

**Evaluating Tradeoffs between Hazard-Resistance and Environmental Impacts: A
Multi-Criteria Approach to Building Design and Life Cycle Performance**

by

SARAH J. WELSH-HUGGINS

M.S., University of Colorado Boulder, 2016

B.S., A.B., Lafayette College, 2012

A thesis submitted to the

Faculty of the Graduate School of the

University of Colorado in partial fulfillment

of the requirement for the degree of

Doctorate of Philosophy

Department of Civil, Environmental and Architectural Engineering

2017

This dissertation entitled:

**Evaluating Tradeoffs between Hazard-Resistance and Environmental Impacts: A
Multi-Criteria Approach to Building Design and Life Cycle Performance**

written by Sarah J. Welsh-Huggins

has been approved for the Department of Civil, Environmental and Architectural Engineering

Abbie B. Liel (Chair)

Sherri Cook

Joseph Kasprzyk

Tonatiuh Rodriguez-Nikl

Wil V. Srubar III

Date: April 19, 2017

The final copy of this thesis has been examined by the signatories, and we find that both the content and the form meet acceptable presentation standards of scholarly work in the above mentioned discipline.

Welsh-Huggins, Sarah Joy (Ph.D., Civil, Environmental and Architectural Engineering)

Evaluating Tradeoffs between Hazard-Resistance and Environmental Impacts: A Multi-Criteria Approach to Building Design and Life Cycle Performance

Thesis Directed by Associate Professor Abbie B. Liel

Principles of green building design and hazard-resistant design are often employed individually to enhance building performance, but for different objectives and evaluated with different units of measurement. At a fundamental level, however, hazard resistant design and green building design are motivated by shared principles and evaluated with shared assessment tools, although often with outcomes presented in different units of measurement. The goal of this research is to quantify the influence of hazard resistant design principles on green building performance—namely, life cycle environmental impact—and, conversely, to quantify the influence of green building design principles on hazard resilience, focused here on seismic performance.

This dissertation represents a compilation of three studies that combine to evaluate and quantify how a) structural design principles for hazard resistance influence life cycle environmental impacts of a building and b) principles of green building design influence building hazard-resistance. Each chapter examines the life cycle environmental impacts and seismic performance of a series of code-conforming, reinforced concrete office buildings in southern Los Angeles, varied with respect to non-structural green building features, structural frame and member configurations, and structural concrete properties. When taken together, the results of each study provide insight into the tradeoffs and synergies between life cycle hazard performance and environmental impact. The results also support broader goals for the intersection of hazard-resistant and green design, not limited in application to buildings (nor only reinforced concrete as a structural material). A key methodological contribution of this dissertation is development of an innovative approach that transforms building component damage fragilities into specific material volumes for post-hazard component restoration and then translates these material quantities into distributions of post-hazard environmental impacts. Finally, this dissertation applies the concepts of multi-objective analysis and life cycle assessment to evaluate the multi-metric, systems-based nature of building design, construction, operation, and performance in the 21st century.

DEDICATION

To my grandparents—Pat, Tom, Mary Anne, and Richard—each of whom taught me to value perseverance and curiosity in all that I strive to accomplish.

ACKNOWLEDGMENTS

My studies and research at the University of Colorado were funded in large part by a grant from the National Science Foundation (NSF), while the final semester of my doctorate has been funded by a Dissertation Completion Grant from the CU Boulder Civil, Environmental, and Architectural Engineering (CEAE) Department. This support is greatly appreciated. Much of this work utilized the Janus supercomputer, which is a joint effort of the University of Colorado Boulder, the University of Colorado Denver and the National Center for Atmospheric Research, funded by NSF award number CNS-0821794. I appreciate the computational support to my work from use of Janus. In addition, I gratefully acknowledge the Haselton Baker Risk Group for providing access to the SP3 software prior to its public release.

A number of individuals have contributed significantly to the research presented in this dissertation. Most importantly, I would like to thank my advisor, Professor Abbie Liel, for sharing with me her enthusiasm for and knowledge of structural and earthquake engineering, civil systems thinking, and engineering education. She has also taught me what it means to be a compassionate and motivating leader, and inspires me daily to hold myself to the highest standards of research and professionalism, while also maintaining a healthy and happy work-life balance. Under her tutelage and mentorship, I have grown as an engineer, academic, writer, and an advocate for women in engineering and the sciences. I am lucky to have spent my time at CU Boulder as her student and I look forward to our future collaborations together.

I would also like to thank Professors Wil V. Srubar III, Sherri Cook, Joseph Kasprzyk, and Tonatiuh Rodriguez-Nikl for their thoughtful comments on my research, models, and results during my time at CU Boulder. I appreciate, as well, the insights given by Professors Paul Chinowsky and David Veshosky during initial development of my research framework. I also thank CEAE administrative staff past and present, especially Araceli Warren, Ken LaFon, Pamela Halstead Williamson, and Robyn Sandekian for their dedication to our department's students.

Now-Drs. Siamak Sattar, Jared DeBock, and Meera Raghunandan provided a welcome environment for me during my first year as a Ph.D. student. I am forever grateful for their patient help with my early forays into nonlinear computational analysis and the personal encouragement

they have continued to bestow upon me after their own graduations. Although this dissertation is the product of my own efforts, my work has benefitted greatly from conversations about coding, structural design, and structural analysis with members of my research group, especially Cody Harrington, Rob Chase, and Travis Marcilla. Fellow CEAE graduate students Juan-Pablo Gevaudan, Adriana Souto, Topher Jones, and Liz Shilling have provided invaluable assistance to my studies of life cycle analysis and concrete chemistry. In addition, I shared an office over the years with a wonderful cohort of graduate students and post-docs, who brightened my days in the Engineering Center. I thank, in particular, Derek Kozak, Lan Nguyen, Emily Elwood, Holly Bonstrom, Jakub Valigura, Derya Deniz, and Shahlaa Al Wakeel.

To my dear friend and former officemate Yolanda Lin, your support—from hand-made gifts, to phone dates, to pool workouts, to paper editing advice—has meant the world to me and I know we have years of post-graduate school adventures together. Thank you as well to Kristen Hess and Rebecca Scheetz for having kept me smiling, calm, fed, and caffeinated during the final six months of my dissertation. To the old Civil Systems cohort of Drs. Laura Kohler, Kyle Kwiatkowski, Amy Schweikert, and Jeff Walters, thank you for your always-valuable feedback on my presentations and writing. To the original “Rungineers,” Leigh Gilmore Terry and Kaitlin Litchfield, thank you for your friendship across the many miles, on and off the trails. I have been lucky during my time in Boulder to have built a large community of fun, like-minded friends and I am so grateful to know each of you (in particular: thank you to Toni Escalas, David Faulon, and Jenny Ramirez).

Next, but never last in my mind or my heart, to my family. Mom, Dad, Emma, and Thomas, who all knew me first as Seismic Sarah, thank you for your ever-present love and support. And finally, to Xavi, for the adventures we have shared, for your endless depth of patience and encouragement, and for the joy you bring each day to my life, I am so thankful...and I can't wait for the new chapter we are beginning together now.

TABLE OF CONTENTS

Abstract.....	iii
Dedication.....	iv
Acknowledgments	v
Chapter 1 Introduction.....	1
1.1 Intersection of green and resilient design principles.....	1
1.2 Points of departure	3
1.3 Scope and organization	6
Chapter 2 Green Building and Hazard-Resistant Design: Examining the Seismic Impacts of Buildings with Green Roofs	9
2.1 Introduction.....	9
2.2 Points of departure	10
2.3 Proposed framework for green-resilient building design and assessment	12
2.4 Life cycle assessment of buildings with green roofs in high seismic areas	13
2.5 Nonlinear modeling and analysis	17
2.6 Loss analysis	22
2.7 Environmental impact analysis	29
2.8 Limitations	37
2.9 Conclusions.....	37
Chapter 3 Is Hazard Resilience Sustainable? Evaluating Multi-Objective Outcomes from Enhanced Seismic Design Decisions	41
3.1 Introduction.....	41
3.2 Background.....	42

3.3	Case study building designs.....	43
3.4	Nonlinear modeling and dynamic analysis	46
3.5	Seismic loss analysis results	49
3.6	Multi-objective analysis of economic and environmental metrics.....	63
3.7	Conclusions.....	66
Chapter 4 Reduce, Reuse, Resilience: Tradeoffs in Life Cycle Seismic Performance Associated with the Use of Fly Ash or Recycled Concrete Aggregate in Reinforced Concrete Buildings		68
4.1	Introduction.....	68
4.2	Life cycle seismic performance of buildings	69
4.3	Case study	74
4.4	Conclusions.....	101
Chapter 5 Conclusions.....		104
5.1	Summary.....	104
5.2	Findings.....	105
5.3	Future work.....	110
5.4	Concluding remarks	113
References.....		114

LIST OF TABLES

Table 2.1 Hazard levels considered for Los Angeles site.	18
Table 2.2 Pushover results for case study buildings.	19
Table 2.3 Example calculation of material quantities needed for repair actions for curtain wall units.	27
Table 2.4 Median repair costs for total building post-earthquake losses from Monte Carlo simulation of all potential component repair and building replacement costs.	28
Table 2.5 Allocation unit environmental impacts for curtain wall repair materials.	32
Table 2.6 Strengths and weaknesses identified during life cycle assessment of building design tradeoffs for environmental impact and hazard performance.	39
Table 3.1 Design variables and seismic analysis outcomes for all 30 case study buildings.	52
Table 4.1. Mix designs with alternative concrete materials.	75
Table 4.2. Properties of case study buildings with alternative concretes, showing concrete properties and building period and strength.	79
Table 4.3. Seismic analysis results for study buildings designed with each alternative concrete type.	81
Table 4.4. Distances between potential material extraction/processing sites to concrete mix plant site in southern Los Angeles.	88
Table 4.5. Results of uncertainty analysis showing how unit embodied carbon impacts for concrete mix materials influence unit concrete and total upfront building embodied carbon impacts due to a) variations in cement unit embodied carbon impact, and b) variations in virgin aggregate transport distances.	91
Table 4.6. Material repair quantities and concrete embodied carbon impact parameters varied in uncertainty analysis of post-earthquake embodied carbon outcomes.	97

LIST OF FIGURES

Figure 2.1 Framework for “green-resilient” building design and assessment.	13
Figure 2.2 2D elevation representation of the four study buildings, with diagram of the different green roof systems (based on Sailor 2008).....	15
Figure 2.3 Column and beam designs for all four buildings (same size member dimensions at each floor for each building, but reinforcement ratios vary depending on member location in the building). Concrete and steel material strengths are the same for all buildings.	17
Figure 2.4 Results of static pushover analysis for all buildings.....	20
Figure 2.5 Peak IDRs as a function of ground motion intensity for (a) control building, (b) shallow green roof building, (c) deep green roof building and (d) retrofit green roof building (showing only non-collapse results in all cases).	21
Figure 2.6 Collapse fragility curves for all four buildings.....	22
Figure 2.7 Fragility functions developed for shallow and deep green roof systems (based on data from Carmody et al. 2009).....	24
Figure 2.8 Damage to curtain wall units for shallow green roof building over all realizations at each hazard level, showing (a) median damage state and (b) box plot of number of damaged units (25 th , 50 th and 75 th percentiles).....	26
Figure 2.9 Median material quantities needed for curtain wall repair for shallow green roof building (including collapse cases).	28
Figure 2.10 Tons of CO ₂ emissions or equivalent associated with post-earthquake repairs of curtain walls in the shallow green roof building: (a) deaggregated by material requirement and (b) showing uncertainty in the estimate (box plot with 25 th , 50 th , and 75 th percentiles).	33
Figure 2.11 Climate change potential (CO ₂ eq.) from life cycle stage of: (a) product manufacturing, (b) operating energy and (c) post-hazard repair (mean log values from lognormal distribution) for all four buildings after each of the nine ground shaking intensity scenarios.....	35

Figure 2.12 Environmental impact exceedance curve (representing CO₂ emissions fragility function) for exceedance of 100 tons of CO₂ during post-earthquake repairs. 36

Figure 2.13 Radar plot showing tradeoffs in building performance (where repairs are considered at a ground shaking intensity of $S_a(T_1=1.00 \text{ s}) = 0.86 \text{ g}$) and environmental impact is considered in terms of climate change potential (referred to as CCP and in terms of CO₂ equivalents). 39

Figure 3.1 Influence of seismic design on upfront embodied carbon showing a) effect of ultimate base shear strength on embodied carbon for 4-story strength design space frames and b) effect of ductility capacity on 4-story ductility design space frames. (1 kip. = 4,448 N.; 1 ton = 987 kg.)..... 47

Figure 3.2. Nonlinear static pushover results (per frame line) for 4-story a) strength design space frames and b) ductility design space frames. (1 kip. = 4,448 N.). The labels RDR_{yield} and RDR_{ult} on Figure 3.2(b) demonstrate the points used to calculate the ductility capacity of a given building design. RDR_{yield} refers to the roof drift ratio at the maximum lateral strength capacity achieved by a building, while RDR_{ult} refers to the roof drift ratio at which 20% of the lateral strength has been lost for a design..... 48

Figure 3.3. Median post-earthquake economic cost for strength design space frames for a) 4-story and b) 12-story buildings at each hazard level. (denotes code-compliant designs)..... 53*

Figure 3.4. Post-earthquake economic costs deaggregated by non-collapse and collapse costs at each hazard level for selected 4-story above-code (SCWB = 2.5) and below-code (SCWB = 0.6) ductility design space frames..... 53

Figure 3.5. Expected annual post-earthquake economic cost for 4-story strength design a) space frames, b) perimeter frames, c) 4-story ductility design space frames, and d) 12-story ductility design perimeter frames. Losses are annuities and expressed as percentage of total building replacement cost. (* denotes code-compliant designs). 55

Figure 3.6. Median post-earthquake embodied carbon for 4-story strength design a) space frames and b) perimeter frames at each hazard level. (* denotes code-compliant designs. 1 ton = 987 kg.)..... 57

Figure 3.7. Expected annual post-earthquake embodied carbon loss for 4-story space frames for a) strength designs and b) ductility designs. Losses are annuities and expressed as percentage of total building replacement embodied carbon values. (* denotes code-compliant designs)..... 58

Figure 3.8. Deaggregated component contributions to seismic losses in terms of economic costs and embodied carbon loss for 4-story strength design space frames: a) above-code ($R = 4$), and b) below-code ($R = 12$), at the nine different ground shaking intensities analyzed at hazard levels defined by $S_a(T_1)$ 60

Figure 3.9. Total post-earthquake embodied carbon for 4-story space frames with respect to a) base shear strength for strength designs, and b) ductility capacity for ductility designs, showing the effect of discount rate on these calculations. 62

Figure 3.10. Influence of ultimate base shear strength on total seismic embodied carbon loss for Los Angeles, CA study site, compared to sites of higher and lower seismic hazard. Expected results for a building with 20% greater design strength in Los Angeles also shown. (1 kip = 4,448 N.; 1 ton = 987 kg.). 63

Figure 3.11. Multi-objective analysis results comparing design and analysis outcomes for 4-story space frame a) strength design buildings and b) ductility design buildings. Results are presented with respect to a selected “baseline” design (code-compliant 4-story space frame), i.e. the value associated with the baseline design is subtracted from the value for the design of interest. Metrics are plotted on y-axis such that less desirable outcomes are at the top and more desirable are at the bottom. 65

Figure 4.1. Life cycle system boundary showing stages inside the scope of current study. 73

Figure 4.2. Static pushover results (per frame line) for a) distributed plasticity and b) lumped plasticity models of functional unit when designed with fly ash concrete; and c) distributed plasticity and d) lumped plasticity models of functional unit when designed with RCA concrete (1 kip = 4,480 N). 80

Figure 4.3. a) Vulnerability functions quantifying median post-earthquake economic costs for the normal concrete building and the RCA concrete buildings; b) post-earthquake economic costs deaggregated by median non-collapse and collapse at hazard level corresponding to $S_a(T_1=0.87s)=1.50g$ for normal concrete and RCA concrete functional unit variations. 83

Figure 4.4. Expected annualized post-earthquake economic costs, expressed as annuities and normalized by total building replacement cost, for each RC building variation or functional unit.....	84
Figure 4.5. System boundary for production of one cubic foot (0.03 m ³) of normal concrete, without any alternative materials.....	86
Figure 4.6. System boundaries for production of the functional unit when constructed with either fly ash or RCA concrete variations.....	87
Figure 4.7. Map showing relative locations of material sources, processing plants, potential concrete mix plants, and building site assumed in this study.....	88
Figure 4.8. Results of uncertainty analysis, showing how distributions of concrete unit embodied carbon vary with respect to changes in a) cement unit material embodied carbon impact, b) transport distance between cement production facility and concrete plant, c) virgin aggregate unit embodied carbon impact, and d) transport distance between virgin aggregate source and the concrete plant. The legend on Figure 4.8(c) shows key boxplot features. (1 lb = 0.45 kg).....	91
Figure 4.9. System boundary for production of a functional unit (code-conforming, 4-story, RC space frame building), which is constructed with alternative types of structural concrete.....	92
Figure 4.10. Sensitivity of upfront embodied carbon for a functional unit constructed with normal concrete. The parameters on the left are material quantities for structural and non-structural building components, while the parameters on the right are inputs to a unit of concrete. (1 ton = 987 kg).	94
Figure 4.11 Vulnerability functions quantifying changes in median post-earthquake embodied carbon when the functional unit is constructed with each alternative concrete type, considering median unit impacts, transportation distances, and material quantities. (1 ton = 987 kg).	96
Figure 4.12. Distributions of post-earthquake embodied carbon, considering uncertainties in quantities of repair materials and alternative concrete impact assumptions at a) $S_a(T_1=0.87s)=1.50g$; and b) $S_a(T_1=0.87s)=2.91g$. Figure 4.8(c) shows legend of boxplot features. (1 ton = 987 kg).....	99

Figure 4.13. Total post-earthquake embodied carbon. Results represent median values, considering distributions of all possible embodied carbon outcomes, conditioned on hazard scenario frequencies of occurrence. (1 ton = 987 kg). 101

Chapter 1 INTRODUCTION

1.1 INTERSECTION OF GREEN AND RESILIENT DESIGN PRINCIPLES

Principles of green building design and hazard-resistant design are often employed individually to enhance building performance, but with a focus on different objectives and with different units of measurement. Green building practices aim to mitigate threats from building construction and operations to human health and degradation of the natural environment, through more efficient uses of water, energy and material resources (Bokalders & Block, 2010). Engineering for green buildings encompasses a wide range of design choices, from decisions about structural features, to energy-saving equipment, to building orientation. The green building initiative grew alongside ideas about sustainable development, which recognizes the need to reduce present-day negative environmental impacts to sustain resources for future generations (Berke, 1995; Bokalders & Block, 2010; Schwab & Brower, 1999). Green building rating systems such as LEED in the U.S. (USGBC, 2015) or BREEAM in Europe (BREEAM, 2015) have become popular tools to evaluate “greenness” and to recognize buildings where owners and operators have taken steps towards sustainable design and operations.

Hazard-resistant design has traditionally involved quantification of extreme loads, and probabilistic representation of those loads for generally simplistic inclusion in design codes. More recently, performance-based design methodologies have sought to develop design procedures that satisfy performance objectives for design-level hazard events a priori, where performance is related to different levels of post-disaster functionality (Porter, 2003). A key goal of this paradigm shift is the development of more robust, redundant structures capable of experiencing low levels of hazard-induced damage and limited loss of post-event functionality (Bruneau et al., 2004). In the United States, \$35 million in direct property loss is incurred each year from natural hazard-induced damage, much of which is associated with building damage from structures that could not resist the level of hazard intensity experienced in a given event (Portland Concrete Association, 2012). Losses associated with indirect impacts, e.g. business interruption, may be orders of magnitude higher.

The hypothesis of this dissertation is that hazard-resistant design principles can support achievement of green building objectives for life cycle environmental impacts and that,

simultaneously, green design philosophies should be included in tandem with performance-based engineering goals for hazard resilience. Enhanced building hazard-resistance not only protects human lives, but also supports broader goals for community hazard resilience, health and safety. Damage to buildings (or other structures), under seismic, hurricane, or other extreme event loads can necessitate repair activities that increase life cycle consumption of energy, release of greenhouse gas emissions, and natural resource use. The release of harmful particulates or heavy metals during post-hazard building repair, replacement, or demolition activities can also contaminate air and water sources, further jeopardizing human health and community recovery after a disaster. When buildings or their components are less likely to be experience damage in a hazard event, short and long-term economic costs and environmental impacts from repair and replacement activities may be reduced. Moreover, fewer post-hazard building repairs diverts material and financial resources from restoration of individual buildings towards larger emergency response, relief, and recovery operations. Typical hazard-resistant design practices, however, may only prove environmentally beneficial in the occurrence of a major hazard event. Designing a building for specific “green” objectives, such as lower operating energy, can reduce total life cycle economic and environmental costs, since the majority—or in some cases, the entirety—of a structure’s lifespan will not experience a significant hazard event.

On a more fundamental level, hazard resistant design and green building design are motivated by shared principles and evaluated with shared assessment tools, although often with outcomes presented in different units of measurement. Both design objectives require long-term decision-making perspectives to balance upfront impacts or costs, with uncertain future environmental, societal and safety benefits (Berke, 1995; Mileti & Peek-Gottschlich, 2001; Schwab & Brower, 1999). Successful integration of these two design philosophies requires development of life cycle analysis assessment techniques that provide comprehensive and reproducible metrics of building performance over time. Innovation for system-based solutions to this problem currently are limited by prescriptive design procedures that specify code-defined minimum levels of hazard resistance or assign points based on specific green building actions. A performance-based design approach is therefore needed to support holistic building life cycle assessment, considering variability or uncertainty in outcomes and accounting more completely for the multi-metric nature of upfront and long-term costs of environmental and structural performance (Comber & Poland, 2013; Gromala et al., 2010; Portland Concrete Association,

2012). Such a paradigm shift in building design and performance-based assessment could facilitate adoption of greener, more hazard resistant building technologies.

1.2 POINTS OF DEPARTURE

Practice and assessment of green buildings has not recognized hazard resistance as a component of building sustainability. In the early to mid-2000s, green building rating systems commonly credited buildings for categories like efficient water use, reductions in operating energy, or improved indoor environmental quality, but not for design decisions to improve hazard-resistance (USGBC, 2009). Numerous analyses have also documented building life cycle environmental impacts, accounting for material production and transportation, construction, operating energy, and demolition, without considering the occurrence of a hazard event during a structure's lifespan (Cole & Kernan, 1996; Horvath & Hendrickson, 1998; Johnson, 1996; Junnila & Horvath, 2003; Simion et al., 2013). At the same time, prescriptive and performance-based methods for hazard-resistant design and analysis have grown in isolation from green building philosophies.

The development of resilience rating systems programs like REDi or the United States Resiliency Council over the last five years, however, demonstrates growing interest among policy-makers and communities to design buildings beyond code minimum requirements, to achieve targeted performance goals for resilient post-hazard functionality (Almufti & Willford, 2013; USRC, 2015). In addition, a small number of pilot credits to incorporate resilience in green building certification have recently been introduced to the LEED credit library. These pilot credits encourage developers to account for disaster preparedness and resilience in community development and structural design, including the suggested incorporation of the REDi credits into planning initiatives (USGBC, 2015).

Despite these recent advances, the majority of green building standards contain either no, or limited, mention of safety in their guidelines (as these topics are assumed to be covered in structural building codes), while building codes do not address the environmental impacts potentially produced by code-mandatory design procedures (ACI 318, 2011; BREEAM, 2015; USGBC, 2015). One of the most complete—even nearly seven years after its publication—studies on this topic is FEMA P-798, which focuses on identifying interactions between hazard resistance practices and green building practices. These interactions relate mostly to non-structural design

features, like advanced window shading systems, that receive credits from green building rating systems (Gromala et al., 2010). FEMA P-798 recognizes that—although important for mitigating building environmental impacts—green building features can compromise structural resistance to hazard events (*e.g.* placement of photovoltaic cells on a roof could increase wind uplift forces on a structure). This document, however, does not examine the impact of hazard-resistant design decisions on life cycle environmental impact, nor does it provide methods to quantify these green and hazard-resistant interactions. The Portland Cement Association (PCA) has also entered the discussion about connecting resilient and sustainable design ideals, suggested that “greener” buildings should be designed for higher seismic and other extreme loads to reduce environmental impacts associated with post-hazard repairs (Portland Concrete Association, 2012). Despite offering target recommendations for design levels of resistance in green buildings, the PCA does not provide any analytically or experimentally-founded method to quantify the improved performance (environmental or otherwise) associated with these increases in building strength. Finally, when the FEMA P-58 seismic loss analysis methodology was published in 2012, initial suggestions were included for linking probabilistic seismic loss analysis approaches to associated environmental impacts from post-earthquake repairs (Court et al., 2012). However, advancement of this work to develop performance-based environmental impact assessment methodologies for seismic loss is still in progress.

In the academic sphere, a number of frameworks have been suggested in recent years to evaluate building life cycle environmental impacts with consideration of the potential for disasters or extreme event (*e.g.* Bocchini, Frangopol, Ummenhofer, & Zinke, 2014; Court, *et al.*, 2012; Padgett & Li, 2016; Rodriguez-Nikl, 2015). These frameworks each offer similar approaches, each adding a “post-hazard” stage to the traditional building life cycle (construction, operation, demolition, etc.) in an attempt to quantify lifetime environmental impacts from post-disaster repair/replacement actions. Such studies have examined the influence of specific structural system decisions—almost exclusively for reinforced concrete buildings or bridges—for seismic design by quantifying CO₂ emissions and economic losses from building construction and post-earthquake repairs. For example, Chiu *et al.* (2013) examine returns on investment, both in terms of reduced economic costs and CO₂ emissions, for seismic retrofits to reinforced concrete buildings. Hossain and Gencturk (2014) conduct a cradle-to-grave life cycle assessment of reinforced concrete buildings subjected to seismic hazards that quantifies upfront and post-hazard repair environmental

impacts, presented as single environmental impact outcomes score. Simonen *et al.* (2015) evaluate post-hazard environmental impacts of tall buildings (over 40 stories) based on changes in seismic response from use of innovative seismic force resisting systems (fixed-base, base-isolated, and damped-outrigger) and structural design configurations (code-minimum and above-code). Meanwhile Wei *et al.* (2016a and 2016b) present a cost-benefit analysis approach for evaluating seismic retrofit decisions in the context of life cycle CO₂ emissions, comparing upfront CO₂ emissions produced from retrofit actions with avoided environmental impacts from reduced post-earthquake damage. The work of Wei *et al.* shows that initial investments in seismic retrofit can be environmentally and economically positive; despite slightly increasing pre-hazard service life environmental impacts, seismic retrofits can help reduce potential post-earthquake repair-related CO₂ emissions. However, the specific approach taken to translate seismic demand and building damage into environmental impacts is not well-documented in these previous studies. As well, most studies attempt to combine results of multiple design and analysis categories into a single “environmental impact” score or to monetize all life cycle impacts. There is a lack of existing approaches to appropriately evaluate and quantify the multi-metric nature of building life cycle analyses, in support of real-world decision-making or design prioritization for jointly green *and* hazard-resistant buildings.

Other researchers have sought in recent years to quantify economic and environmental savings from novel materials, including concretes created by supplementing conventional concrete mixes with materials traditionally considered waste products. These studies primarily focus on properties of alternative concretes (*e.g.* those that replace cement with fly ash) like constitutive material properties, unit CO₂ emissions, or durability under chemical intrusions. Only a few studies that analyze alternative concrete mixes have considered broader building life cycle impacts, with respect to both hazard loads and environmental impacts, from constructing a building with varying types of structural materials. Changqing and Jianzhuang (2013) conduct full-scale shake table tests of a mid-rise building constructed with recycled aggregate concrete, where seismic demand is quantified in terms of drifts and accelerations. Srubar (2014) introduces a framework to combine traditional life cycle environmental impact assessment with models of material service life durability, using the example of recycled aggregate concrete, while Flint *et al.* (2014) present a modular, performance-based engineering framework to incorporate material degradation into consideration of hazard-resistance over the service life of a building. Studies of fly ash concrete

meanwhile have been almost exclusively limited to investigation of mechanical properties like in Langley, *et al.* (1989) or Siddique (2004), or quantification of CO₂ emissions from production of fly ash concrete, as in Huntzinger and Eatmon (2009) or O'Brien *et al.* (2009), but have generally not assessed the use of fly ash concretes at a whole building level. Rodriguez-Nikl *et al.* (2012) presents one of the few studies that considers the impact of alternative materials like recycled concrete aggregate and fly ash in concretes on life cycle seismic performance and environmental impacts of an entire reinforced concrete bridge.

Despite these recent investigations of integrated green and hazard-resistant design principles, further research is needed to quantify and assess the life cycle of an entire building, with respect to upfront environmental impact, structural material properties, and hazard performance when using alternative structural materials (Comber, Poland, & Sinclair, 2012; Feese, Li, & Bulleit, 2014; Menna, Asprone, Jalayer, Prota, & Manfredi, 2013). From the findings of the literature described above, there is still a lack of knowledge about the influence of green building design practices on hazard-resistance and, conversely, the influence of systematic hazard-resistant design techniques, such as increasing lateral strength, for life cycle environmental impacts. In response, this dissertation seeks to develop probabilistic life cycle performance assessment methodologies to account for potential hazard event occurrences in the context of green/sustainable design and vice versa. The proposed methodology can be used to explore multiple design decisions (*e.g.* non-structural green building features, enhanced structural systems for seismic design, and/or alternative, “green,” structural materials) to evaluate tradeoffs from these different choices on performance objectives for upfront and post-hazard green building and hazard-resistant design.

1.3 SCOPE AND ORGANIZATION

The goal of this research is to quantify the influence of hazard resistant design principles on green building performance—namely, life cycle environmental impact—and, conversely, to quantify the influence of green building design principles on hazard resilience, focusing here on seismic performance. In doing so, this project also develops and describes a life cycle assessment framework for the holistic evaluation of green and hazard resistance performance. This dissertation represents a compilation of three studies that combine to evaluate and quantify how a) structural design principles for hazard resistance influence life cycle environmental impacts of a building

and b) principles of green building design influence building hazard-resistance. Chapters 2-4 of this dissertation are adapted from a series of journal papers developed over the course of the author's doctoral studies. Chapter 5 summarizes the findings of these three studies and provides concluding thoughts on how economic and environmental metrics of different design and analysis categories may be considered together to enhance decisions surrounding building life cycle environmental and seismic performance. The concluding chapter also identifies limitations to the work presented herein and suggests remaining knowledge gaps that could be addressed by other researchers in future studies. A large number of sources have been reviewed for this thesis. In place of a single chapter on literature review, discussion of the relevant references is presented at the beginning of the relevant section in each chapter.

Chapter 2: This study is motivated by the knowledge that building design and performance are increasingly being scrutinized from perspectives of both sustainability and hazard-resistance. However, the approaches taken to consider these perspectives are disconnected; green building ratings systems do not consider hazard resistance in their assessments, while performance-based engineering methods have tended to neglect consideration of environmental impacts. This chapter presents a framework to assess building life cycle performance in terms of social, environmental, and economic impacts using probabilistic approaches, considering the possible occurrence of an earthquake or other extreme event. The framework is illustrated by a case study of an office building in Los Angeles, designed with and without different types of vegetated (green) roofs, and at risk from varying earthquake hazard scenarios. This chapter has been published in *Structure and Infrastructure Engineering* (Welsh-Huggins and Liel, 2016).

Chapter 3: This study investigates the idea that “green” buildings should be designed to withstand higher extreme loads (i.e. loads associated with earthquakes or other hazards), to reduce environmental impacts associated with post-hazard repairs. The study assesses the seismic performance and associated environmental impact of 30 modern reinforced concrete buildings with varying lateral strengths and ductility capacities, considering 4- and 12-story space and perimeter frames. The structural engineering community is currently engaged in an epistemological debate regarding the value of ductility capacity for life cycle building design. Previous studies have investigated how design strength and ductility capacity affect building performance in terms of economic losses, but not environmental impacts. The analysis presented

in this chapter seeks to further understanding about the tradeoffs between lateral strength and ductility capacity in terms of joint life cycle environmental and seismic performance. This chapter also demonstrates how multi-objective analysis, a decision-making approach more common in water resources engineering, may act as a useful tool for evaluating multi-metric building life cycle analysis outcomes. This chapter has been accepted as an article for review by the *Journal of Structural Engineering*.

Chapter 4: This study conducts a life cycle environmental impact assessment of concrete's contribution to climate change from upfront building construction and from additional life cycle CO₂ emission produced during post-hazard building repair and restoration. This chapter quantifies changes in seismic performance of a modern, 4-story reinforced concrete building when the concrete is designed with fly ash replacing cement or recycled concrete replacing coarse aggregate. Unit embodied carbon, accounting for uncertainties in material transport distances and quality of concrete mix emissions data, is correlated to unit embodied carbon impacts of cement and to assumptions about transportation distances for virgin aggregate. The research in this chapter seeks to unify the many existing, yet largely disconnected, studies about material properties and environmental impacts, of these alternative concretes, in the context of a comprehensive life cycle assessment of structural systems. Chapter 4 holistically investigate changes in building performance at two key life cycle stages—upfront (pre-service life) and hazard event/post-hazard repair (service life)—from use of these alternative concretes as structural materials. Following final submission of this dissertation, this chapter will be submitted for review as an article in the *International Journal of Life Cycle Assessment*.

Chapter 2 GREEN BUILDING AND HAZARD-RESISTANT DESIGN: EXAMINING THE SEISMIC IMPACTS OF BUILDINGS WITH GREEN ROOFS¹

2.1 INTRODUCTION

This paper conducts a life cycle assessment evaluating impacts of green and hazard-resistant design decisions for buildings within an integrated green-resilience framework. Investigation of the synergies between green building design and hazard-resistant building design is a developing field of research. The building sector accounts for over 40% of primary energy consumption in the United States (DOE, 2012). Activities in each building life cycle stage, i.e. material extraction, construction, operation, etc., release CO₂, CO, NO_x, SO₂ emissions, volatile organic compounds and particulates, which can harm human health and the natural environment. Green building rating systems such as LEED (USGBC, 2009) or BREEAM (BREEAM, 2015) have become popular tools to credit buildings where owners and operators have taken steps towards sustainable design and operations. At this time, programs such as the *Resilience-Based Earthquake Design Initiative* and the U.S. Resiliency Council (USRC) are still-developing systems to rank building resilience and hazard performance (Almufti & Willford, 2013; USRC, 2015).

However, the development of resilience rating systems programs such as REDi or the USRC demonstrates the increasing interest from both policy-makers and communities to design buildings for beyond code minimum requirements, in order to achieve targeted performance goals for resilient post-hazard functionality. In addition, several pilot credits to incorporate resilience into LEED certification have recently been introduced, to encourage developers to consider disaster preparedness and resilience in community development and structural design, including the suggested incorporation of the REDi credits into their planning initiatives (USGBC, 2015).

Goals for green, sustainable design and hazard-resilient buildings cannot be seen as separate or competing objectives. Modern structural engineers must balance structural integrity

¹Adapted from Welsh-Huggins, S. J., & Liel, A. B. (2017). A life-cycle framework for integrating green building and hazard-resistant design: examining the seismic impacts of buildings with green roofs. *Structure and Infrastructure Engineering*, 13(1), 1-15.

and resilience with sustainability (Feese et al., 2014). Academic research is needed to understand how a greener 21st century building stock will perform in the context of being placed near or alongside hazards such as floodplains and fault lines (Comber & Poland, 2013; Comber et al., 2012; Menna et al., 2013). Probabilistic life cycle performance assessment methodologies can provide a means to account for potential occurrences of hazard events in the context of green/sustainable design and vice versa.

This article opens with the motivation for the proposed green-resilience framework. We illustrate the framework with a case study of a Los Angeles office building, designed with and without different vegetated or green roof systems, and at risk from varying seismic ground shaking hazard scenarios. The objective of this case study is to explore how inclusion of green roofs in structural design affects both building environmental impact and hazard losses. We close with a discussion of case study findings and future applications for the proposed holistic life cycle framework for building design and assessment.

2.2 POINTS OF DEPARTURE

Green building design strives to minimize resource use in building construction and operations and to provide healthier and more environmentally friendly living and working spaces, offering benefits such as reduced operating energy, lower water consumption, improved indoor environmental quality and enhanced occupant productivity (USGBC, 2009). Rating systems such as LEED are intended to evaluate the ‘greenness’ of new and existing buildings. The green building initiative grew alongside ideas about sustainable development in the urban planning community. The concept of sustainable development stemmed from the broader sustainability movement, which recognizes the need to reduce present-day negative environmental impacts to sustain resources for future generations (Berke, 1995; Schwab & Brower, 1999).

Life cycle analysis (LCA) can be used to systematically quantify economic and environmental impacts of a product or system over its lifespan (Hendrickson, Horvath, Joshi, & Lave, 1998; Lawson, Bersani, Fahim-Nader, & Guo, 2002; Sharrard, Matthews, & Ries, 2008). LCA can be used to demonstrate the benefits of different green building design features. Process-based environmental LCA describes the inflow of material processes and outflow of environmental impacts during a product’s lifespan. By comparison, input–output LCA defines life cycle costing

and environmental impacts based on U.S. Department of Commerce data for goods and services production and related energy and material consumption. For both approaches, a typical system boundary encompasses impacts associated with extraction of raw materials, product manufacturing, construction, operations/maintenance, repairs and demolition/end-of-life.

A seminal study by Junnila and Horvath (2003) quantifies life cycle impacts of reinforced concrete office buildings. Junnila and Horvath demonstrate that steel production dominates manufacturing impacts, given the high volume required for the structural reinforcement, external envelope, HVAC and water piping systems and other internal non-structural components. Compared to manufacturing, the impact of construction activities was found to be relatively low. In the operations and use stage, lighting, heating and cooling have the largest impact on electricity consumption. During maintenance, replacement of steel components and re-painting of building interiors contribute greatly to life cycle heavy metal and summer smog impacts. Impact from the end-of-life and decommissioning of buildings depends largely on whether components are recycled, reused or disposed of in a landfill (Carbon Leadership Forum, 2012; Thormark, 2007).

In parallel to environmental impacts studies, engineers have developed the concept of performance-based engineering (PBE) to formalize hazard-resistant design practices that aim to satisfy societal and owner's performance objectives (Moehle & Deierlein, 2004). PBE was originally envisioned as a method to quantify building seismic performance in terms of death, dollars and downtime. Recently, engineering philosophy has moved towards a more holistic thinking, encompassing societal, structural and economic concerns through resilient design, which seeks robust, redundant structures that incur low levels of hazard-induced damage and limited loss of post-disaster functionality (Bruneau et al., 2004).

The interplay between green design and hazard resilience has the potential to change life cycle environmental and post-disaster impacts and to change how we assess these impacts. From one perspective, green building practices can impact how a building resists hazard events, a potentially negative influence (Gromala et al., 2010). At the same time, poor hazard performance of a building may contribute to greater environmental impacts and economic costs over the building lifespan. Yet, beyond a few pilot credits, many current established green building rating systems have not adopted considerations of building hazard performance (BREEAM, 2015;

USGBC, 2015) into their rankings, nor have PBE methodologies been developed to fully account for environmental impacts.

The work presented in this chapter joins a small, but growing body of the literature aiming to examine both building environmental impact and hazard performance through the addition of a “hazard event” stage in building LCA. For example, researchers have proposed framework improvements to LCA that account for life cycle stages associated with hazard events—such as Hossain and Gencturk (2014) or Padgett and Tapia (2013)—and structural deterioration, like Flint *et al.* (2014). Each of these frameworks produces a final life cycle impact score that presents the results from each life cycle stage summed either in terms of dollars or environmental impact indicators. In this vein, the ATC-86 initiative (Court *et al.*, 2012) have proposed the inclusion of environmental impacts from seismic hazard damage within the PBE paradigm.

Nevertheless, a holistic framework that assesses the building life cycle in terms of social, environmental and economic impacts without default to a common, dollar-based, denominator and using probabilistic approaches is lacking. Thus, this study expands assessment of “green” buildings to include consideration of the environmental consequences of hazard resilience. The proposed framework combines environmental impact assessment for green building and hazard performance design objectives, which have, up to this point, largely been quantified separately.

2.3 PROPOSED FRAMEWORK FOR GREEN-RESILIENT BUILDING DESIGN AND ASSESSMENT

Figure 2.1 presents a graphical representation of the so-called “green-resilience” framework developed and applied in this study. The *conceptual design* stage involves development of an initial building, designed to meet building codes, hazard performance objectives and green building rating system goals selected by the owner and/or building professional as appropriate for the function and location.

The second stage involves three consecutive, interrelated analyses of the initial design: (1) *structural analysis* to predict building response to hazard events, (2) *loss analysis* to quantify potential economic losses and material quantities associated with hazard-related repair needs and (3) *environmental analysis* to evaluate the life cycle impact of the design decisions, including environmental impacts from potential hazard events. The third stage, *integration of analysis*

results, combines the results from the analyses in terms of the multi-objective social, economic and environmental losses and benefits to consider potential outcomes probabilistically. In the final stage, *implementation of green-resilient building design*, decision-makers evaluate the results to develop more holistic building designs. The case study presented here illustrates the framework and demonstrates how it can improve understanding of potential tradeoffs between designing for green building objectives, such as a green roof, and designing for hazard resistance goals.

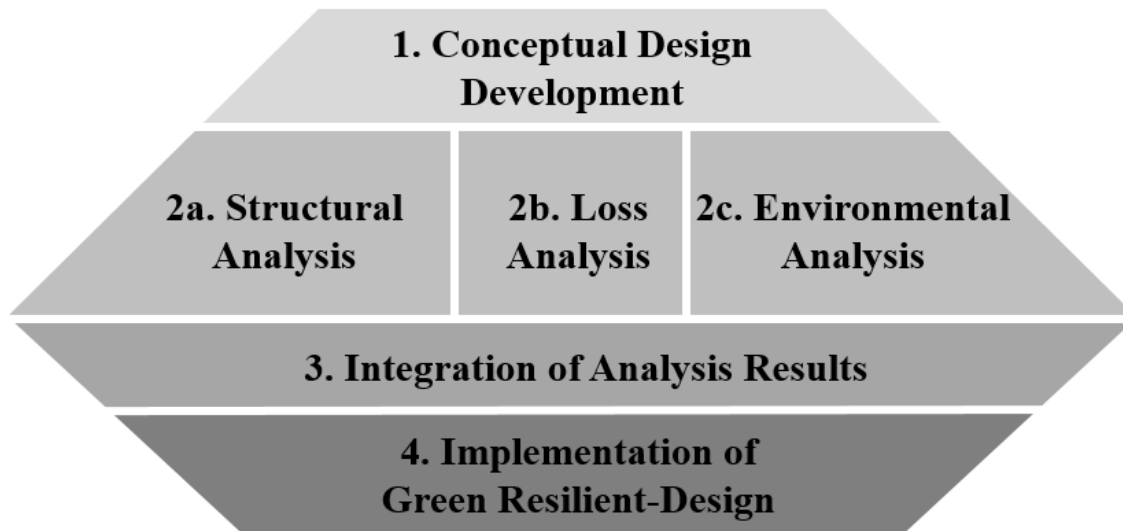


Figure 2.1 Framework for “green-resilient” building design and assessment.

2.4 LIFE CYCLE ASSESSMENT OF BUILDINGS WITH GREEN ROOFS IN HIGH SEISMIC AREAS

2.4.1 GREEN ROOFS

Engineering for green buildings encompasses a wide range of design choices, from decisions about structural features, to energy-saving equipment, to building orientation. Some of these design options may also impact building performance during hazard events. The construction of vegetated (green) roofs in high seismic areas offers both potential benefits and tradeoffs for building life cycle impact. In dense urban environments, plants on these roofs can lower ambient building air temperatures, reducing heat island effect (Saiz, Kennedy, Bass, & Pressnail, 2006). Green roofs also can help to manage storm water, reducing run-off and slowing release time of precipitation. Other benefits include improved air quality, external noise control and provision of wildlife habitat; green roofs may also improve psychological health for building occupants (General

Services Administration [GSA], 2011). Although U.S. adoption of green roofs lags behind Europe, the construction of buildings with green roofs is on the rise: Chicago leads the U.S. in terms of square footage of green roof coverage (DOE, 2012), while Seattle's 2009 *Green Factor* legislation requires 30% vegetated roof cover for all new development in residential and commercial districts (Weiler & Scholz-Barth, 2009).

The basic structure of all green roofs is a plant or grass layer, supported by an engineered soil mixture. Protective, insulating and structural materials placed beneath the soil include filter fabrics, foam insulation and root barriers, waterproofing membrane and structural decking (NRCA, 2007). In this study, green roof types are distinguished by their soil depth following classifications from GSA (2011) and other green roof professionals. "Shallow" green roofs, which are used predominately for storm water management and to mitigate heat island effect, are covered by sedum or other succulent grasses and defined as those with a soil depth of less than six inches. "Deep" green roofs have 8–24 in of soil and provide the same benefits as shallow roofs, along with wildlife habitat and occupant access to green space (GSA, 2011). For both types of green roofs, granite pavers or light aggregate acts as drainage perimeters around green roofs to store excess storm water before its release into the ground and provide roof access (NRCA, 2007). All green roofs require supplemental irrigation for the first three years after construction, but roofs with deeper growing media and larger plants may need permanent irrigation systems, especially in arid places (Weiler & Scholz-Barth, 2009).

2.4.2 BUILDING DESIGNS

The proposed framework is illustrated through a case study of four commercial buildings in Los Angeles, as shown in Figure 2.2. The basic design of this modern code-designed four-story office building is adopted from Goulet *et al.* (2007) and Haselton *et al.* (2008, 2011). The special reinforced concrete space frame has a floor area of 120 ft by 180 ft with six frame lines resisting lateral loads in each direction. The story height at the first story is 15 ft, all others are 13 ft, and column spacing is 30 ft. The case study site in Los Angeles places the building in seismic design category D (ASCE, 2010). This site has a design spectral acceleration for short periods (SDs) of 1.0 g and a design spectral acceleration at 1.0s (SD₁) of 0.6 g.

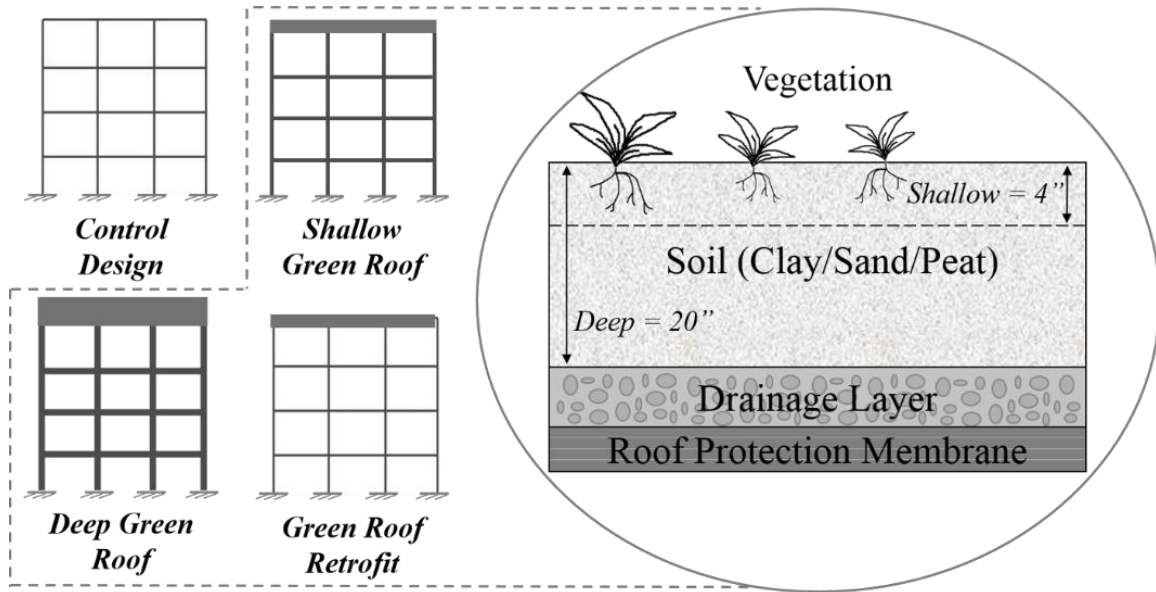


Figure 2.2 2D elevation representation of the four study buildings, with diagram of the different green roof systems (based on Sailor 2008).

2.4.2.1 GREEN ROOF DESIGN

The control building does not have a green roof. The other three buildings consider three different green roof cases. The roof system designs resulted from correspondence with practicing engineers and a literature review of common material, structural and environmental requirements for green roofs. The shallow green roof building has a green roof with 4 in of soil. The deep green roof building uses 20 in of soil, with around 1500 ft² of paved area for occupant roof access. The shallow and deep green roof buildings have larger member sizes and greater amounts of reinforcing steel (larger reinforcement ratios) than the control building to account for the added weight and seismic mass. The fourth building is a “green retrofit” case, in which a shallow green roof is placed on the building without modification, using the same structural system as the control building.

2.4.2.2 STRUCTURAL DESIGN

The soil, with a saturated density of 120 pcf, is the heaviest component of green roof systems. The weight of small plants is less than 10 psf, providing only a small contribution to the total superimposed dead load (personal communication, 2013). In the shallow green roof building, the vegetated green roof system covers a roof area of 21,000 ft². The drainage pavers add 1.3 psf along the roof perimeter and are supported by one inch of soil. Therefore, considering the entire roof area, the average weight of the shallow green roof system is 47.9 psf. The average roof dead load

for the deep green roof building is 200 psf, due to the deeper soil. In addition to the calculated dead loads for each building, the International Building Code designates that “where roofs are to be landscaped, the uniform design live load in the landscaped area shall be 20 psf” (ICC, 2009). The shallow green roof building is therefore designed for this recommended 20 psf of live load, because occupant access is expected to be sparse on these systems. By comparison, the deep green roof live load increases to 100 psf across the entire roof area, because it is designed to support more frequent roof access by occupants.

Seismic design utilizes the equivalent lateral force method (ASCE, 2010). The special moment-resisting space frame system of these building has a response modification coefficient (R) of 8, indicating that stringent seismic capacity design and detailing requirements were met in accordance with ASCE 7-10. The control building has a design base shear of 193 kips resisted by each frame. The heavier load for the green roofs increases the lateral load, producing a design base shear of 212 and 258 kips for the shallow and deep green roof buildings, respectively. The retrofit green roof building is modeled with the same member sizes and ratios of reinforcement steel as the control building, because we assume that the additional roof mass is not accounted for in the original design. For each building, the size of columns and beams was assumed to be the same at each story, although reinforcement ratios varied (smaller areas of steel were placed in the exterior column lines for the control and retrofit buildings, and the shallow and deep green roof buildings have larger areas of reinforcement at upper stories to support the heavier roof masses). Key design variables are summarized in Figure 2.3. The member sizes and reinforcement ratios were designed to ensure that overstrength and ductility were as similar as possible between the different buildings.

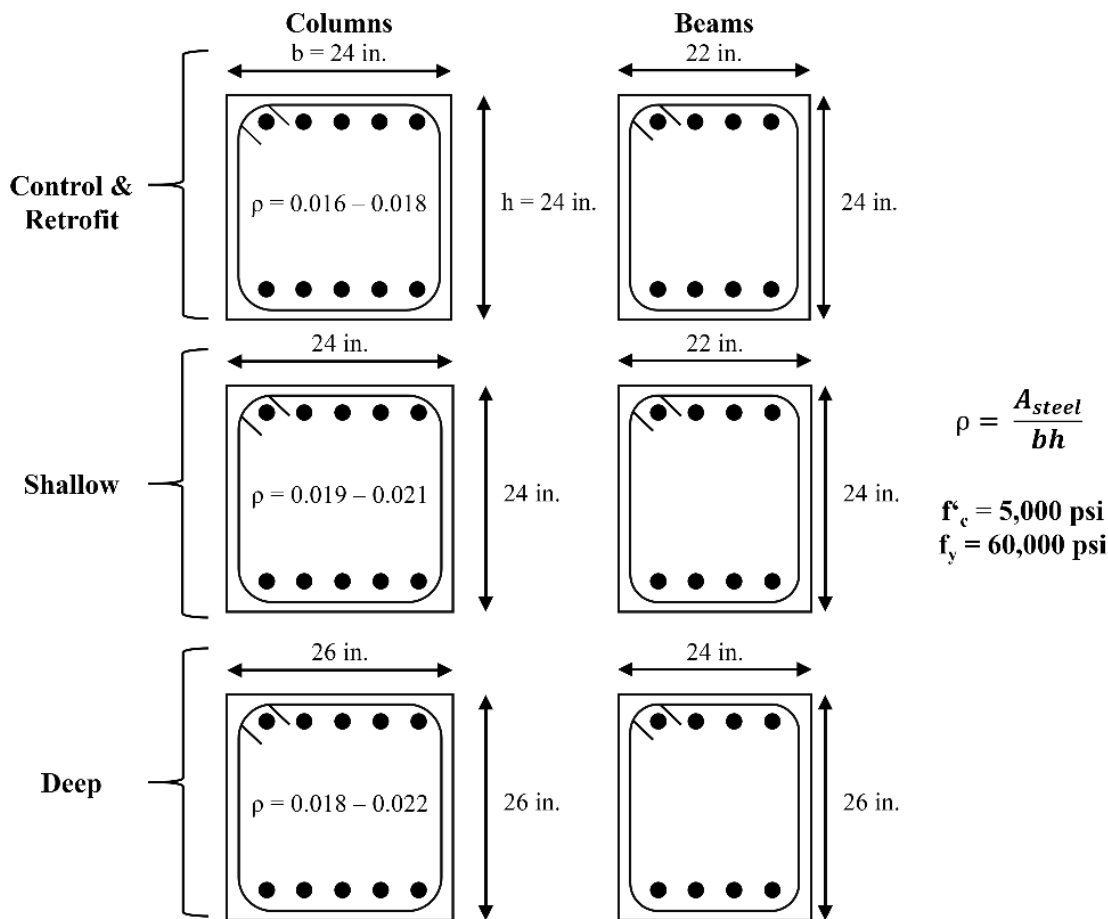


Figure 2.3 Column and beam designs for all four buildings (same size member dimensions at each floor for each building, but reinforcement ratios vary depending on member location in the building). Concrete and steel material strengths are the same for all buildings.

2.5 NONLINEAR MODELING AND ANALYSIS

2.5.1 GROUND MOTION SELECTION AND SCALING

The seismic response of each of the buildings is simulated using a multi-stripe dynamic analysis (MSA) procedure. In MSA, a structure is subjected to a set of ground motion records at each of several hazard levels, creating multiple observations of structural response at each hazard level (Jalayer & Cornell, 2009). For the purposes of this study, the MSA approach is considered superior to incremental dynamic analysis because MSA permits the selection of ground motions that more appropriately represent the expected spectral shape at each hazard level (Baker, 2015).

This study employs the conditional mean spectrum (CMS) method for selecting ground motion records. A CMS curve represents the expected response spectra shape, conditioned on

occurrence of a target spectral acceleration value at a period of interest for a particular site, corresponding to the hazard level of interest (Baker, 2011). Ground motion sets are selected to match (in terms of mean and standard deviation) the expected shape and amplitude of the CMS following a procedure defined by Lin, Harmsen, Baker, and Luco (2013). For this study, nine levels of seismic hazard, ranging from 50% in 50 years to 1% in 50 years, were chosen (see Table 2.1). Since the CMS changes shape at each ground motion intensity level, we selected a suite of twenty ground motions at each hazard level of analysis. The ground motion sets differ between buildings due to the different fundamental periods of each building model. Relatively small scale factors (between 0.4 and 1.9) were applied to ground motion records in this process.

Table 2.1 Hazard levels considered for Los Angeles site.

Hazard Level	Sa(T₁=1.00s) [g]	Return Period (years)
1	0.22	72 [50% in 50 years]
2	0.40	224
3	0.48	336
4	0.55	475
5	0.65	712
6	0.74	975
7	0.86	1,462
8	1.05	2,475
9	1.32	4,975 [1% in 50 years]

2.5.2 NONLINEAR BUILDING MODELS

The *OpenSEES* seismic analysis program (PEER, 2014) was used to conduct a non-linear analysis of two-dimensional, three-bay models of each of the four buildings. Beams and columns are modeled with elastic elements and concentrated hinge springs, *i.e.* a lumped plasticity approach. These hinges were assigned a material model developed by Ibarra, Medina, and Krawinkler (2005), which is capable of capturing the effect of strain softening at large deformations associated with concrete spalling and rebar buckling. The hinge model can also capture cyclic deterioration. The properties of the hinge are calibrated to experimental results of more than 250 concrete columns, such that modeling of different components represents differences in design and detailing. For dynamic analysis, the buildings were assumed to have 5% damping, using Rayleigh damping in the first and third modes and assigned only to the models' elastic elements. More details about the structural modeling approach are available in Haselton *et al.* (2008, 2011).

In the *OpenSEES* models, the green roof is considered only in terms of the added mass and its column, beam and reinforcement sizes. Recent experimental studies of green roof seismic

performance suggest that water content in the soil layer may provide greater damping during seismic excitation (Carmody, Jasarevic, Omenzetter, Clifton, & Fassman, 2009), but, to date, this effect is poorly quantified and we did not consider it here. Eigenvalue analysis was used to calculate the first-mode period of the building models, which varies between 1.24 and 1.35 sec. These values account for cracked section properties. Static pushover analysis results illustrate the as-modeled properties of the buildings in Figure 2.4, including ductility capacity and overstrength (defined as the ratio of peak strength from pushover to design base shear). Table 2.2 presents the overstrength ratio and fundamental period of each building.

The retrofit green roof building was not intended to carry the heavier load of the shallow green roof, which gives this building the lowest maximum base shear and overstrength values. The building follows a similar ductility trend to the control building, however, and experiences a loss of strength at a roof drift ratio of about 5%. The designs for the shallow and deep green roof buildings aimed to achieve the same ductility and overstrength of the control building as closely as possible. The control model and the deep and shallow green roof models show similar trends in ductility, although the deep and shallow green roof models experience a slightly earlier loss of lateral load capacity at a roof drift ratio of around 4% due to the more significant P-Delta effects. Despite this, the shallow and deep green roof buildings exhibit greater overstrength due to the larger gravity loads dominating the design.

Table 2.2 Pushover results for case study buildings.

Building	Overstrength Ratio	Fundamental Period (T_1), [sec]
<i>Control</i>	1.64	1.24
<i>Shallow green roof</i>	1.74	1.31
<i>Deep green roof</i>	1.85	1.35
<i>Retrofit green roof</i>	1.49	1.33

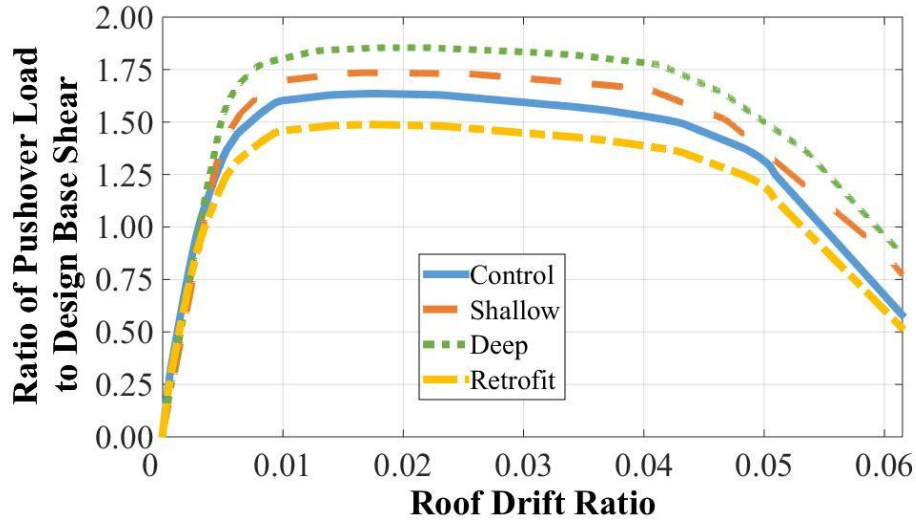


Figure 2.4 Results of static pushover analysis for all buildings.

2.5.3 DYNAMIC ANALYSIS RESULTS

Following the design and preliminary static analysis of the buildings, the framework moves into the *analysis* stage, beginning with a dynamic structural analysis. The four non-linear building models were analyzed under 20 different ground motion records at each of the nine levels of seismic intensity. The results of the analysis are compared at each intensity level in terms of interstory drift ratios (IDR), maximum floor accelerations and collapse fragilities.

As shown in Figure 2.5, all four buildings experience higher IDR and floor acceleration values at increasing levels of shaking intensity, with similar results (across all four buildings) at the lower levels of shaking. At the two highest levels of ground shaking, however, the IDR results were greatest for the shallow and retrofit green roof buildings, due to the extra mass at the top of the building, which impacted the response in the nonlinear range. Similar trends were observed for the maximum floor accelerations: at all but the highest intensity levels, the three green roof buildings have maximum floor accelerations similar to those of the control building. Although the shallow green roof building has a stronger gravity and lateral system compared to the retrofit building, at a shaking intensity of $Sa(T_1=1.00s)$ of 1.05 and 1.32 g, the retrofit building actually showed slightly lower interstory drifts and floor accelerations than the shallow green roof, likely due to relative differences in mass and stiffness and the related non-linear effects.

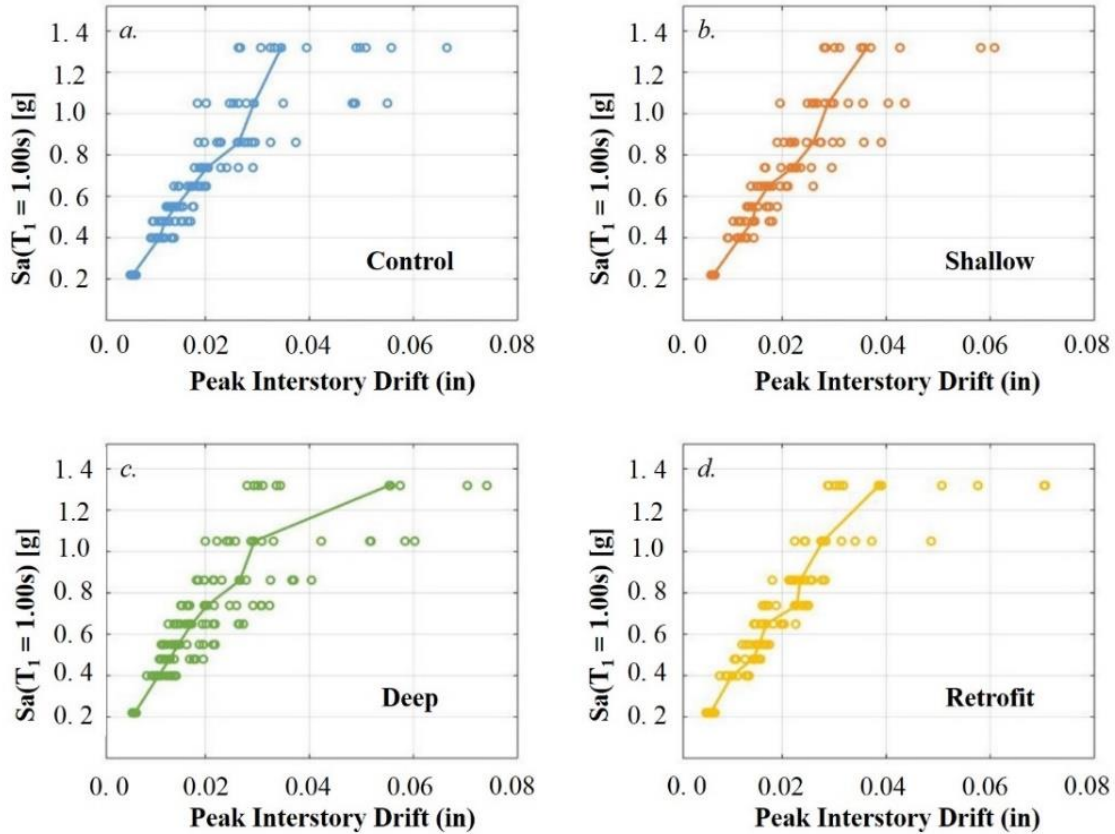


Figure 2.5 Peak IDRs as a function of ground motion intensity for (a) control building, (b) shallow green roof building, (c) deep green roof building and (d) retrofit green roof building (showing only non-collapse results in all cases).

Collapse fragility curves, which show collapse probability as a function of ground motion intensity, are provided in Figure 2.6. The median collapse capacity of all four buildings is similar, ranging from 1.1 to 1.25 g. However, the retrofit model experienced the greatest instances of collapse, while the deep roof building had the fewest instances of collapse. The difference in collapse risk between all four buildings is greatest at higher levels of excitation. At low levels of excitation, the shallow green roof building has a lower collapse probability than the retrofit green roof building, but this performance is reversed at higher levels of shaking, where the shallow green roof building demonstrates a slightly higher probability of collapse.

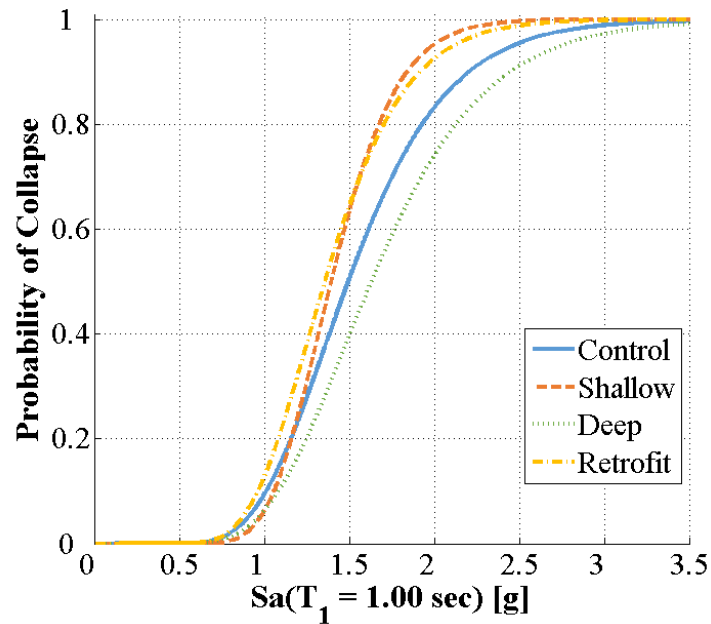


Figure 2.6 Collapse fragility curves for all four buildings.

Overall, the MSA results demonstrate the complexities of adding green roofs to buildings. The “up-sizing” of structural members was required to support the heavier green roof systems. These buildings could have been designed without larger member sizes, but this would not have satisfied building code requirements for lateral force resistance. Conversely, the retrofit green roof building was not designed for the green roof, demonstrating a tradeoff between savings in operational energy and a potential loss of collapse capacity if additional structural support is not provided when a green roof is added after service life begins.

2.6 LOSS ANALYSIS

The next step in the analysis stage of the framework is loss analysis. Loss analysis refers to the probabilistic analysis of building performance in terms of damage and repair costs. This analysis considers the different possible damage states for structural and non-structural components, taking dynamic structural analysis results as input. In loss estimation, damage analysis for each building component is based on empirically built fragility curves that express the probability that a component is in or exceeds a specified damage state as a function of the engineering demands on a building. Engineering demand parameters (EDPs) include peak IDRs and peak floor accelerations, depending on to which response quantity a component is most sensitive (Mitrani-

Reiser et al., 2007). Each damage state for a specific type of component is associated with a specific repair action. The consequences of incurring this state are quantified in terms of repair costs and repair time (Porter et al., 2004).

The basis for our loss analysis approach comes from advancements in seismic performance and probabilistic loss estimation developed by the FEMA P-58 project (ATC, 2012a). The FEMA P-58 software, *Performance Assessment Calculation Tool* (PACT), incorporates building occupancy schedules, inventories of structural and non-structural components and results of structural dynamic analysis into predictions of seismic repairs and associated costs (ATC, 2012b). PACT takes an assembly-based approach, wherein total building repair costs and repair times are sums of losses associated with different building components (Porter, Kiremidjian, & LeGrue, 2001). Given our interest in forecasting building performance for a specific site and at specific hazard levels, we conducted an intensity-based assessment.

2.6.1 INPUTS TO LOSS ANALYSIS

Loss estimation requires data for structural and non-structural quantities at each floor. The structural components considered here are the following: beams, columns, concrete roof and concrete floor slabs. The non-structural components are the following: water piping and HVAC systems, gypsum wall partitions, raised access office flooring, suspended ceiling systems and concrete roof tiles (for the control building). The inventory of components within the building was calculated from typical quantities provided by PACT that depend on building occupancy type and gross building area. Previous studies suggest that repair costs after an earthquake are dominated by damage to the structural framing system, interior partition walls and interior paint (Goulet et al., 2007), making it particularly important to estimate accurately the quantity of and possible damage to these components.

At present, the PACT fragility library does not contain damage information for any green building features, including green roofs. We created user-defined components for the shallow and deep green roofs based on the limited body of experimental data pertaining to the seismic response of green roofs. Carmody *et al.* (2009) used a shaking table to test green roof scale models with and without plants under varying levels of excitation. This study quantified the peak roof acceleration that led to detrimental soil displacement, for different fundamental periods of hypothetical buildings. For the purposes of this study, the data for the Carmody *et al.* (2009) roof without plants

are assumed to represent the response of a shallow green roof, while that study's data for the roof with plants represent the response of a deep green roof. These data were used to create fragility functions following recommendations from Porter, Kennedy, and Bachman (2007) and produced median detrimental roof accelerations of 0.59 and 0.78 g and dispersions of 0.39 and 0.40 for the shallow and green roof systems, respectively, as shown in Figure 2.7

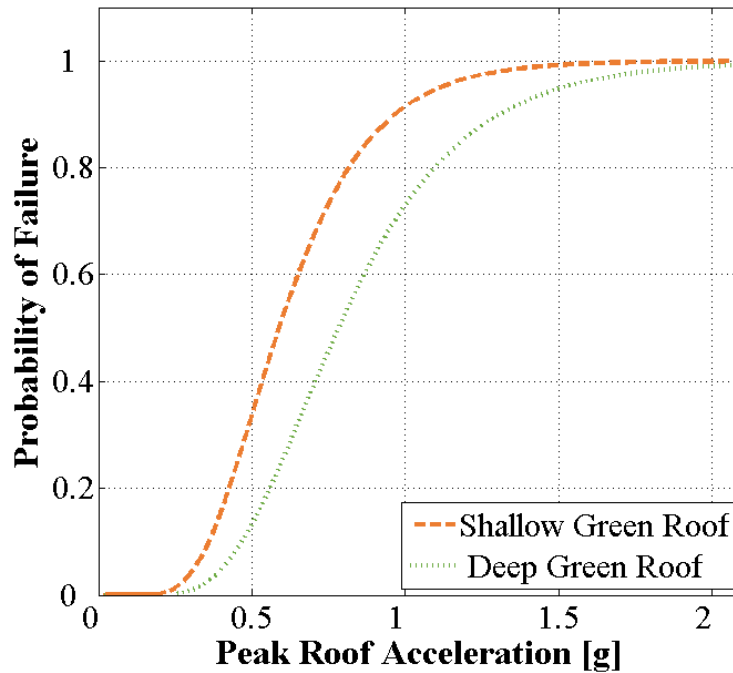


Figure 2.7 Fragility functions developed for shallow and deep green roof systems (based on data from Carmody et al. 2009).

The user-defined green roof fragility function in PACT was completed by defining repair costs for damage to green roof components, based on industry standard minimum and maximum repair costs per square foot. The fragility functions are based on economies of scale. Repairs for roof areas 100 ft² or less were assumed to cost \$12.50/ft² for the shallow roof system and \$19.90/ft² for the deep roof system. Repairs for roof areas greater than 600 ft² were assumed to cost \$10.30/ft² for the shallow roof system and \$16.20/ft² for the deep roof system (General Services Administration, 2011; Peck & Kuhn, 2003). The roof pavers around the green roof systems were represented in PACT by the existing component for unsecured clay roof tiles.

The estimated replacement cost for the buildings is \$12.5 million for the control building, \$12.75 million for the shallow green roof building and \$12.9 million for the deep green roof building. The replacement costs come from a study of the same four-story control building, which

used RS Means to estimate the construction costs (Ramirez et al., 2012). It is assumed that total collapse of a building would require the total replacement cost, equal to the capital cost.

2.6.2 REPAIR OUTCOMES AND BILL OF REQUIRED MATERIALS

PACT uses a Monte Carlo simulation procedure to estimate a lognormal distribution of possible repair outcomes at each of selected hazard levels. At each realization for each hazard level, PACT estimates the EDPs in the building from the structural analysis results, and then simulates the damage states $DS \in \{1, 2, 3, \dots, m\}$ experienced by a component, based on its fragility functions. Damage states in PACT are sequential, meaning that each subsequent damage state cannot be reached until the previous one has been exceeded. Some of the sequential damage states are also divided into mutually exclusive damage states, representing two or more distinct sub-states with different probabilities of occurrence, where only one state can exist at a time and each represents a distinct state of progressive damage. For example:

$$P(ME_{1,2}) = P(ME_{1,2}|S_2) * P(S_2) \quad \text{Equation 2-1}$$

quantifies the occurrence of the mutually exclusive damage state ($ME_{i,k}$), which is a subset of sequential damage state of $S \in \{1, 2, \dots, k\}$. Given a predicted damage state, PACT also reports the expected value of the repair cost for the component.

The

To calculate the material quantities needed for repairs of the damaged components, the first step is to determine the number of units of each component type damaged in each realization. This information is not directly provided in the PACT output. In this study, calculation of the number $C_{c,j} = TU_{c,j} * (UC_{c,i} * P_i + UC_{c,i+1} * P_{i+1} + \dots + UC_{c,n} * P_m)$ Equation 2-2, which states that, for each realization, j , the cost of repairing a given type of component, c , from PACT is equal to:

$$C_{c,j} = TU_{c,j} * (UC_{c,i} * P(i) + UC_{c,i+1} * P(i + 1) + \dots + UC_{c,n} * P(m)) \quad \text{Equation 2-2}$$

where $C_{c,j}$ is the expected total repair cost for component c . $TU_{c,j}$ is the total number of units damaged for component c , and m is the total number of damage states for this component. $UC_{c,i}$ is the unit cost for repairs at (DS_i), and $P(i)$ could be either $P(S_i)$ or $P(ME_i)$, depending on the $C_{c,j} = TU_{c,j} * (UC_{c,i} * P_i + UC_{c,i+1} * P_{i+1} + \dots + UC_{c,n} * P_m)$ Equation 2-2 can be

rearranged to calculate total number of damaged units, $TU_{c,j}$, for component type c , as well as the number of units within each damage state, based on the repair cost, probabilities of the different damage states and mean unit costs.

This process is illustrated in Figure 2.8(a) with damage to the curtain walls in the shallow green roof building. The first sequential curtain wall damage state (DS_1) describes how the glass will crack at a median story drift ratio of 0.021. The second damage state (DS_2) is more severe, involving glass falling from the curtain wall frame occurring at a median story drift ratio of 0.024. Following the trends of the structural analysis, the curtain walls move into more severe damage states with larger floor displacements. The Monte Carlo simulation enables probabilistic representation of the results, as in Figure 2.8(b) which shows box plots (25th, 50th and 75th percentiles) of the number of damaged curtain walls as a function of the hazard level. As for most components, the lower hazard levels have larger coefficients of variation. Similar results are observed for all component types.

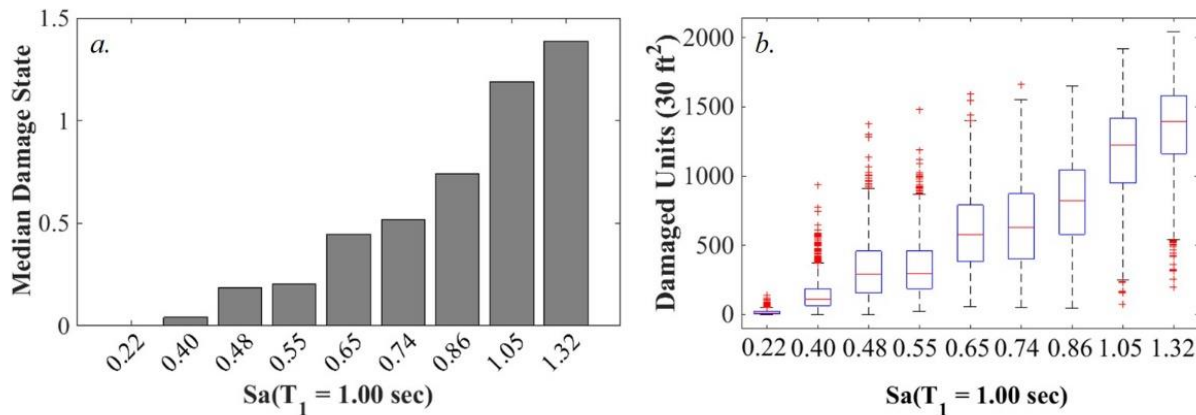


Figure 2.8 Damage to curtain wall units for shallow green roof building over all realizations at each hazard level, showing (a) median damage state and (b) box plot of number of damaged units (25th, 50th and 75th percentiles).

PACT also lists qualitative descriptions of repairs for each damage state of each component. We used these descriptions along with industry data sheets for non-structural components and architectural drawings provided in *Building Construction Illustrated* (Ching, 2014) to convert the qualitative repair actions into numerical material quantities. Table 2.3 provides example calculations for the exterior curtain walls. The PACT repair description suggests that the curtain wall damage for DS_1 is light enough to warrant only replacement of the glass, while

DS₂ requires new glass, as well as plywood to cover the area during replacement (ATC, 2012a). Therefore, repairs for a single 30 ft² unit (the PACT normative unit for this component) of curtain wall were converted into material volumes of 2,610 in³ of glass (assuming double glazed window thickness of 0.5 in, from standard industry specifications) for DS₁ and the same volume of glass plus a volume of plywood equal to 1,080 in³ (assuming a thickness of 0.25 in) for DS₂.

Table 2.3 Example calculation of material quantities needed for repair actions for curtain wall units.

Damage State Description	Repair Action Description	Required Material quantities per Damaged 30ft² unit (in³)
DS 1: Glass cracking	Replace glass	Glass = 2,160
DS 2: Glass falls from frame	Replace glass; cover exposure in meantime	Glass = 2,160 Plywood = 1,080

The total volume of required materials to repair the curtain walls at each hazard level for the shallow green roof building is shown in Figure 2.9. The results show how damage at the lower hazard levels mainly involves repair of the glass, but damage at higher hazard levels also requires plywood, to cover damaged openings during more intensive repairs. Similar repair descriptions were translated into material quantities at each damage state for each component. Material quantities for repair came from combining repair costs and multi-state damage probabilities from PACT with the estimated repair action quantities. We then multiplied the estimated damaged unit quantities for each damage state in each realization by the material quantities required to repair damaged units of a given component. The total number of materials—such as concrete, rebar and grout for the beam–column components—for a single realization of one hazard level is the sum of materials for repair of a given component.

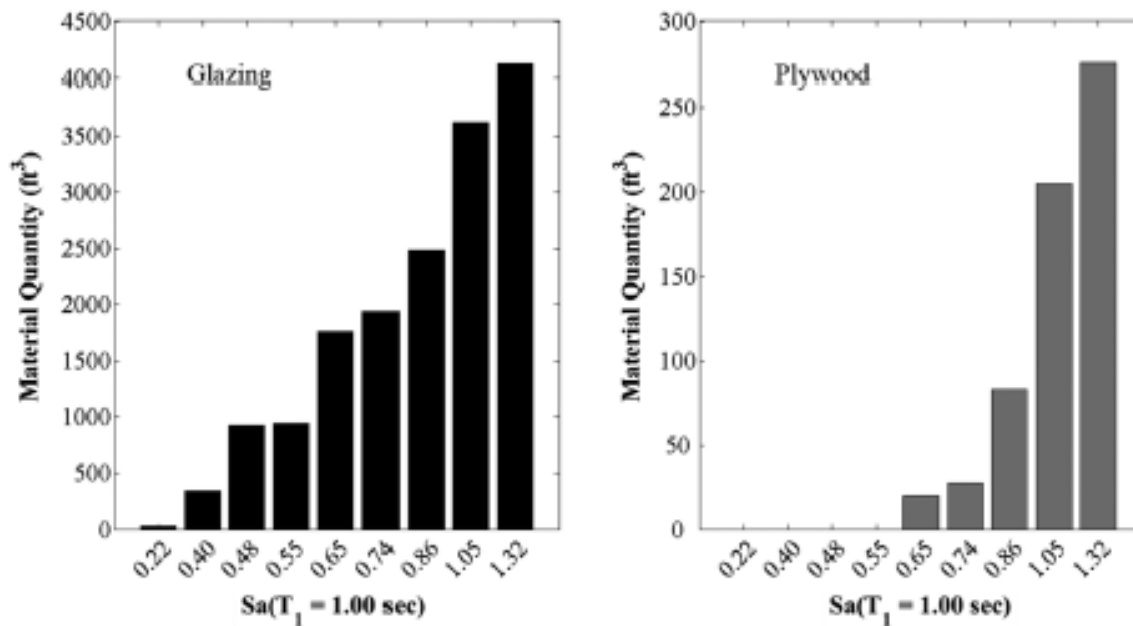


Figure 2.9 Median material quantities needed for curtain wall repair for shallow green roof building (including collapse cases).

The median repair costs presented in Table 2.4 are the sum of all component repair and replacements costs for each building at each hazard level. At the lower hazard levels, the damage is concentrated in the non-structural curtain walls and interior wall partitions, while the beams, columns and floor slabs dominate the losses at higher hazard levels. The retrofit green roof building has higher potential median losses than the other three buildings. Similarly, while the shallow and deep green roof building have fewer losses at less intense hazard losses, they incur greater potential losses than the control building at hazard levels of 1.05 and 1.32 g.

Table 2.4 Median repair costs for total building post-earthquake losses from Monte Carlo simulation of all potential component repair and building replacement costs.

Hazard Levels	Median Total (Collapse + Non-Collapse) Building Repair Costs			
	Control	Shallow Green Roof	Deep Green Roof	Retrofit Green Roof
1	\$ 702,00	\$ 680,000	\$ 571,000	\$ 901,000
2	\$ 1,984,00	\$ 1,484,000	\$ 1,434,000	\$ 2,429,000
3	\$ 2,403,000	\$ 2,402,000	\$ 2,055,000	\$ 3,434,000
4	\$ 2,724,000	\$ 2,531,000	\$ 2,669,000	\$ 4,116,000
5	\$ 3,392,000	\$ 3,533,000	\$ 3,005,000	\$ 4,775,000
6	\$ 4,108,000	\$ 3,807,000	\$ 3,842,000	\$ 5,623,000
7	\$ 4,838,000	\$ 4,535,000	\$ 4,352,000	\$ 6,818,000
8	\$ 5,596,000	\$ 6,126,000	\$ 6,387,000	\$ 7,788,000
9	\$ 6,146,000	\$ 7,163,000	\$ 7,858,000	\$ 9,105,000

2.7 ENVIRONMENTAL IMPACT ANALYSIS

2.7.1 LIFE CYCLE BOUNDARY AND SCOPE

Following structural and loss analysis, the framework enters the final analysis stage, environmental analysis. LCA, in general, begins with definition of the functional unit for comparison, the system boundaries and the impact methodology (ISO IEC, 2006). In our case, the functional units (Ciroth & Srocka, 2008) for comparison are the four buildings. This definition introduces a series of challenges due to the inherent complexity of buildings, compared with a simpler product such as a plastic cup (Vieira & Horvath, 2008). Here, the functional unit of each building is broken into separate structural and non-structural components, providing the basis for the assessment of the total material quantities associated with manufacturing or repair of these components.

The study takes a “cradle-to-gate” approach in which building performance is compared in terms of the impacts produced by the extraction and manufacturing of new products and the operating energy, but not routine maintenance activities or end-of-life disposal. The system boundary was determined by identifying those life cycle stages that differ between the buildings. In the product manufacturing stage, the impacts of only structural members (beams, columns and floor slabs) and roofing systems are considered, since the structural, but not the non-structural, design varies between the buildings. Previous studies (M. M. Bilec, Ries, & Matthews, 2010; Junnila & Horvath, 2003) have demonstrated that environmental impacts from a building’s construction stage, *i.e.* impacts associated with on-site erection of the building, are minimal compared with manufacturing and production of raw materials or annual operating energy of a building. As such, construction impacts are not considered.

The impact of the transportation stage for initial construction and post-earthquake repair activity depends on the distance of manufacturing plants to the building site, and the weight and volume of material being transported. The impact of transportation emissions also depends on the type of freight vehicles, because larger vehicles (Class 6) used to transport materials such as steel and concrete typically have more stringent emissions standards than smaller vehicles (Class 4), which would be used to transport materials such as the green roof soil (EIA, 2016). Transport effects are not considered in the current study.

The operating energy of the buildings is presented in order to quantify the differences between the green roof and non-green roof buildings in this context. The midlife addition of a green roof system on the fourth building requires creation of an additional life cycle stage, entitled midlife roof retrofits, which accounts for only impacts from the manufacturing and production of materials for the new green roof system. In this stage, we assume that the shallow green roof was added five years after initial construction and that the computed impact from this stage comes only from manufacturing the additional materials needed to build the roof.

The final stage included in the system boundary is post-hazard repairs. Based on the loss analysis results, this stage considers the impact from the most heavily damaged building components: the structural members, wall partitions, exterior curtain walls, suspended ceiling tiles and green roof systems. The raised access flooring, water piping systems and HVAC system units are excluded, because the loss analysis suggested that most damage for these components could be repaired by manual labor (*i.e.* no material inputs required). Discussion of end-of-life building disposal is out of the scope of this study, because we chose to focus on in-service building performance, not differences between material disposal options and impacts.

2.7.2 ENVIRONMENTAL IMPACT ASSESSMENT METHODS

The environmental impact of a functional unit and its subcomponents comes from analysis of life cycle inventory (LCI) data. Process-based LCI describes the main flows of energy and materials in and out (e.g. emissions) of the functional unit (EPA, 2008). Multiple databases estimate energy/material flows, as well as their associated emissions to land, water and soil (Cook, 2014; Simion et al., 2013). Here, inventory data were gathered using Ecoinvent, because it is a well-established and comprehensive source, with over 10,000 different processes for analysis (Goedkoop, Oele, Leijting, Ponsioen, & Meijer, 2013). Ecoinvent is a database that provides life cycle inventories for all economic activities at a unit process level (Weidema et al., 2013).

We allocated the impact of the inventory processes using the EPA's *Tool for the Reduction and Assessment of Chemical and other Environmental Impacts* (TRACI). The TRACI methodology transforms a selected process activity into potential impacts associated with raw material production, as well as associated chemical releases (EPA, 2008). While the LCI presents the raw emissions of each process, the TRACI methodology is needed to quantify how these

emissions combine together into environmental impacts, such as fossil fuel depletion or eutrophication, which are more typically presented as LCA results.

We used the process-based life cycle software SimaPro (Goedkoop et al., 2013) to organize environmental impact calculations for all building materials. Product manufacturing impacts were determined based on unit impacts for the amount of concrete, reinforcing steel and roof materials needed for the initial production of building components. In the post-hazard repairs phase, calculations began with collection of the material quantities for earthquake-related repairs; here, we use these material quantities as inputs for the environmental impact analysis. Table 2.5 shows an example of manufacturing environmental impacts, for 1 ft³ each of curtain wall glazing and plywood in the post-hazard repair stage. The table presents results for all ten different SimaPro environmental impact categories. The remainder of this study focuses on only the impact from carbon dioxide (CO₂) equivalents at the life cycle stages of interest. Carbon dioxide equivalents compare emissions from different greenhouse gases with respect to their contribution to climate change. Embodied carbon is considered here as the total amount of greenhouse gas emissions, converted to CO₂ equivalents, required to produce a given material or building product (Werner & Burns, 2012). We refer throughout this study to the embodied carbon from manufacturing products or the CO₂ emissions from operating energy consumption and demand as climate change potential (CCP), considered in terms of tons of CO₂ equivalents.

For each realization of each hazard level, we multiplied the unit environmental impacts by the respective material quantities needed to conduct repairs. The final output for each building was a lognormal distribution of the environmental impacts over the 1,000 realizations of each hazard level. For realizations causing building collapse, it is assumed that all of the components need to be replaced, which therefore considers the environmental impact from restoring the building to full functionality for the remainder of its service life.

Table 2.5 Allocation unit environmental impacts for curtain wall repair materials.

Impact	Units	Glazing (per 1 ft ³)	Plywood (per 1 ft ³)
Ozone Depletion	ton CFC-11 eq.	1.57E-10	2.71E-09
Carbon Dioxide Emissions	ton CO ₂ eq.	1.14E-03	1.98E-02
Smog	ton O ₃ eq.	1.03E-04	2.01E-03
Acidification	ton SO ₂ eq.	9.89E-06	1.64E-04
Eutrophication	ton N eq.	2.81E-06	1.04E-04
Carcinogenics	CTUh	1.66E-10	9.21E-10
Non-Carcinogenics	CTUh	2.64E-10	1.20E-08
Fine Particle Emissions	ton PM _{2.5} eq.	9.36E-07	4.31E-05
Ecotoxicity	CTUe	1.12E-02	0.197
Fossil Fuel Depletion	kWh surplus	13.42	310.77

2.7.3 ENERGY USE ASSUMPTIONS

The energy portfolio impacts from electricity and natural gas production for building operation and the expected annual operating energy at our site are determined from assumptions drawn from survey data compiled by the California Energy Commission (CEC). In Los Angeles, the typical energy supply mix is 33% from coal, 21% from natural gas, 13% from wind power, 10% from nuclear power, 5% from biomass and natural waste, 6% from hydroelectric plants and 12% from other energy sources (Itron, 2006).

Controlling for state-wide differences in climate, the CEC survey suggests that a typical mid-sized commercial building consumes annually 17.72 kWh/ft² in electrical energy and 21.80 kBtu/ft² in natural gas (Itron, 2006). From these data, we assume that the control building would consume 1.53 million kWh/year and 1.88 million kBtu/year. The potential operating energy reduction from the green roof buildings is based on the LEEDv4 new building + construction prerequisite for minimum energy performance (USGBC, 2015). One suggested path in LEED to meet this goal is to follow ASHRAE design guides for advanced energy savings (ASHRAE, 2014). The shallow green roof building was assumed to meet ASHRAE 30% energy reduction standards for mid-sized commercial buildings, consuming 1 million kWh/year and 1.23 million kBtu/year. The deep green roof building, representing design changes for 50% annual energy savings, is assumed to use 765,000 kWh/year and 941,700 kBtu/year goals that would be reasonable to achieve with the chosen green roof systems. Here, the authors choose not to account for future changes in energy efficiency or green building technologies.

2.7.4 ENVIRONMENTAL IMPACT RESULTS

First, the LCA results at a building component level for the damaged curtain walls are presented. Figure 2.10 illustrates how the impacts of earthquake damage influence the climate change potential, or CCP, (in terms of CO₂ equivalents) for curtain walls in the shallow green roof building. The results show, at all hazard levels, that the impacts of the glass replacement in the curtain wall dominate the overall component environmental impact. At higher hazard levels, where the second, more extensive, damage state is more likely to occur, the use of plywood in repair activities contributes more to climate change potential impact than at lower hazard levels.

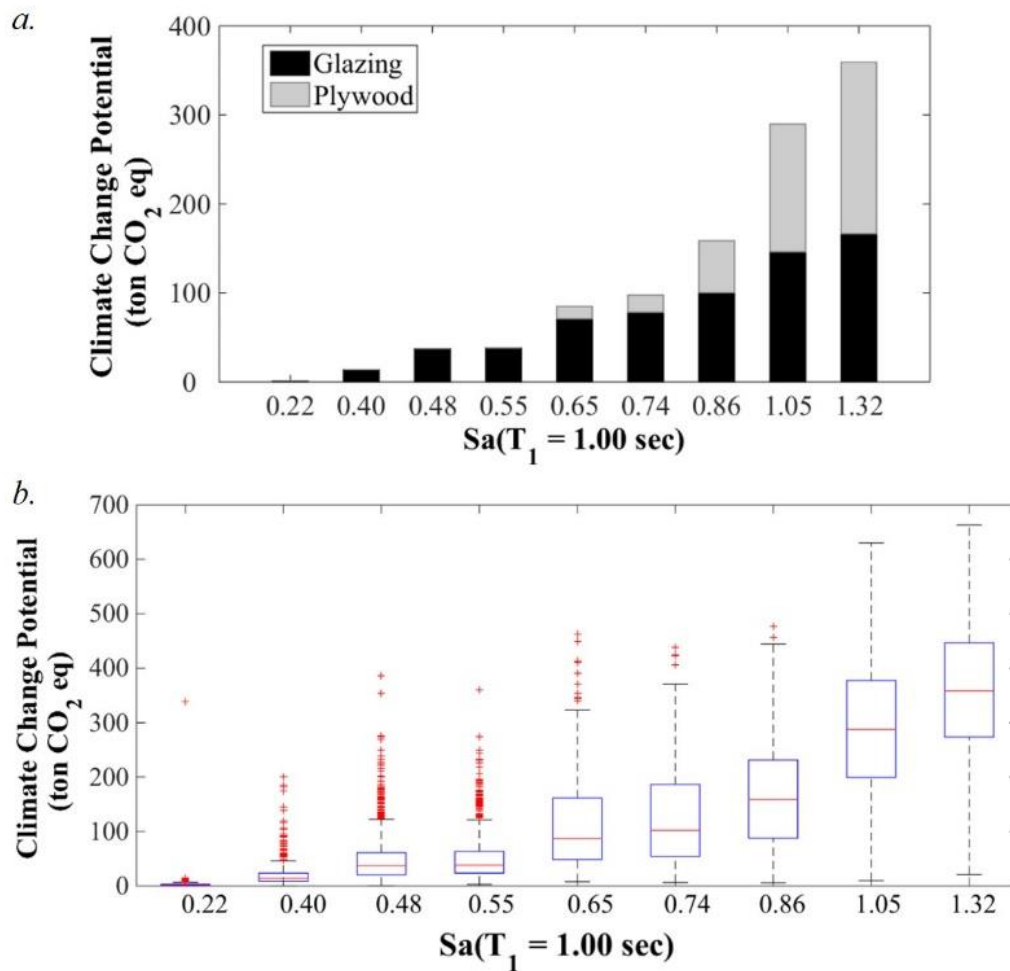


Figure 2.10 Tons of CO₂ emissions or equivalent associated with post-earthquake repairs of curtain walls in the shallow green roof building: (a) deaggregated by material requirement and (b) showing uncertainty in the estimate (box plot with 25th, 50th, and 75th percentiles).

To study the uncertainty of the results, we also computed the median, 25th percentile, 75th percentile and coefficient of variation (COV) for the total number of units damaged and the total environmental impact of each component. For all components, we saw relatively small COV values, almost all less than 1, at lower hazard levels. However, in some cases, at higher hazard levels, the CO₂ emissions COV value for the curtain walls was larger than 2, indicating large uncertainties in the projected results. In this study, the computation of uncertainty considered variability only in the damaged components and material quantities, not in sources of uncertainty from the emissions data, so the true uncertainties are likely substantially higher.

Subsequently, the combined life cycle environmental impacts for all four buildings are compared. Figure 2.11(a)–(c) presents the CO₂ emissions for each building, in terms of the life cycle phases of greatest interest: product manufacturing, operating energy and post-hazard repairs. (The results of the roof retrofit stage are not shown because its impact is minimal compared to the other stages and occurs only for the retrofit green roof building.) We can draw relative comparisons between each of the three life cycle stages presented. For all four buildings, the life cycle impacts are dominated by the operating energy, because the results are shown over the total 50-year lifespan (without any discounting). Among all buildings, the shallow and deep green roof buildings have the highest manufacturing impact for raw materials, due to the larger volumes of concrete and reinforcing steel for the initial construction of the beams, columns and floor slabs required to support the extra green roof loads under gravity and seismic load cases. Therefore, a decision-making tradeoff appears with respect to the upfront environmental impact of the green roof building and the significantly lower annual operating energy impacts.

The impacts of post-hazard repairs assume that at most one earthquake occurs sometime during the building's service life, after addition of the retrofit green roof. Note that the results below are presented in lognormal space, due to the challenge of comparing the scale of the impacts between the lower intensity shaking and higher intensity shaking levels. At all hazard levels, the median impacts are largest for the retrofit building impacts.

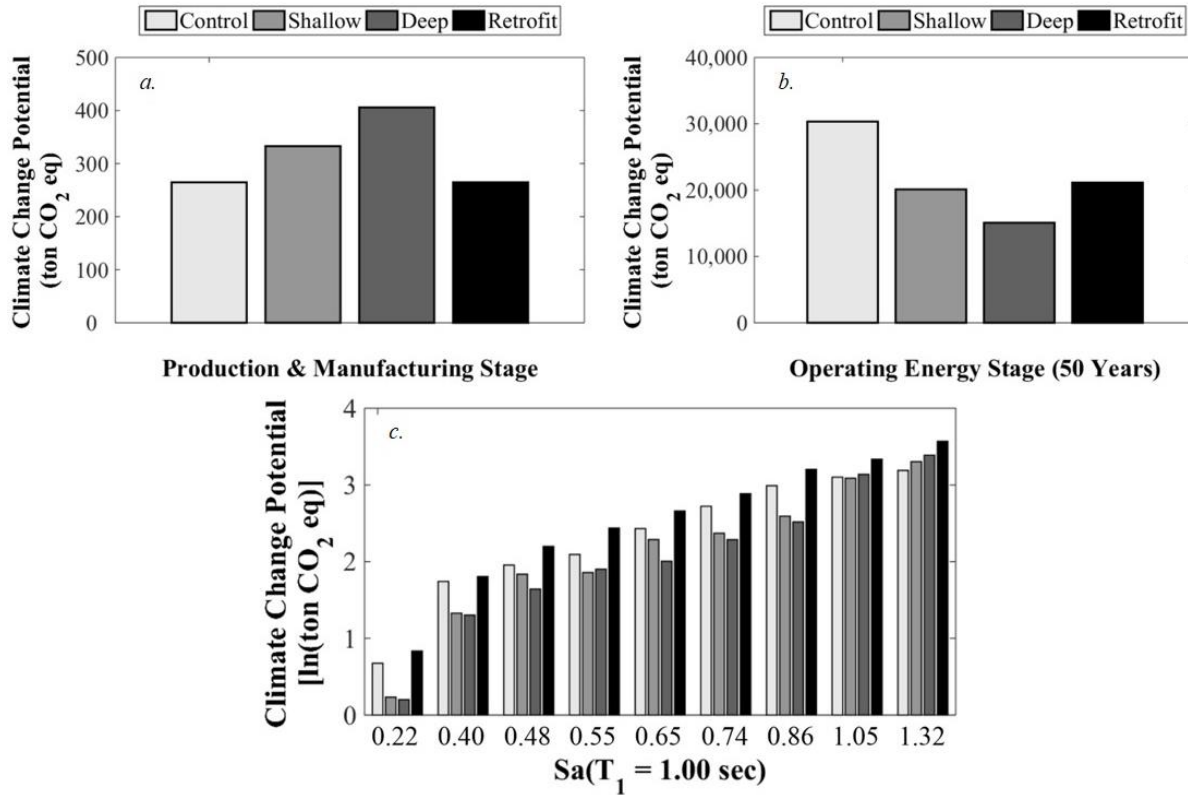


Figure 2.11 Climate change potential (CO₂ eq.) from life cycle stage of: (a) product manufacturing, (b) operating energy and (c) post-hazard repair (mean log values from lognormal distribution) for all four buildings after each of the nine ground shaking intensity scenarios.

If ground shaking with an intensity ranging from $Sa(T_1=1.00s) = 0.2-0.86$ g was to occur, the control building produces the second largest possible CO₂ emissions. Nonetheless, at the highest level of shaking, the non-linear effects and lower seismic performance of the green roof buildings result in much higher environmental impact from post-hazard repairs. For example, at a hazard level of 0.74 g, both the shallow and deep green roof buildings have almost 20% lower CO₂ repair emissions than they produce from repairs at the highest level of shaking. The values presented in Figure 2.11(c) are median values, but we note that the uncertainty and variability in the results increase with greater level of shaking. However, similar trends between buildings are observed in the other percentiles.

At low levels of ground shaking, the results suggest positive tradeoffs between the upfront material choices for the green roof buildings: these buildings provide both lower annual operating energy demand, costs and emissions and fewer post-earthquake losses and environmental impacts. Although the control and retrofit green roof buildings have lower upfront material production

impacts, they trade this low upfront impact for greater operating energy impacts and higher earthquake losses. The retrofit green roof building in particular demonstrates a decision-making dilemma, in that the building can achieve a midlife reduction in operating energy with the addition of the green roof, but the building would perform relatively poorly during any significant seismic event. Design decisions must weigh the costly investments in green design practices, which may not benefit hazard performance in high consequence, low probability events, but may provide smaller annual operating benefits over the total lifespan of a building.

These tradeoffs are demonstrated through an environmental impact exceedance curve, by presenting the results in terms of a fragility function for CCP (CO₂ eq.) at varying hazard levels. Figure 2.12 presents the CCP fragility function for the probability that post-earthquake repair actions for four buildings exceed 100 tons of CO₂ equivalents based on the analysis conducted here (without fitting to a probability distribution).

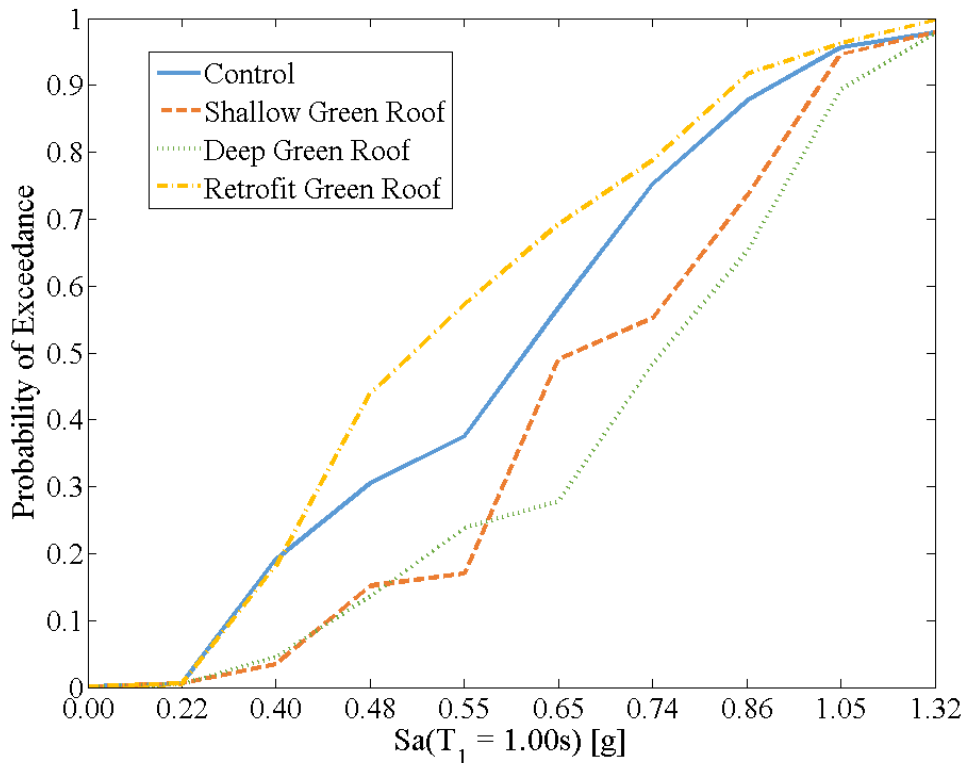


Figure 2.12 Environmental impact exceedance curve (representing CO₂ emissions fragility function) for exceedance of 100 tons of CO₂ during post-earthquake repairs.

2.8 LIMITATIONS

This study has several limitations. First, there exists a significant challenge in comparing environmental and economic impacts at different points in time. Discounting could have been used to place all impacts in the same temporal boundary, but this introduces an ethical debate with respect to selection of appropriate discounting factors (Vieira & Horvath, 2008). Due to the social and ethical complexities of discounting environmental impacts, we chose to exclude discounting for all results and instead deaggregated the impacts in the different stages.

Second, the environmental impact from temporary and permanent irrigation of the green roof systems, as well as changes in storm water management, was excluded from the scope. Inclusion of this component in the analysis would better quantify the benefits of the green building for comparison with the other buildings. Third, additional experimental studies are needed to better represent the response of green roof systems under seismic excitation. More broadly, as many communities seek to “build green” while facing a simultaneous risk of major hazard events, greater experimental testing and computational modeling are needed to study the behavior of green building features under extreme hazard events.

Finally, the specific building-to-building findings presented in this paper may not necessarily be generalized across all building configurations and uses. However, the results provide valuable relative metrics of performance for evaluating the tradeoffs associated with green roof buildings in high seismic areas. Refinements in the procedures may alter some of the specific quantitative values, but not the relative positions of the comparison between buildings. In addition, the case study serves to illustrate the green-resilience framework, providing a novel tool that can be employed for various building types, locations and types of hazards.

2.9 CONCLUSIONS

This paper presents a new framework for the joint assessment of building environmental impact and hazard performance, in the context of green building design choices and earthquake hazard risk. The framework is illustrated through an examination of the seismic performance of office buildings with green roofs with different characteristics, examined through non-linear dynamic analysis and assembly-based loss analysis and environmental impact assessment.

The findings of this study demonstrate key tradeoffs between design choices for green building objectives and performance goals for post-hazard functionality, which are summarized in

Table 2.6 and Figure 2.13. The results of each building's performance in six different arenas, collapse capacity, construction cost, post-hazard cost, construction CCP, post-hazard CCP and operating energy CCP, are normalized against the values for the control building. The results presented here are for a ground shaking intensity of $Sa(T_1=1.00s) = 0.86$ g, but similar plots can be made for each hazard level.

The results from these buildings illustrate the challenging tradeoffs presented for building design decision-makers, as each building offers varying economic, environmental and hazard performance strengths and weaknesses. Although the control building performs moderately well under low probability, high-intensity earthquake events, in terms of post-earthquake economic losses and environmental impact from repair activities, these strengths are counterbalanced by the building's relatively worse performance under high probability, low-intensity earthquake events and its large annual operating energy consumption.

Conversely, all three of the green roof buildings offer significant environmental benefits during the life cycle of a building, provided an earthquake does not occur. This is a scenario under which green buildings, and especially those with green roof systems, are normally considered. The results of our case study, however, suggest that significant environmental impact may result from repair actions due to low probability, high-intensity earthquakes, making the green roof buildings, in effect, less "green" than their control counterpart when considering post-hazard repairs. In addition, the green roof buildings come with additional material expenditures due to the larger beam and column sizes required to support the more massive roofs under gravity and seismic loads.

Table 2.6 Strengths and weaknesses identified during life cycle assessment of building design tradeoffs for environmental impact and hazard performance.

Building	Strengths	Weaknesses
Control	-Lower up-front environmental impact from structural design than Shallow and Deep green roof buildings -Lower collapse risk in rare earthquake events than Green Roof buildings	-Worse performance under frequent earthquake events than Shallow and Deep green roof buildings
Shallow Green Roof	-Lower annual operating energy than control building -Stormwater management/heat island mitigation -Lower environmental impact at high frequency earthquake events than Control and Retrofit buildings	-Larger upfront environmental impact from structural materials than Control building -Worse performance in rare earthquake events (potential for significant economic losses and environmental impact) than Control
Deep Green Roof	-Lowest annual operating energy than Control building -Added occupant comfort from access to green roof -Lower environmental impact at high frequency earthquake events than Control and Retrofit buildings	-Worse performance in rare earthquakes (potential for significant economic losses and environmental impact) than Control
Retrofit Green Roof	-Lower up-front environmental impact than Shallow and Deep Green roof buildings -Mid-life reduction in operating energy	-Larger potential economic and material losses and environmental impact at all levels of earthquake hazard than Control

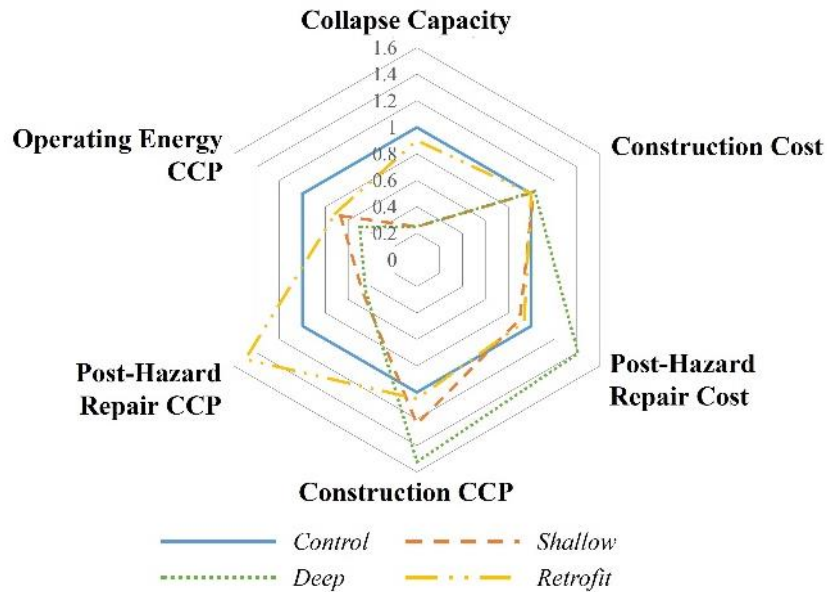


Figure 2.13 Radar plot showing tradeoffs in building performance (where repairs are considered at a ground shaking intensity of $Sa(T_1=1.00\text{ s}) = 0.86\text{ g}$) and environmental impact is considered in terms of climate change potential (referred to as CCP and in terms of CO_2 equivalents).

The framework presented in this paper advances the science of building design and assessment, through an integrated, multi-criteria life cycle assessment procedure for buildings that includes green building design decision-making. The 21st-century building stock faces the challenge and opportunity of a growing number of green buildings, coupled with greater vulnerability to extreme earthquake events from expanding populations and dense urban environments. In order to support urban development objectives for both sustainability and resilience, the proposed framework encourages decision-makers to assess the environmental impacts and hazard resistance of their buildings in tandem, rather than as isolated considerations.

Chapter 3 and Chapter 4 explore other design decisions that contribute to economic and environmental tradeoffs associated with green-resilient building design, expanding the applicability and utility of the framework developed in this chapter.

Chapter 3 IS HAZARD RESILIENCE SUSTAINABLE? EVALUATING MULTI-OBJECTIVE OUTCOMES FROM ENHANCED SEISMIC DESIGN DECISIONS²

3.1 INTRODUCTION

A recent paradigm shift in the structural engineering community recognizes that to design for resilience is to design sustainably. Buildings account for roughly 40% of energy use and 35% of total carbon dioxide (CO₂) emissions in the U.S. (CEC, 2008). As a result, advances in green building design offer the potential to significantly reduce resource and energy usage, and associated environmental impacts. At the same time, resilient design principles have emerged from performance-based engineering, linking building design to desired performance outcomes. Performance-based design seeks to reduce hazard-induced (*e.g.* earthquake) building damage and other consequences (Porter, 2003).

Seeking to connect resilient and sustainable design concepts, recent studies have proposed that “green” buildings should be designed for higher levels of seismic and other extreme loads, in order to reduce environmental impacts associated with post-hazard repairs (Chiu *et al.*, 2013; PCA, 2012; Wei, *et al.*, 2016a; Wei, *et al.*, 2016b). A growing body of work explores the relationship between building design features (*e.g.* steel vs. concrete, construction costs), structural response and damage (*e.g.* story drifts, structural losses), and post-earthquake environmental impacts for various building types and life cycle analysis boundary scopes (*e.g.* Arroyo *et al.*, 2015; Bocchini *et al.*, 2014; Feese *et al.*, 2014; Hossain & Gencturk, 2014; Sarkisian *et al.*, 2011). Other studies have examined how design strength and ductility capacity impact the economic component of seismic losses (*e.g.* Anagnos *et al.*, 2016; Goulet *et al.*, 2007; Haselton *et al.*, 2011; Ryan *et al.*, 2009). However, no studies have systematically quantified the environmental impacts associated

²Adapted from Welsh-Huggins, S. J., & Liel, A.B. (2017). Is hazard resilience sustainable? Evaluating multi-objective outcomes from enhanced seismic design decisions. *Journal of Structure Engineering*, currently under review.

with enhanced seismic design.

This study quantifies and identifies life cycle tradeoffs relating environmental impact and enhanced seismic designs for 30 reinforced concrete (RC) buildings with varying base shear strengths and period-based ductility capacities. Quantifying the embodied carbon—*i.e.* greenhouse gas emissions released by building manufacturing, construction and post-earthquake repairs—associated with these design decisions elucidates life cycle implications for the natural environment and human health from changes in seismic design practice. The study’s primary aim is to investigate whether enhancing seismic design is a meaningful tool to achieve jointly “greener” and more resilient buildings.

3.2 BACKGROUND

Joint quantification of building hazard resistance and environmental impacts is a still-growing field of research and practice, but a number of frameworks have been suggested to evaluate building life cycle impacts for this purpose (*e.g.* Court, *et al.*, 2012; Padgett & Li, 2016; Rodriguez-Nikl, 2015; Welsh-Huggins & Liel, 2016). These frameworks offer similar approaches, adding a “post-hazard” stage to the traditional building life cycle (construction, operation, demolition, etc.) to quantify extra lifetime environmental impacts from hazard-induced repair/replacement actions.

Previous studies have examined the influence of specific building design decisions on building construction and post-earthquake repair impacts by quantifying CO₂ emissions and economic losses. For example, Hossain & Gencturk (2014) conducted Pareto optimization to minimize member size and reinforcement ratios for two RC buildings, under specific design constraints, one with low initial cost and greater design story drifts, and the other with higher upfront cost and lower drifts. They found that larger seismic losses from the low-cost building incurred much higher environmental impacts than the more expensive building. However, the study also suggested that the overall life cycle environmental impact of the low-cost building was 40% lower than that of the high-cost building due to lower material volumes used in construction and removed during end-of-life disposal. Wei *et al.* (2016) evaluated tradeoffs between environmental, social, and economic costs associated with seismic losses in a cost-benefit analysis of retrofits to an existing building. The study computed a combined present value of losses by monetizing post-hazard carbon emissions and fatalities. Results showed that the retrofit design

with the lowest cost and lowest hazard resistance offered the highest present value benefit. Likewise, Welsh-Huggins and Liel (2016) indirectly considered the influence of member size and design strength on environmental and seismic performance, analyzing members that were “up-sized” to support green roof systems. That study showed that the buildings with larger roof loads (and hence higher member sizes) experienced more seismic damage during intense shaking, but better withstood low-to-moderate shaking. Damaged buildings with higher roof loads were associated with greater post-hazard CO₂ emissions, due to larger material volumes needed for repair/replacement of larger structural members.

Other studies have investigated how design strength and ductility capacity can impact building performance in terms of economic losses, but not environmental impacts. Ramirez *et al.* (2012) quantified the economic seismic losses for the same buildings assessed in this study and found that enhanced lateral strength can reduce post-earthquake economic costs. That study, however, also suggested that enhanced ductility capacity can increase economic seismic losses for low to mid-rise buildings, due to greater damage to non-structural components and associated losses. Porter (2016) likewise argued against the prevailing idea to design resilient buildings to be more ductile, but weaker. To the contrary, he suggested that a stronger building is more cost-effective for building owners, based on the results of a San Francisco earthquake scenario. Davis and Porter (2016) further suggested that buildings with greater ductility capacity experience larger permanent structural deformations, which can lead to more costly repairs. Those studies pointed to a public desire for building functionality beyond provision of life-safety, which may not be achieved by a design focus solely on ductility.

3.3 CASE STUDY BUILDING DESIGNS

3.3.1 STRUCTURAL DESIGN

This study considers a range of structural configurations for special moment RC perimeter and space frames, divided into two design sets. The first set varies by design lateral strength (herein called the “strength design” set), while the second set varies by ductility capacity (the “ductility design” set). Ductility capacity is computed from pushover analysis (described below), following calculations similar to those employed elsewhere (ATC, 2012a). The ductility capacity is defined here as the ratio of post-capping deformation capacity (indicated by the roof drift ratio at which

20% of the lateral strength of the structure has been lost) to yield deformation capacity in terms of roof drift ratio. In all other aspects, each building is code-conforming (ACI, 2011; ASCE, 2010; ICC, 2009). Design parameters for both building sets are listed in Table 3.1.

The structural designs of the study's modern 4 and 12-story office buildings are adopted from Haselton *et al.* (2011). Each building has a 120 ft. by 180 ft. (36.6 m. by 54.9 m.) footprint. In each direction, the space frames have six lateral load-resisting RC frame lines, while the perimeter frames have two. Column dimensions are the same for interior and exterior space frame lines, while the perimeter frames use smaller square gravity columns at interior columns measuring 12.5 in. (0.32 m.). The first-story height of all buildings is 15 ft. (4.6 m.); all others are 13 ft. (4.0 m.); column spacing is 30 ft. (9.1 m.). The buildings are in Seismic Design Category D, based on a Los Angeles site location, with a design spectral acceleration for short periods of 1.0g and 0.6g at 1 s (ASCE, 2010). All buildings have 8 in. (20.3 cm.) concrete floor slabs.

For the strength design set, the response modification coefficient or “R factor”, an inverse modifier on design strength, is changed for each structure. U.S. design standards specify $R = 8$ for special RC moment frames (ASCE, 2010). The strength design set includes buildings weaker than code requirements ($R > 8$) and buildings that are stronger ($R < 8$). For the ductility design set, the design strong-column-weak-beam (SCWB) ratio is varied. For a special moment frame, ACI 318 requires that the sum of column moment strengths at each joint exceed 1.2 times the sum of beam strengths (ACI, 2011). This provision promotes distribution of inelastic structural response over multiple stories, enhancing deformation capacity of the structure (Moehle, *et al.*, 2008). Here, we consider design SCWB ratios ranging from 0.4 to 3.0. Design for above-codes seismic parameters (lower R or higher SCWB ratios) requires larger member sizes and more reinforcing steel. Certain building designs (indicated in Table 3.1) require greater concrete compressive strengths to satisfy target strengths or ductility capacities.

The 4-story buildings results are the primary focus of this paper. Examples of the 12-story results are described briefly in each section to illustrate the effect of building height on the results.

3.3.2 ARCHITECTURAL DESIGN

The inventory of non-structural building components are based on typical office buildings quantities provided by the SP3 loss estimation software (Haselton Baker Risk Group, 2016). These

quantities vary depending on building occupancy type and gross building area. The non-structural components considered here are: staircases; exterior glazed curtain walls; exterior concrete cladding; interior wall partitions; suspended ceiling tiles; carpeted floor tiles; concrete roof tiles; HVAC ducts; hot and cold water pipes; sanitary waste pipes; and fire sprinkler systems. The quantities and distribution of non-structural components are the same for buildings of the same height such that only structural member dimensions and quantities vary between building designs.

3.3.3 EMBODIED CARBON ASSOCIATED WITH UPFRONT CONSTRUCTION

Life cycle analysis (LCA) quantifies potential economic and environmental impacts of a material, product, or system over a given period of time (Hendrickson et al., 1998). In this study, we assess life cycle environmental impacts with respect to the amount of *embodied carbon* produced at different stages of the building lifespan. Embodied carbon is the total amount of greenhouse gas emissions, converted to CO₂ equivalents, required to produce a given material or building product (Hammond & Jones, 2008). CO₂ equivalents account for the contribution of various greenhouse gas emissions to climate change. We estimate the main input and output flows of energy/materials (*e.g.* emissions) through a process-based life cycle analysis of each functional unit of analysis (EPA, 2008), *i.e.* each study building. We use the *SimaPro* software to organize life cycle inventory quantities from the Ecoinvent database to calculate building life cycle environmental impacts (Goedkoop, *et al.*, 2013). Next, the Tool for the Reduction and Assessment of Chemical and other Environmental Impacts (TRACI) is used to quantify resulting impacts from raw emissions associated with each inventory process (EPA, 2008).

The building life cycle stages assessed here are: 1) material manufacturing/production for upfront (pre-service life) building construction, and 2) material manufacturing for post-earthquake building repairs or replacement. The life cycle environmental impact analysis is conducted for only the upfront and post-hazard material manufacturing because environmental impacts from other stages, *e.g.* on-site construction activities or building operations/routine maintenance actions, are assumed equal for each building, regardless of the structural design. Material transportation to the construction site could produce variations in building life cycle impacts, depending on the type of vehicle used or volume of structural materials transported, but quantification of these impacts is beyond the scope of the current study. Quantification of demolition/debris removal impacts is also excluded, as is consideration of sources of uncertainty in emissions inventory data.

Upfront embodied carbon for a building is computed from the embodied carbon associated with material manufacturing of all structural and non-structural building components. The upfront embodied carbon of the non-structural members is the same for all buildings of the same height, but the structural member contribution to embodied carbon depends on the member sizes, quantity of steel reinforcing, and required concrete compressive strength. Higher concrete strength requires greater quantities of Portland cement, which increases concrete's unit embodied carbon impact. This effect is accounted for here with a multiplier on the embodied carbon impact of normal strength concrete (5,000 psi), based on calculations by Hammond and Jones (2006, 2008).

Table 3.1 presents the upfront embodied carbon for all 30 buildings in this study. Consistent with Guggemos and Horvath (2005), we find that production of structural materials releases higher levels of greenhouse gas and other emissions than production of non-structural component materials. Figure 3.1(a) shows how upfront embodied carbon varies with lateral strength, such that stronger buildings are associated with greater upfront embodied carbon. Levels of embodied carbon do not correlate linearly with enhanced lateral strength due to other design requirements (gravity loads, drift limits *etc.*) that also impact member sizes, especially at lower lateral load levels. In Figure 3.1(b) the below-code ductility design buildings have similar levels of upfront embodied carbon. Changes in design SCWB and ductility capacity are associated with redistribution of material from columns to beams without adding much extra material. However, Figure 3.1(b) also demonstrates a notable increase in embodied carbon for buildings with above-code ductility capacities, due to associated increases in member size and steel required to achieve SCWB ratios greater than 2.0.

3.4 NONLINEAR MODELING AND DYNAMIC ANALYSIS

3.4.1 NONLINEAR STRUCTURAL MODELING

Two-dimensional, three-bay models of the study buildings were built in the *OpenSEES* seismic analysis program (PEER, 2014). Beam-columns are modeled with elastic elements and concentrated hinge springs, *i.e.* a lumped plasticity approach. These hinges have been assigned a material model capable of capturing concrete spalling and rebar buckling effects at large deformations (Ibarra, *et al.*, 2005). The hinge model also captures cyclic deterioration and accounts for bond-slip. The hinge properties have been calibrated to experimental results of over 250

concrete columns, such that modeling of different components represents differences in design and detailing (Haselton, Liel, Taylor-Lange, & Deierlein, 2016). The models also capture P-Δ effects. The perimeter frame models do not consider the strength and stiffness of the interior (gravity) framing. Rayleigh damping of 5% is applied to the models’ first and third modes and assigned only to elastic elements. Haselton and Deierlein (2007) and Haselton *et al.* (2011) provide further details about the structural modeling approach.

Nonlinear static pushover analysis of the buildings verifies that the models exhibit the desired changes in base shear strength and ductility capacity. Figure 3.2(a) presents the pushover results for the 4-story strength design space frames, showing that greater design loads increases the base shear capacity, while ductility capacity remains similar. Increasing the SCWB ratio enhances ductility capacity, as well as base shear strength, as shown in Figure 3.2(b). Although not shown, the trends are similar for the perimeter frames and 12-story buildings.

Table 3.1 presents the fundamental period, ultimate base shear strength, and ductility capacity for all buildings. The larger member sizes of the stronger, more ductile designs leads to decreased fundamental periods. Overstrength (the ratio of ultimate to design lateral strength) ranges from 1.6 to 4.3 for the 4-story buildings and from 1.6 to 3.2 for the 12-story buildings. The weaker buildings have higher overstrengths due to gravity loads and other design considerations.

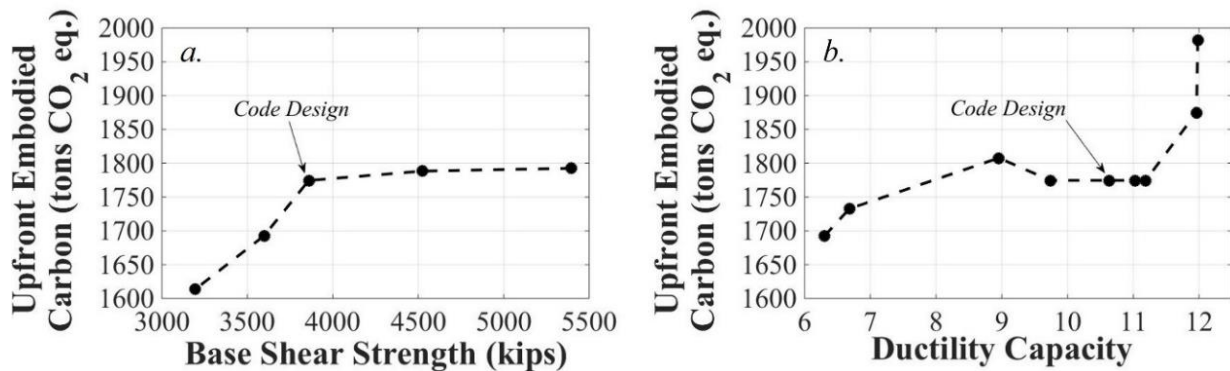


Figure 3.1 Influence of seismic design on upfront embodied carbon showing a) effect of ultimate base shear strength on embodied carbon for 4-story strength design space frames and b) effect of ductility capacity on 4-story ductility design space frames. (1 kip. = 4,448 N.; 1 ton = 987 kg.).

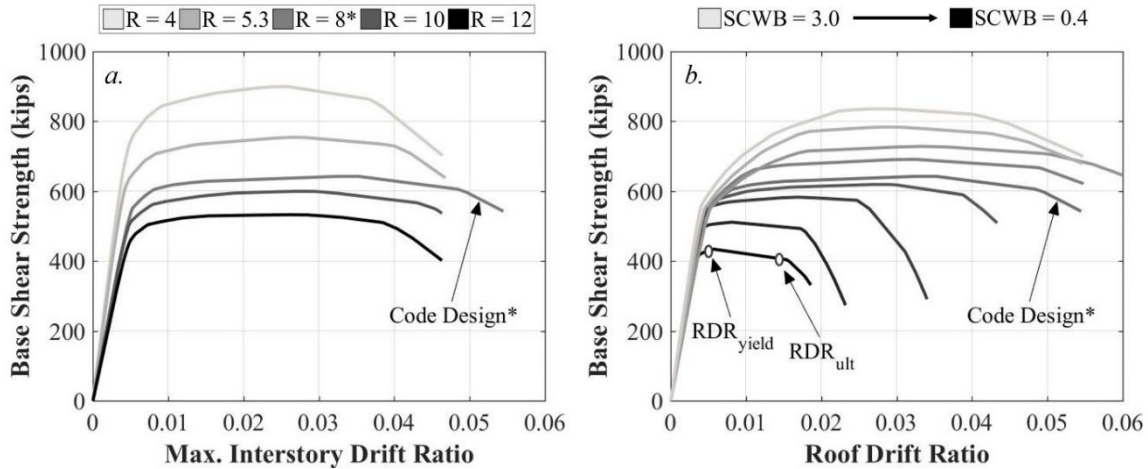


Figure 3.2. Nonlinear static pushover results (per frame line) for 4-story a) strength design space frames and b) ductility design space frames. (1 kip. = 4,448 N.). The labels RDR_{yield} and RDR_{ult} on Figure 3.2(b) demonstrate the points used to calculate the ductility capacity of a given building design. RDR_{yield} refers to the roof drift ratio at the maximum lateral strength capacity achieved by a building, while RDR_{ult} refers to the roof drift ratio at which 20% of the lateral strength has been lost for a design.

3.4.2 DYNAMIC ANALYSIS RESULTS

The seismic performance of the case study buildings is computed with Incremental Dynamic Analysis (IDA) (Vamvatsikos & Cornell, 2002). In IDA, the building model is subjected to recorded ground motion acceleration time histories. At first, records are scaled to a small value of the spectral acceleration at a building’s fundamental period, $Sa(T_1)$, and then structural response is analyzed at increasing scale factors, until collapse is observed. Collapse is defined as occurring when story drifts greater than 12% are recorded at any story, following Haselton *et al.* (2011). The IDA uses a set of thirty strong ground motions recorded from California earthquake, with magnitudes between 6.5-6.9, and at firm sites with site-to-source distances ranging from 15-33 km (Vamvatsikos & Cornell, 2006). These records are representative of the type of crustal ground motions expected at the study site. The seismic hazard analysis for the LA site is obtained from USGS (Petersen *et al.*, 2008) for nine different ground shaking hazard levels, which range from 50% in 50 years, corresponding to an intensity of $Sa(T = 1s) = 0.25g$ (referred to here as Hazard Level 1, or HL 1) to 1% in 50 years (HL 9), associated with $Sa(T = 1s) = 1.25g$. In this study, HLs are defined solely in terms of the spectral acceleration intensity measure and ground motion selection for the study did not consider the influence of spectral shape. Previous analysis results of the same buildings for different ground motions are found in Haselton and Deierlein (2007) and Haselton *et al.* (2011).

The IDA results show that enhanced base shear strength and ductility capacity both increase median collapse capacity (quantified in Table 3.1 in terms of $S_a(T = 1s)$ for all buildings), compared to code-compliant or below-code designs. Strength designs for the 4 and 12-story perimeter frames and 12-story space frames are highly governed by lateral load demands, making their collapse capacities especially sensitive to design base shear changes. In addition, the below-code 12-story buildings experience damage localization in fewer stories, likely from increased P- Δ effects on weaker, more flexible structures (Haselton & Deierlein, 2007). The buildings designed for enhanced ductility capacity exhibit better collapse performance, as column hinging is prevented and lateral deformation is more evenly distributed along building height (Ramirez et al., 2012).

The IDA results confirm past studies' observations that even subtle design variable changes can strongly affect structural response. Due to the shorter periods of stronger and more ductile buildings, above-code structures dynamically experience larger floor accelerations and smaller story drifts than code-compliant or below-code designs. Perimeter frame design is lateral load-dominated, so base shear strength changes to these buildings have a larger influence on building stiffness and drift and acceleration demands.

3.5 SEISMIC LOSS ANALYSIS RESULTS

Probabilistic seismic loss analysis quantifies building performance under seismic loading in terms of building damage and associated seismic losses. The losses are referred to here as *economic costs* (dollar value of post-earthquake component repairs and building replacement) and *embodied carbon* (CO₂ equivalents released by post-earthquake material manufacturing for repairs and replacement of damaged components and structures).

3.5.1 ECONOMIC COSTS ASSOCIATED WITH SEISMIC LOSSES

The seismic loss analysis approach for quantifying post-earthquake economic costs follows the seismic performance and probabilistic loss-estimation procedures developed by the FEMA P-58 project (ATC, 2012a). Here, we have implemented these calculations with SP3, a web-based tool for organizing FEMA-58 loss calculations (Haselton Baker Risk Group, 2016). In this approach, fragility curves quantify the probability that a given structural or non-structural component is in or exceeds a specified damage state (DS) as a function of the engineering demands on a building, expressed as either peak floor accelerations or story drifts (ATC, 2012a, 2012b). Here, these losses

are computed conditioned on a particular hazard level, defined in terms of $Sa(T_I)$. Although the variability and magnitude of these losses may be influenced by the selected intensity measures, this analysis choice is not expected to change greatly the overall comparisons between the different building designs in this study.

The expected seismic loss, $E[SL|HL]$, at each hazard level (shown in $E[SL|HL = x_i] = [1 - P(C|HL = x_i)]E[SL|NC, HL = x_i] + P(C|HL = x_i)E[SL|C]$ Equation 3-1) is computed as the sum of expected non-collapse building repair costs and total building replacement cost in the case of collapse, considering the collapse probability at that hazard level (ATC, 2012a).

$$E[SL|HL = x_i] = [1 - P(C|HL = x_i)]E[SL|NC, HL = x_i] + P(C|HL = x_i)E[SL|C] \text{ Equation 3-1}$$

In $E[SL|HL = x_i] = [1 - P(C|HL = x_i)]E[SL|NC, HL = x_i] + P(C|HL = x_i)E[SL|C]$ Equation 3-1, $P(C|HL = x_i)$ is the probability of collapse at the hazard level (HL) of interest (x_i). $E[SL|NC, HL = x_i]$ is the sum of seismic losses associated with repairing all damaged structural and non-structural components in order to restore the building to its initial undamaged state. $E[SL|C]$ is the expected seismic loss (in this section, economic cost) associated with total building replacement resulting collapse. $E[SL|C]$ is assumed to be the same as the cost (or embodied carbon) of initial construction for each building based on typical construction economic costs tabulated by the Haselton Baker Risk Group (2016) and Ramirez *et al.* (2012) and reported in Table 3.1.

The loss analysis calculations incorporate several thousand Monte Carlo realizations of potential damage outcomes for each structural and non-structural building component at each hazard level. Each individual realization represents a different level of acceleration and drift, potential damage state entered by the component, and thus varying outcomes for expected non-collapse building repairs costs and total building replacement costs (ATC, 2012a). The number of Monte Carlo realizations varies between analysis of the 4-story and 12-story buildings due to increased computational expense from analyzing a greater number of stories in the taller buildings. For analysis of each building type, the number of Monte Carlo realizations is large enough to ensure that results are not sensitive to this choice.

Figure 3.3 shows the median post-earthquake economic costs at each hazard level. The trends presented here are consistent with general observations made in previous studies of the same buildings and other similar designs (Goulet *et al.*, 2007; Ramirez *et al.*, 2012). The strength design

buildings in Figure 3.3(a) illustrate a correlation between enhanced lateral strength and decreased economic costs at most hazard levels. In addition, enhanced lateral strength is also associated with greater percent contributions from non-structural losses due to decreased structural member damage and lower probabilities of collapse. Higher post-earthquake economic costs for stronger buildings at certain hazard levels (*e.g.* 12-story building results shown in Figure 3.3(b)) arise from the sensitivity of certain non-structural and structural components to story drifts and floor acceleration demands, which are sensitive to the buildings' fundamental period. This effect is discussed in more detail below.

Table 3.1 Design variables and seismic analysis outcomes for all 30 case study buildings.

Code Design Parameter	No. Stories/ Frame Type	Upfront Cost/ sq. ft (USD)	Upfront Embodied Carbon (tons CO ₂ eq.)	T ₁ (sec) ³	Base Shear Strength (kips) ⁴	Ductility Capacity ⁵	Median Collapse Capacity Sa(T = 1s) (g)	Post-EQ Economic Cost (Mil. USD) ⁶	Post-EQ Embodied Carbon (tons CO ₂ eq.) ⁷
R = 4	4P ¹	220	2083 *	0.54	5153	21.0	6.70	0.2%	1.6%
R = 8		220	1682 *	1.16	1845	12.5	1.14	7.1%	20.1%
R = 12		220	1439 *	1.15	1393	16.9	0.88	7.4%	22.8%
R = 4	4S ²	230	1793	0.74	5397	10.5	3.77	2.7%	9.6%
R = 5.3		230	1788	0.78	4526	12.6	3.10	6.1%	17.2%
R = 8		230	1775	0.86	3859	10.6	2.94	8.9%	26.1%
R = 10		230	1693	0.92	3597	10.2	2.31	10.6%	29.0%
R = 12		230	1614	0.97	3196	10.3	1.91	11.0%	30.5%
R = 4	12P	278	5007 **	1.50	2109	2.9	3.36	2.6%	6.2%
R = 8		278	4778 **	2.07	1260	11.9	3.40	4.0%	7.8%
R = 12		278	4500 **	2.93	662	4.6	2.82	8.0%	12.3%
R = 4	12S	291	5739 **	1.93	2409	11.2	2.72	3.2%	1.7%
R = 5.3		291	5728 **	2.11	1911	15.4	2.49	4.7%	7.3%
R = 8		291	5507	2.31	1572	12.9	1.62	5.1%	7.3%
R = 10		291	5318 **	2.38	1288	10.9	1.46	4.6%	6.5%
R = 12		291	5081 **	2.60	1237	10.2	1.19	5.8%	8.5%
SCWB = 3.0	4S	230	1982	0.77	5012	12.0	0.93	9.3%	28.0%
SCWB = 2.5		230	1875	0.82	4701	11.2	0.37	12.9%	36.2%
SCWB = 2.0		230	1775	0.88	4369	12.0	0.09	11.6%	30.4%
SCWB = 1.5		230	1775	0.88	4146	11.0	0.68	11.4%	28.1%
SCWB = 1.0		230	1775	0.86	3714	9.7	0.47	10.9%	24.9%
SCWB = 0.8		230	1693	0.86	3497	9.0	0.32	11.2%	25.5%
SCWB = 0.6		230	1808 *	0.88	3067	6.7	0.24	11.0%	23.1%
SCWB = 0.4		230	1733 *	0.88	2603	6.3	0.22	11.8%	25.0%
SCWB = 3.0	12P	278	5810 *	1.89	1283	22.5	0.71	0.9%	24.7%
SCWB = 2.5		278	5733 *	1.93	1260	20.1	0.60	2.7%	5.6%
SCWB = 2.0		278	5516 *	2.06	1258	13.9	0.46	3.6%	6.8%
SCWB = 1.5		278	5377	2.07	1191	13.1	0.41	3.8%	6.7%
SCWB = 0.9		278	5195 **	2.07	1273	11.9	0.32	27.8%	21.5%

* Entire building designed with concrete compressive strength (f_c) > 5,000 psi (34.5 MPa). ** Bottom stories designed with f_c > 5,000 psi.

¹ "P" denotes perimeter frame design. ² "S" denotes space frame design.

³ Period from eigenvalue analysis of simulation models, considering cracked section properties.

⁴ Ultimate base shear, for entire building, as determined by nonlinear static pushover analysis (1 kip = 4,448 N).

⁵ Period-based ductility capacity as determined by nonlinear static pushover analysis.

⁶ Total loss expected over 50 years, discounted at 3%, normalized by total building replacement cost.

⁷ Total loss expected over 50 years, discounted at 0%, normalized by total building replacement embodied carbon (1 ton = 987 kg.).

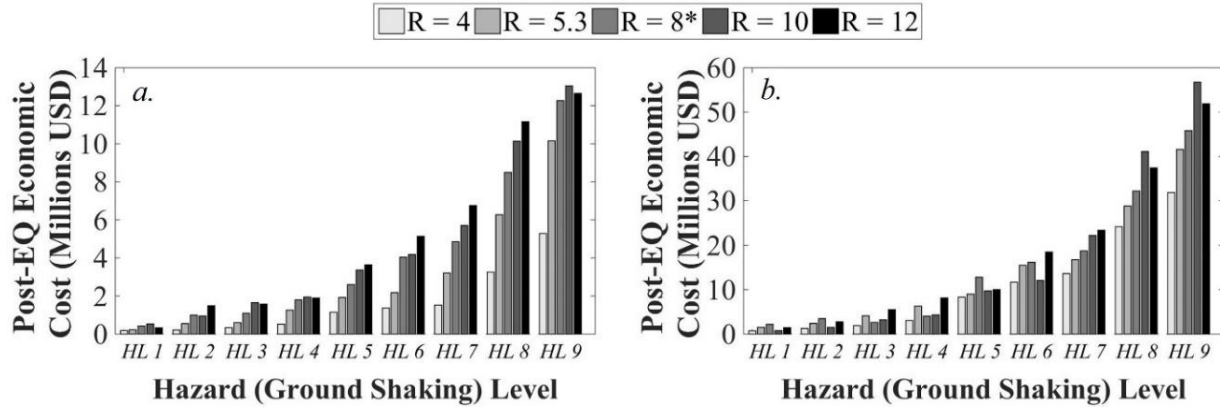


Figure 3.3. Median post-earthquake economic cost for strength design space frames for a) 4-story and b) 12-story buildings at each hazard level. (* denotes code-compliant designs).

Enhanced (above-code) ductility capacity, although improving collapse capacity, generally does not reduce economic seismic losses. For the above-code buildings, more even distribution of lateral deformation, due to greater ductility capacity, also increases the percent contribution and magnitude of non-structural losses. Figure 3.4 compares how the percent contribution to total post-earthquake economic cost from non-collapse and collapse seismic losses varies with ductility capacity. The more ductile building (e.g. SCWB = 2.5) has significantly lower collapse loss contributions than a below-code, less ductile building (e.g. SCWB = 0.6). The below-code building has lower total (collapse plus non-collapse) seismic economic losses at each hazard level, but much larger percent contribution from collapse. The selected 4-story buildings presented in Figure 3.4 are representative of the general trends observed for these buildings.

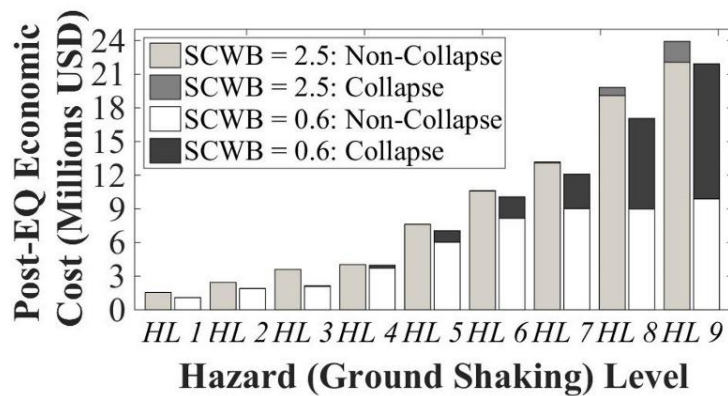


Figure 3.4. Post-earthquake economic costs deaggregated by non-collapse and collapse costs at each hazard level for selected 4-story above-code (SCWB = 2.5) and below-code (SCWB = 0.6) ductility design space frames.

We also quantify the expected annualized losses (EAL) for each building. EAL is calculated based on each hazard level’s frequency of exceedance and estimated loss (either dollar

or, below, CO₂ equivalents) following the analytical EAL solution described by Baker and Cornell (2003). This calculation is presented in Equation 3-2, where the expected annualized seismic loss considers the magnitude of losses at each hazard level, as well as the likelihood of each hazard level occurring:

$$EAL = \sum\{E[SL|HL = x_i] * \Delta\lambda_{HL}(x_i)\} \text{ Equation 3-2}$$

In this case, $E[SL/HL = x_i]$ is the expected seismic loss computed for a given hazard level x_i and $\Delta\lambda_{HL}(x_i)$ is a vector representing the mean frequency of exceedance for each hazard level.

Figure 3.5 presents the expected annualized economic costs for selected 4 and 12-story buildings. Increasing lateral strength decreases EAL, regardless of building height. Conversely, enhancing ductility capacity does not necessarily imply lower seismic loss in low- to mid-rise (*e.g.* 4-story) structures, because the distribution of lateral deformation throughout a greater number of building stories increases the magnitude of non-collapse (especially non-structural) losses in the entire structure. The 12-story ductility designs, however, reverse the trend of their 4-story counterparts, demonstrating lower post-earthquake economic costs with increasing ductility capacity, due to more localized damage in taller buildings.

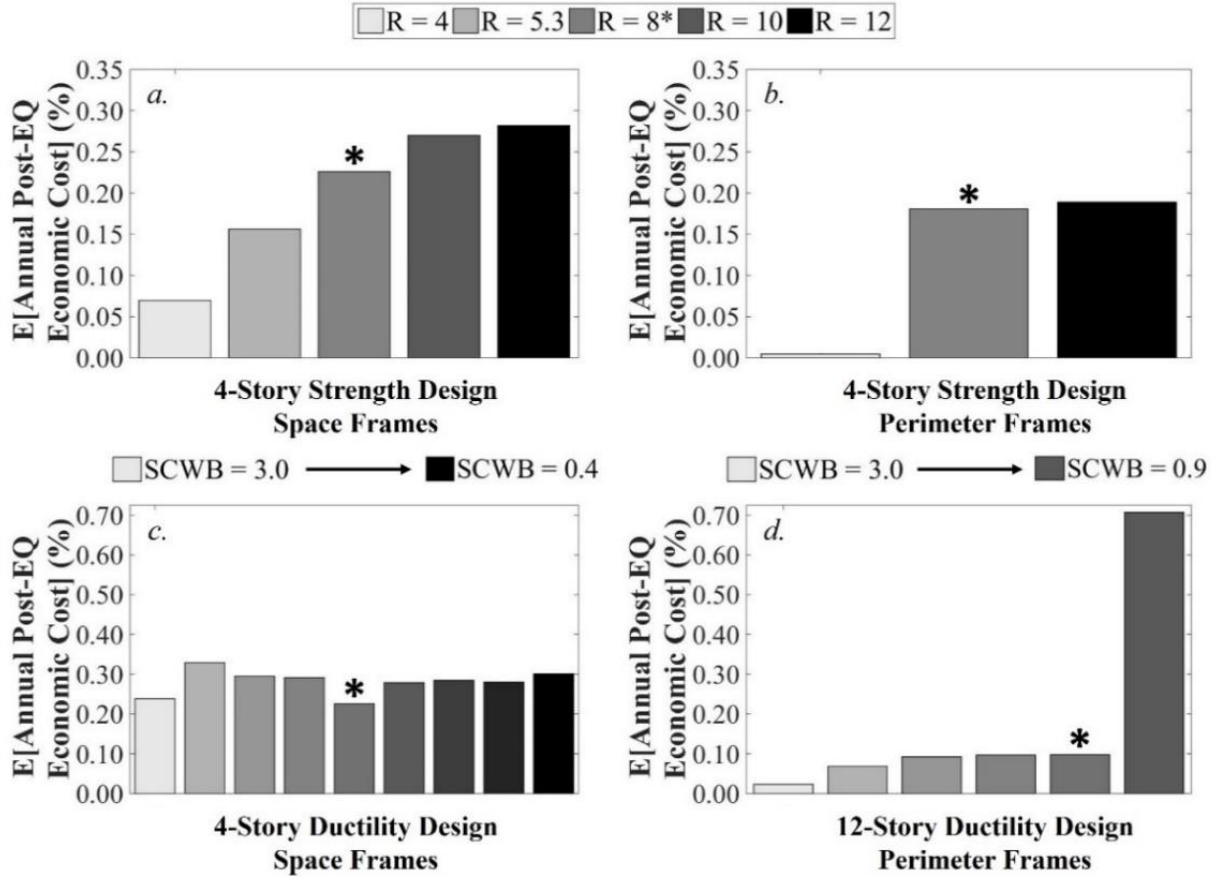


Figure 3.5. Expected annual post-earthquake economic cost for 4-story strength design a) space frames, b) perimeter frames, c) 4-story ductility design space frames, and d) 12-story ductility design perimeter frames. Losses are annuities and expressed as percentage of total building replacement cost. (* denotes code-compliant designs).

3.5.2 EMBODIED CARBON ASSOCIATED WITH SEISMIC LOSSES

Quantification of environmental impacts associated with seismic losses is a still-growing field of research. This study links seismic damage to the embodied carbon associated with manufacturing the materials required for potential post-earthquake building repairs. Previous work by the authors (Welsh-Huggins & Liel, 2016) details our approach for translating damaged component quantities into material volumes for specific repair actions at each hazard level. That study cataloged each non-structural and structural repair action recommended in FEMA P-58 (ATC, 2012b) by material needs and quantities, following typical construction practices described in Ching (2014). Thus, through this approach, at each Monte Carlo realization in the loss analysis, damage states and repair actions are identified for each component in the building, and then the embodied carbon impact from the required repair or replacement materials (e.g. structural steel, glass, etc.) is

computed (Welsh-Huggins & Liel, 2016). For collapse case, calculation of embodied carbon loss accounts for the lower total replacement embodied carbon quantities (from smaller structural members) of below-code (weaker or less ductile) buildings. We assume that building repairs and replacement will use the same materials/components as in the original construction (*i.e.* no post-hazard event upgrades). The result of these calculations for each building is a lognormal distribution of embodied carbon released by repair/replacement activities at each hazard level.

Figure 3.6 presents median post-earthquake embodied carbon at each hazard level for the 4-story strength designs, showing the same general trend as the economic seismic losses. Normalized embodied carbon (median post-earthquake embodied carbon at each hazard level divided by total replacement embodied carbon) is also lower for perimeter frames than for space frames, and lower for taller buildings than for their 4-story equivalents. Although not shown, 4-story ductility design trends in embodied carbon as a function of hazard level differ than those observed for economic losses. The greater magnitude of non-structural damage for more ductile buildings and lower replacement embodied carbon for less ductile buildings results in higher post-earthquake embodied carbon for above-code ductility designs.

The trends in post-earthquake embodied carbon losses also highlight the influence of fundamental period on structural response and on associated non-structural component response and damage, particularly for the structures designed to vary by lateral strength. The stronger, stiffer buildings, with lower fundamental periods, experience lower story drifts and higher peak floor accelerations than weaker designs. The response of stiffer buildings is associated with higher non-structural losses, because the fragility functions of most non-structural components are acceleration-sensitive (as seen in Figure 3.6(a)). The code-compliant space frame ($R = 8$) has a slightly higher collapse capacity than the weaker frames, but experiences higher floor accelerations. Therefore, at shaking intensities greater than 10% in 75 years (HL 6), non-collapse repairs for the code-compliant space frame produce more embodied carbon than below-code designs, due to a greater number of damaged non-structural components that also require more carbon-intensive repair actions or total component replacement, with only somewhat reduced collapse losses.

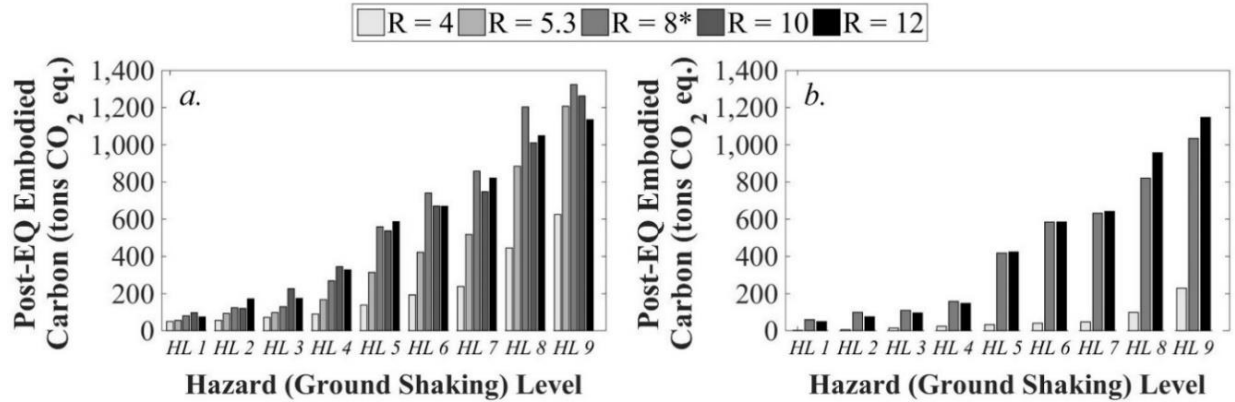


Figure 3.6. Median post-earthquake embodied carbon for 4-story strength design a) space frames and b) perimeter frames at each hazard level. (* denotes code-compliant designs. 1 ton = 987 kg.)

Figure 3.7(a) and (b) show that trends in annualized embodied carbon for all 4-story buildings generally follow the observations described above for hazard level loss, *i.e.* stronger buildings have *lower* annualized expected embodied carbon (63% lower than the code-compliant design in the case of the strongest space frame), while more ductile buildings mostly have *higher* expected annual embodied carbon (19% more than the code-level design for the most ductile design). Although not depicted in Figure 3.7, the results for the 12-story strength design buildings (presented in Table 3.1) follow the same trend as their 4-story counterparts. By comparison, the 12-story ductility design results, as shown in Table 3.1, demonstrate enhancing ductility capacity in taller buildings offers only a limited advantage for reduced post-earthquake embodied carbon. The above-code 12-story ductility designs reduce annual post-earthquake embodied carbon only at SCWB ratios below 3.0; above this SCWB ratio, the higher non-structural losses for this design result in a post-earthquake embodied carbon impact greater than 3.5 times that of the code-compliant design.

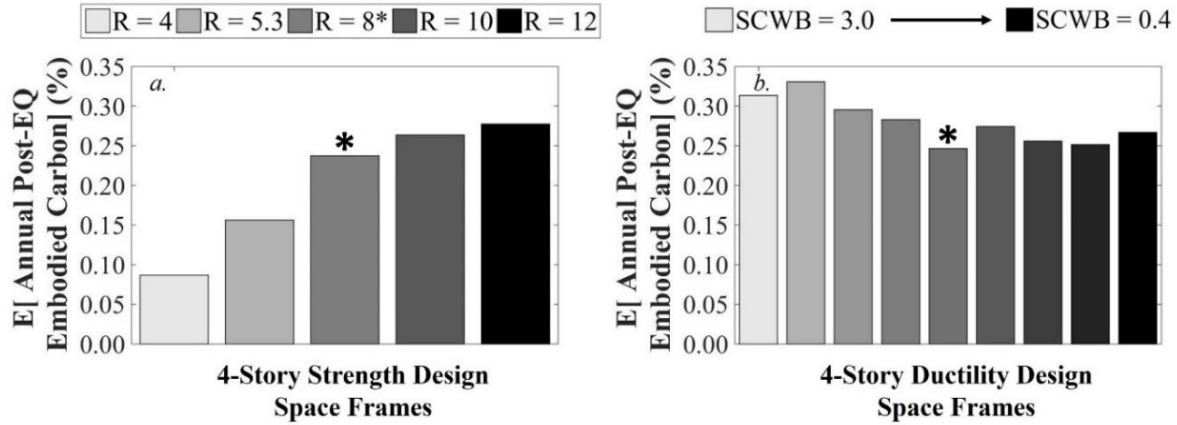


Figure 3.7. Expected annual post-earthquake embodied carbon loss for 4-story space frames for a) strength designs and b) ductility designs. Losses are annuities and expressed as percentage of total building replacement embodied carbon values. (* denotes code-compliant designs).

3.5.3 COMPONENT-LEVEL CONTRIBUTION TO SEISMIC LOSSES

Changes in seismic design also affect which building components contribute the most to seismic losses at each hazard level. Here, seismic losses are deaggregated at each of the hazard levels with respect to the contributing component, or so-called “performance groups.” The cost of post-collapse total building replacement is defined as its own performance group (“collapse”) to evaluate the impact of rebuilding the entire structure as compared to that of repair or replacement of specific damaged components.

Figure 3.8 shows component contributions to seismic loss for selected 4-story strength design space frames at each of the considered hazard levels. The left column illustrates post-earthquake economic costs (presented as median values at each hazard level in Figure 3.3(a) and, in the right column, embodied carbon (median values at each hazard level in Figure 3.6(a) as percentages of total seismic loss. The dominant building components contributing to seismic loss at each hazard level vary with the analysis metric of interest, due to differences in associated repair cost or CO₂ emissions consequences per damaged unit. In particular, depending on the damage state(s) entered at a hazard level, certain components (such as ceiling tiles, interior partitions, or HCAV ducts) may require more CO₂-intensive repairs than other components with higher economic costs (like beam-columns or exterior concrete cladding). At low to middle hazard levels, relatively expensive repairs to exterior concrete cladding dominate non-collapse economic costs for the above-code 4-story building (HL 5 to HL 8 in Figure 3.8(a)). However, for the same building and hazard levels, embodied carbon contributions are dominated by repair/replacement

activities for ceiling tiles and interior partitions. The weakest 4-story building (Figure 3.8(b)) has higher probabilities of collapse (and thus, of total building replacement) at higher levels of shaking, leading to larger contributions from structural repairs and total replacement to both economic cost and embodied carbon seismic losses. Trends are similar for the 12-story strength design set, with greater contribution from full building replacement for taller, below-code buildings than for their 4-story equivalents.

Varying ductility capacity (not shown in Figure 3.8) exhibits similar trends in component contribution to seismic losses. At higher hazard levels, however, non-structural component contribution for the most ductile buildings is larger than for the most above-code strength design 4 or 12-story buildings when either metric is considered. This trend occurs because enhanced ductility is associated with greater water conveyance pipe and HVAC duct damage, and repairs to these components require, for a given floor, significant quantities of steel and member replacement in large interconnected units. As discussed above, selection of a different intensity measure or suite of ground motions could change these results slightly, due to variations in structural and non-structural member response, but are not expected to influence overall trends in results.

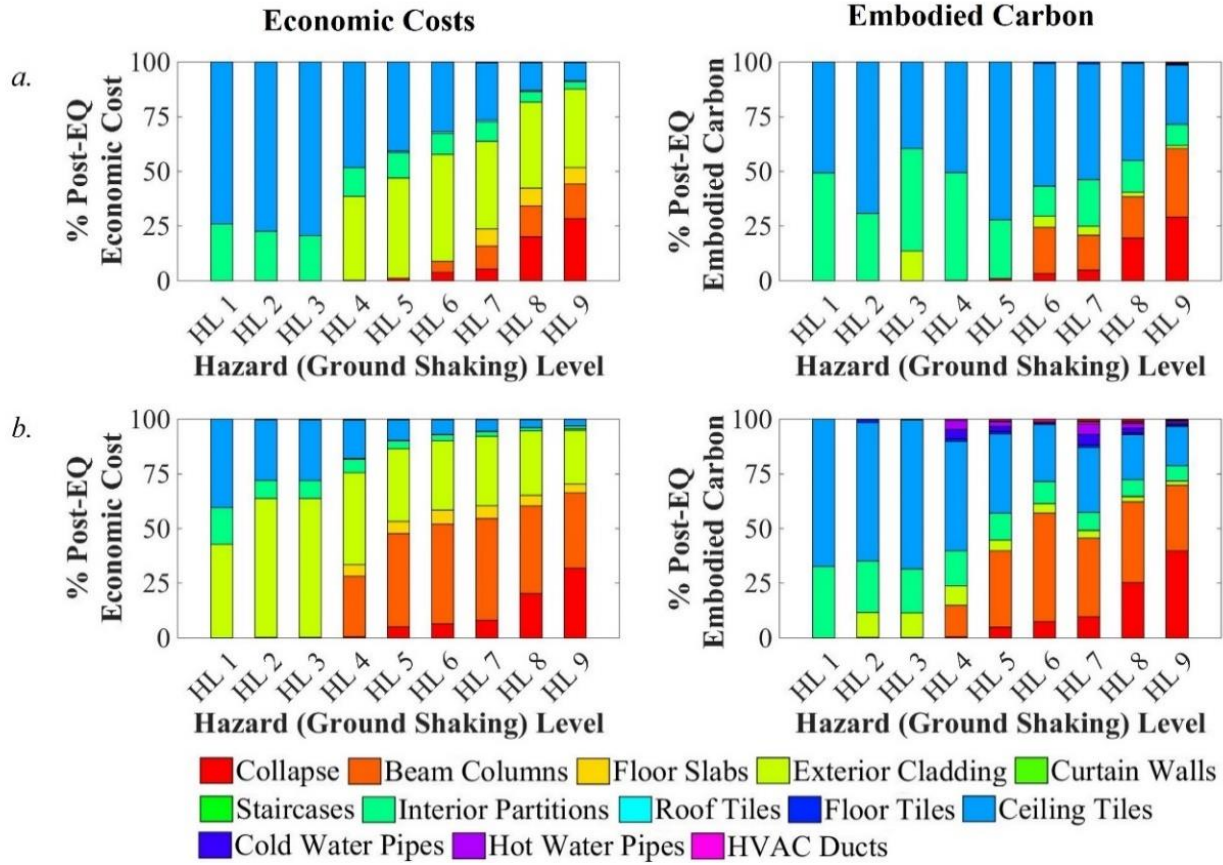


Figure 3.8. Deaggregated component contributions to seismic losses in terms of economic costs and embodied carbon loss for 4-story strength design space frames: a) above-code ($R = 4$), and b) below-code ($R = 12$), at the nine different ground shaking intensities analyzed at hazard levels defined by $Sa(T_1)$.

3.5.4 TOTAL EMBODIED CARBON SEISMIC LOSSES

Computation of the present value of future (*i.e.* uncertain) seismic losses considers present day implications of different seismic design decisions over time. Present value calculations are typically made using engineering economic equations wherein a discount rate is applied to future losses. Applying a discount factor accounts for the time value of money, where costs incurred in the future are valued less than if they occurred today (Cowing, *et al.* 2004); 3% is perhaps the most commonly recommended discount rate in engineering economic analyses (Pate-Cornell, 1984). However, climate change science questions the ethics of applying discount factors for total calculation of non-monetary metrics like carbon emissions. Consequently, many scholars recommend either no or a very low discount rate for environmental impact present value analysis (Jacquet, *et al.* 2013; Schelling, 1995; Tol, 2011). We address this concern regarding present value discounting of environmental impacts by first computing present value (total) post-earthquake

embodied carbon loss at four different discount rates from the annualized losses. The present value seismic loss is computed in terms of the CO₂, not dollar, equivalents of embodied carbon to avoid discussion of appropriate economic valuation of future carbon emissions. A 50-year building service life is assumed for these calculations.

Figure 3.9 shows how total post-earthquake loss decreases as discount rate increases, implying that higher discount rates decrease the value placed on future societal impacts from embodied carbon. In addition, for both design sets, increasing the discount rate has more effect on embodied carbon losses of a higher magnitude, *i.e.* generally associated with the weaker buildings, thus reducing the relative importance of those losses when compared to stronger buildings. As such, the remainder of this study assumes a 0% discount rate (essentially the sum of embodied carbon annuities over 50 years), for computing total embodied carbon losses and also assumes a 3% discount rate when computing the economic losses.

Figure 3.9 compares the influence of base shear strength and ductility capacity on present value post-earthquake embodied carbon. As shown previously in Figure 3.1, upfront embodied carbon increases with enhanced strength or ductility capacity. However, consistent with the seismic loss analysis, total post-earthquake embodied carbon decreases with enhanced lateral strength. For these 4-story space frames, upfront material production for the most above-code strength design releases 18 more tons (16,300 kg) of CO₂ equivalents than upfront material production for the code-level design. However, at a 0% discount rate, post-earthquake repair/replacement activities for the same enhanced design releases 133 fewer tons of CO₂ equivalents (120,660 kg) than the code-compliant design, indicating a net reduction when both upfront and total post-earthquake CO₂ are considered. This result supports an idea posited by the Portland Concrete Association that one tool for achieving “greener” buildings is to design for expected seismic forces 20% higher than required by current standards (PCA, 2012). Shown in Figure 3.10, a 20% increase in strength leads to significant savings in avoided embodied carbon due to lower seismic losses, compared to the original code-compliant design. These analyses (also generalizable to the 12-story designs) demonstrate that increased upfront embodied carbon for enhanced lateral strength can be offset by significant reductions in future post-earthquake embodied carbon from lower seismic losses.

However, enhanced ductility capacity can increase total post-earthquake embodied carbon

Figure 3.9(b). Results for the ductility designs assessed in this study suggest that, depending on building height and desired ductility capacity, above-code designs can increase both upfront embodied carbon (from larger structural member sizes to achieve enhanced SCWB ratios) and total seismic loss embodied carbon (due to greater non-structural damage). Even in cases where the post-earthquake embodied carbon decreases with enhanced ductility, this reduction is not sufficient to counteract the additional upfront carbon produced from the above-code designs.

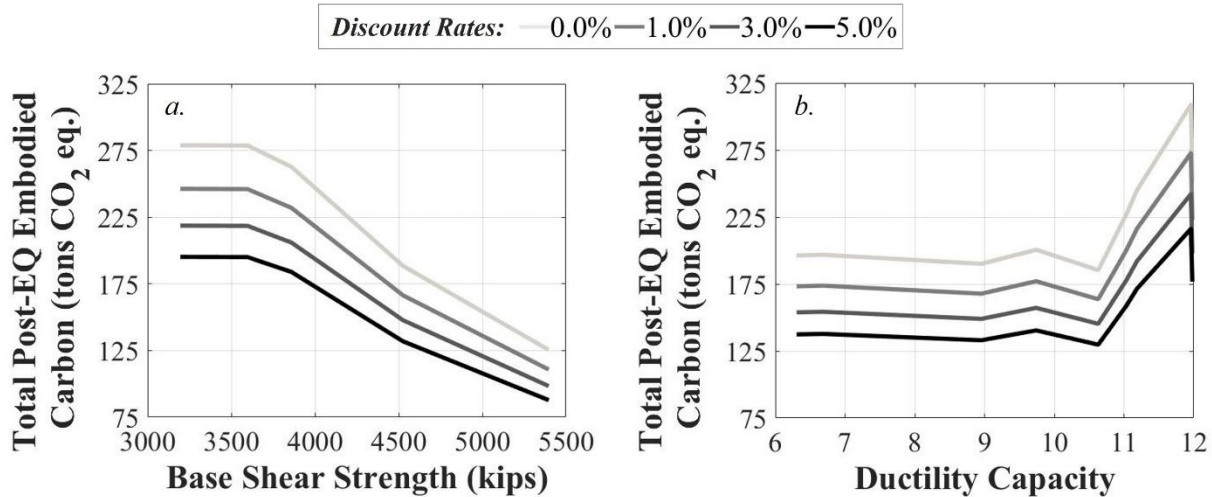


Figure 3.9. Total post-earthquake embodied carbon for 4-story space frames with respect to a) base shear strength for strength designs, and b) ductility capacity for ductility designs, showing the effect of discount rate on these calculations.

3.5.5 INFLUENCE OF SEISMIC HAZARD ON EMBODIED CARBON SEISMIC LOSSES

The relative influence of enhanced seismic design also will depend on the geographic region for which a building is designed, due to differences in seismic hazard. Figure 3.10 compares the predicted present value of embodied carbon seismic losses, should the 4-story strength design space frames be constructed at sites with higher (Pasadena, CA) or lower (Reno, NV) seismic hazard than at the presumed location in Los Angeles (Petersen et al., 2008). The three locations have the same soil site class (D) and similar fault types.

The results presented in Figure 3.10 show that for any of the considered building designs, as expected, lower hazard levels decrease the total embodied carbon associated with seismic losses. It is important to note, however, that code-specifications for lateral strength would vary based on the expected seismic hazard of these different sites, as indicated in the figure by the symbols for expected “code-design” values of base shear strength in Reno and Pasadena. In Pasadena,

enhancing lateral strength offers a major reduction in total post-earthquake embodied carbon compared with designing to-code. In Reno, there is smaller difference in post-earthquake embodied carbon from designing above-code or at the code-minimum. These results suggest that for sites with high seismic hazard, increasing a building’s design lateral strength can significantly reduce embodied carbon from seismic losses, but this effect will be less significant in areas of lower seismicity.

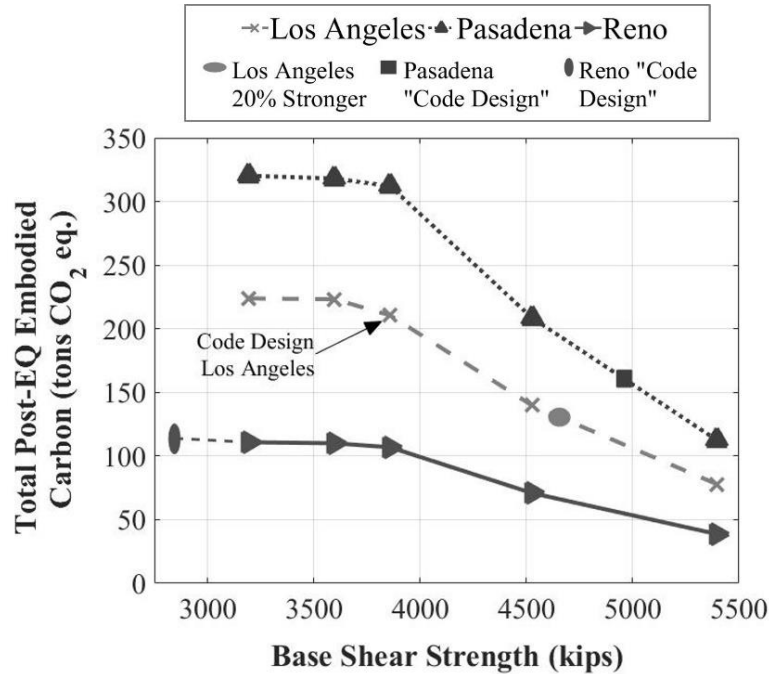


Figure 3.10. Influence of ultimate base shear strength on total seismic embodied carbon loss for Los Angeles, CA study site, compared to sites of higher and lower seismic hazard. Expected results for a building with 20% greater design strength in Los Angeles also shown. (1 kip = 4,448 N.; 1 ton = 987 kg.).

3.6 MULTI-OBJECTIVE ANALYSIS OF ECONOMIC AND ENVIRONMENTAL METRICS

Multi-objective analysis (MOA) is implemented here to identify and quantify relative strengths and weaknesses of the chosen design variations, across multiple design variable and possible analysis outcome categories. MOA is not used in this study for design optimization, which is already the subject of a number of structural engineering life cycle assessment and seismic design studies. Rather, in the form employed here, MOA allows us to represent and assess the complexity of real-world decision-making and the nuanced technical, social, economic, and environmental importance inherent to the specific units of measurement of each category (Kajikawa, 2008).

Figure 3.11 illustrates the MOA design objectives—upfront embodied carbon, base shear strength, and ductility capacity; and seismic analysis outcomes—collapse capacity, and total economic and embodied carbon seismic losses. Figure 3.11(a) presents the MOA results for the 4-story strength designs, where the results of the code-compliant space frame are used as a baseline case for comparison (shown as the black horizontal line). The figure demonstrates that the above-code ($R = 4$) strength design building has the most desirable attributes apart from upfront embodied carbon (for which it is slightly less desirable than the above-code, $R = 5.3$ design). However, the building's higher upfront embodied carbon (73 tons, or approximately 66,000 kg., more CO₂ equivalents than the baseline design) is offset by significant savings in reduced seismic losses. Moreover, the structural design of this building achieves enhanced lateral strength without a major increase in upfront embodied carbon. These and other MOA results suggest that enhanced lateral strength can produce more resilient (higher collapse capacities and lower economic seismic loss) and greener (lower seismic loss embodied carbon) outcomes than a code-compliant design. Moreover, upfront increases in embodied carbon can be offset by avoided post-earthquake impacts, *i.e.* a net reduction in life cycle embodied carbon, compared to the code-compliant design.

Comparatively, Figure 3.11(b) presents the MOA results with respect to the 4-story ductility design buildings, using the same code-compliant design as a baseline. The challenge of enhancing seismic design through increased ductility capacity is evident in the MOA results for the above-code ductility design space frames ($SCWB > 1.2$). Although these buildings have higher ultimate base shear strength and improved ductility capacity compared to the baseline design, their complex collapse mechanisms and non-structural component damage when subjected to large drifts result in much less desirable seismic loss outcomes. Overall, the MOA results shown in Figure 3.11(b) demonstrate that enhancing ductility capacity upfront does not enhance life cycle embodied carbon or economic costs associated with post-earthquake losses.

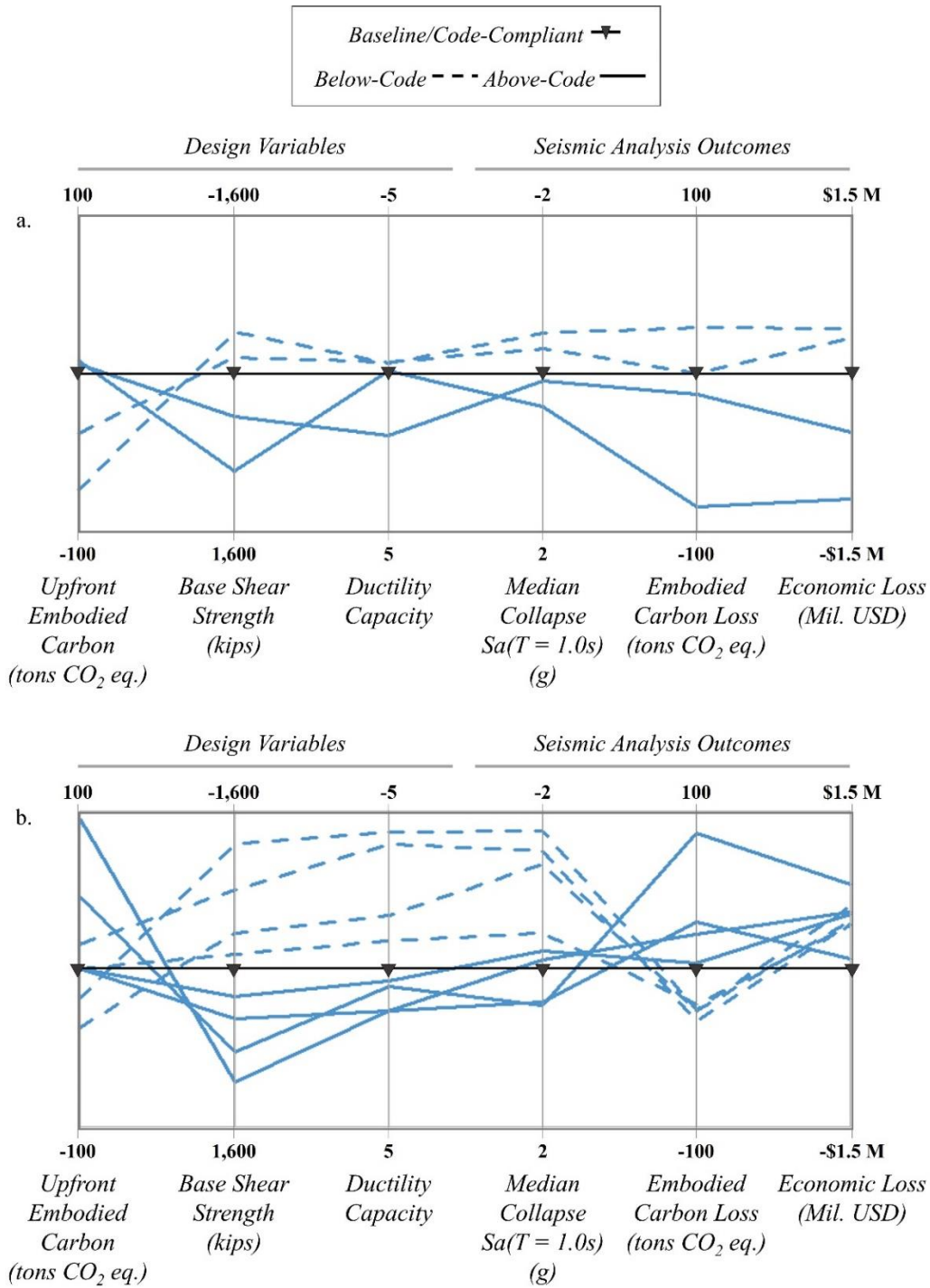


Figure 3.11. Multi-objective analysis results comparing design and analysis outcomes for 4-story space frame a) strength design buildings and b) ductility design buildings. Results are presented with respect to a selected “baseline” design (code-compliant 4-story space frame), i.e. the value associated with the baseline design is subtracted from the value for the design of interest. Metrics are plotted on y-axis such that less desirable outcomes are at the top and more desirable are at the bottom.

3.7 CONCLUSIONS

This study investigates the idea that designing “green” buildings to withstand higher earthquake and other extreme loads offers a potential tool to reduce environmental impacts associated with post-hazard repairs. To do so, seismic performance and life cycle embodied carbon are quantified for 30 RC buildings varying by lateral strength, ductility capacity, frame type, and height using nonlinear dynamic simulation and probabilistic loss assessment.

Changes in structural member sizes to vary design lateral strengths or ductility capacities influence upfront embodied carbon, which increases with enhanced lateral strength and, more so, with enhanced ductility capacity. Higher lateral strengths decrease economic seismic losses, but increase non-collapse, non-structural loss contributions. Trends from enhanced ductility with respect to seismic losses are inconclusive; although improved ductility reduces the magnitude of collapse-induced costs relative to code-level designs, it also increases non-collapse, non-structural losses. These trends apply to both the 4-story and 12-story buildings examined here.

This study quantifies the life cycle (total) environmental impacts from seismic losses in terms of the embodied carbon associated with post-earthquake repair and replacement activities. The findings show that increasing lateral strength reduces total embodied carbon seismic losses. Trends in seismic losses for ductility designs are less clear because embodied carbon losses relate to the percentage and magnitude of contribution from non-collapse versus collapse losses; collapse losses tend to decrease with higher ductility capacity, but at the expense of larger non-collapse losses. Improved ductility capacity is thus less influential to achieve more resilient or greener life cycle outcomes.

In conclusion, we find that increases in upfront embodied carbon required to achieve enhanced lateral strength can be offset by significant reduction in future post-earthquake losses, for a net savings in embodied carbon. Thus, this study demonstrates that enhancing lateral strength is a possible design tool for achieving greener buildings. These benefits from enhanced strength will be more significant in regions of high seismicity. The decision to enhance lateral strength above code-mandatory levels to achieve “green” goals will depend on the desired life cycle objectives of a designer, but offers a possible avenue for incorporating principles of hazard-resistance into green building rating systems. For example, structures in regions with significant

seismic, or other extreme load, hazard risks could be credited by demonstrating capacity increases above the code-minimum specifications. Future work on this topic could also expand the analysis presented herein to quantify total impacts (considering all life cycle stages) of a building designed to achieve jointly performance-based goals for hazard-resistance and objectives for green building rating system standards. The overall findings of this study suggest a need in building design and analysis for holistic consideration of both economic and environmental impacts through life cycle assessment of seismic losses.

Chapter 4 REDUCE, REUSE, RESILIENCE: TRADEOFFS IN LIFE CYCLE SEISMIC PERFORMANCE ASSOCIATED WITH THE USE OF FLY ASH OR RECYCLED CONCRETE AGGREGATE IN REINFORCED CONCRETE BUILDINGS³

4.1 INTRODUCTION

4.1.1 MOTIVATION

Concrete is one of the most widely consumed materials in the world, with some estimates suggesting that nearly 1 ton (987 kg) of concrete is produced for every person on the planet each year (Flower & Sanjayan, 2007). Concrete production is an energy-intensive and environmentally-impactful activity; for example, global manufacturing of Ordinary Portland Cement for concrete (referred to for the remainder of this chapter as simply “cement”) accounts for 5-7% of global carbon dioxide (CO₂) emissions (Worrell, Price, Martin, Hendriks, & Meida, 2001). In addition to cement, concrete also requires fine (sand) and coarse (gravel) aggregate, as well as water and chemical admixtures. In addition to environmental impacts from manufacturing concrete for new construction, damage from an earthquake or other hazard event can require production of new concrete and other materials for repairs, increasing life cycle environmental impacts (Menna et al., 2013; Welsh-Huggins & Liel, 2017). Reducing upfront and post-hazard repair-related emissions from concrete production for building applications may offer a significant step toward lowering global CO₂ emissions and combating climate change.

Numerous advancements have been made in recent years to develop alternative concrete materials with environmental and other goals in mind. These alternatives repurpose materials once viewed as waste for use in new concrete applications, potentially reducing concrete’s environmental impacts. One alternative involves replacement of cement with fly ash, a byproduct of coal combustion (Juenger, Winnefeld, Provis, & Ideker, 2011; RILEM, 1991). Over 50% of

³ This chapter will be adapted and submitted as a journal paper for review to the *International Journal of Life Cycle Assessment* following completion of this dissertation.

ready-mix concretes made in the U.S. currently contain some percentage of fly ash (ASTM C618, 2015). However, the current U.S. building code (ACI 318, 2011) restricts use of fly ash to an upper cement replacement limit of 25%, due to concerns regarding chloride intrusion from deicing materials in fly ash concretes. Recycling concrete for use as coarse aggregate (RCA) in new concrete offers another possibility for reducing the environmental impact of concrete production. This material is common in non-structural and transportation applications (e.g. sidewalks), but examples worldwide of RCA concrete use in buildings or structural applications are limited. However, some shake table tests of full-scale RCA concrete buildings have been conducted recently, demonstrating the material's feasibility in larger-scale structures (Changqing & Jianzhuang, 2013; Etxeberria, Marí, & Vazquez, 2007). The introduction of materials like fly ash or RCA in concrete (referred to together in this study as "alternative concretes") holds the potential to reduce CO₂ emissions at the beginning of a structure's life, by replacing traditional concrete materials. In addition, the use of these alternative concretes may support goals for hazard resilience, through potential savings from lower CO₂ emissions associated with post-hazard repair activities and possibly superior seismic performance. These relationships between alternative material choices, seismic performance, and life cycle environmental impacts are investigated here.

4.2 LIFE CYCLE SEISMIC PERFORMANCE OF BUILDINGS

4.2.1 OVERVIEW OF LIFE CYCLE ANALYSIS APPROACH

As described in Chapters 2 and 3, life cycle analysis (LCA) provides a tool to identify, assess, and analyze the environmental impact of a material, product, or service over its entire lifespan. This chapter takes a more rigorous adherence to LCA methodologies than the two previous studies. Two LCA approaches exist: 1) process-based analysis, where the impacts of known environmental inputs and outputs are computed within a specific process boundary, or 2) input-output analysis, where environmental impacts are calculated through matrices of macro-level process interactions. In addition, a LCA can be structured either as attributional, which models environmental flows into and out of a life cycle and its subsystems, or consequential, which models the consequences of a decision (a change to the system) in comparison with a baseline scenario (Ekvall & Weidema, 2004). Attributional analyses are typically used to compare the impacts of two products for the same functional unit (Goedkoop et al., 2013). The International Organization for Standardization (ISO) 14000 has developed international standards for conducting life cycle analyses for mass and

energy flows through a system (Hendrickson et al., 1998). The standard LCA procedure is outlined by ISO in two documents: *ISO 14040:2006* and *ISO 14044:2006* (ISO IEC, 2006). The ISO standards provide an iterative framework for attributional LCA, which consists of four phases:

1. *Goal and scope*, which defines the general purpose of the study and the level of detail of the system boundary.
2. *Life cycle inventory analysis*, which builds an inventory of input and output products and emissions (to water, air, soil etc.) data for the system under consideration.
3. *Life cycle impact assessment*, which seeks to quantify the overall environmental consequences and significance of the compiled emissions inventory data. This phase classifies environmental consequences into several major impact categories.
4. *Interpretation*, which summarizes the life cycle inventory and impact assessment results and identifies the greatest life cycle stage contribution to each impact category.

The ISO approach suggests drawing a *cradle to grave* system boundary, wherein environmental inputs and outputs are quantified over a product's entire lifespan, from raw material acquisition, production, use or operating life, to end-of-life treatment and disposal (ISO IEC, 2006). The LCA approach for large-scale systems, like buildings, is more complicated than for a single product, like a unit of concrete, due to the large number of manufactured products in a building. For each material that composes a building, all respective input and output emissions and associated environmental impacts must be accounted for, inventoried, and quantified (Althaus, Kellenberger, Doka, & Künniger, 2005; M. Bilec, Ries, Matthews, & Sharrard, 2006).

4.2.2 INCORPORATING SEISMIC PERFORMANCE INTO BUILDING LIFE CYCLE ANALYSES

Damage to buildings (or other structures and infrastructure systems), under seismic, hurricane, or other extreme event loads can necessitate repair activities that increase life cycle consumption of energy, release of greenhouse gas emissions, and natural resource use. When buildings or their components are less likely to be experience damage in a hazard event, short and long-term economic costs and environmental impacts from repair and replacement activities may be reduced.

In recent years, a number of frameworks have been proposed to consider the potential for acute hazard events in building life cycle environmental impact assessments (Bocchini et al., 2014; A. Court et al., 2012; J. Padgett & Li, 2016; Rodriguez-Nikl, 2015; Welsh-Huggins & Liel, 2016).

These frameworks take similar approaches, adding a “post-hazard” stage to the traditional building life cycle (construction, operations, end-of-life, *etc.*) in attempts to quantify lifetime environmental impacts from post-disaster repair/replacement actions. In a similar vein, other studies have proposed frameworks to incorporate chronic hazards (*e.g.*, earthquakes, material degradation, *etc.*) with material serviceability concerns (*e.g.*, material quality or strength) into building life cycle impact assessments. For example, Srubar (2014) introduced a framework to incorporate material service life and durability models into building life cycle analyses, using the example of RCA concretes. Flint et al. (2014) likewise presented a modular framework to incorporate material degradation into considerations of resistance to climate hazards over a building’s service life.

Such frameworks can be used to examine the influence of building design decisions. Welsh-Huggins and Liel (2017), for example, examined seismic design decisions, showing that increasing the lateral strength capacity of a building offers a tool to reducing post-earthquake environmental impacts, due to reduced damage and subsequent material repair needs that outweigh the impacts of larger member sizes on emissions associated with building production.

Other recent studies have sought to quantify economic and environmental savings from novel structural materials, including alternative concretes. Studies of concretes that use materials like RCA or fly ash have been almost exclusively investigations of mechanical material properties, such as strength and stiffness (as in Langley, Carette, & Malhotra, 1989; Mehta & Gjørsv, 1982; Siddique, 2004; Xiao, Li, & Poon, 2012), quantification of unit CO₂ emissions from production of these alternative types of concrete (Gartner, 2004; Huntzinger & Eatmon, 2009; O’Brien et al., 2009; Serres, Braymand, & Feugeas, 2016), or material durability under chemical intrusions (Evangelista & de Brito, 2010; Malhotra, 1990; Sagoe-Crentsil, Brown, & Taylor, 2001). Indeed, only a few studies of alternative concretes have considered the broader building life cycle impacts of constructing a building with varying types of structural materials, in terms of economic and environmental impacts. Changqing and Jianzhuang (2013) tested a mid-rise building constructed with RCA in full-scale shake table experiments, finding similar deformation capacities for both the natural aggregate and RCA buildings, but showing that the RCA building was more likely to develop a weak story mechanism. Rodriguez-Nikl *et al.* (2012) considered the impact of alternative materials, including RCA and fly ash concretes, on life cycle seismic performance and environmental impacts of an RC bridge. That study showed that such alternative concrete materials

can alter worsen structural response and lower seismic performance of a structure due to more variable compressive strengths and permeability. In addition, the results suggested RCA concrete may increase life cycle energy use and greenhouse gas emissions, but can reduce virgin aggregate impacts. The study also posited that fly ash concrete will decrease life cycle energy use and greenhouse gas emissions, but will have negligible impact on virgin aggregate usage.

4.2.3 METHODOLOGY FOR ASSESSING LIFE CYCLE SEISMIC PERFORMANCE OF RC BUILDINGS

This section presents a step-by-step overview of the study's methodology to assess changes in life cycle seismic performance of a reinforced concrete (RC) building when concrete is designed with (i) fly ash replacing cement or (ii) RCA (recycled concrete replacing coarse aggregate).

4.2.3.1 GOALS AND SCOPE

Following the ISO standards for LCA procedures, we first define the study goal and scope. The goal of this assessment is to determine how the use of alternative concrete materials influences the life cycle seismic performance of a building, quantified in terms of earthquake-related economic impacts (repair costs), and the life cycle embodied carbon (*i.e.* greenhouse gas emissions expressed as carbon dioxide equivalents, emitted during upfront and post-earthquake material manufacturing activities). There are multiple categories in which environmental impacts may be evaluated, such as resource depletion, embodied carbon, embodied energy, human health (Menna et al., 2013), but this study chooses to focus on embodied carbon, because it acts as a proxy for how the life cycle environmental impacts of a structure will influence global climate change.

The functional unit is a seismically-designed code-compliant reinforced concrete 4-story building in southern California, with an assumed lifespan (or use) time of 50 years. Life cycle inventory results are evaluated and presented for two stages in the functional unit's life cycle:

1. Building production from cradle to gate (from raw material extraction to building site), referred to as the "upfront" life cycle stage in this study.
2. Service life, which includes the possible occurrence of earthquake hazard events.

ISO permits the deletion of a life cycle stage if this decision is not expected to significantly change the study's overall conclusions (ISO IEC, 2006). In this case, the environmental impacts from building operational energy are excluded, as are impacts from on-site construction activities for upfront or post-earthquake repairs, because these effects are expected to be 1) less significant

relative to the impacts of the life cycle stages of upfront material production and post-hazard repair activities (Junnila & Horvath, 2003), and 2) nearly identical for all buildings. One limitation of the study is that end-of-life impacts—such as from different disposal options—are not calculated, because the boundary only considers the operational lifespan of the building and the structures are assumed to be repaired to full functionality after any potential hazard event occurs. Figure 4.1 presents the system boundary for the entire life cycle of the functional unit, with a dashed line indicating the stages considered in this study.

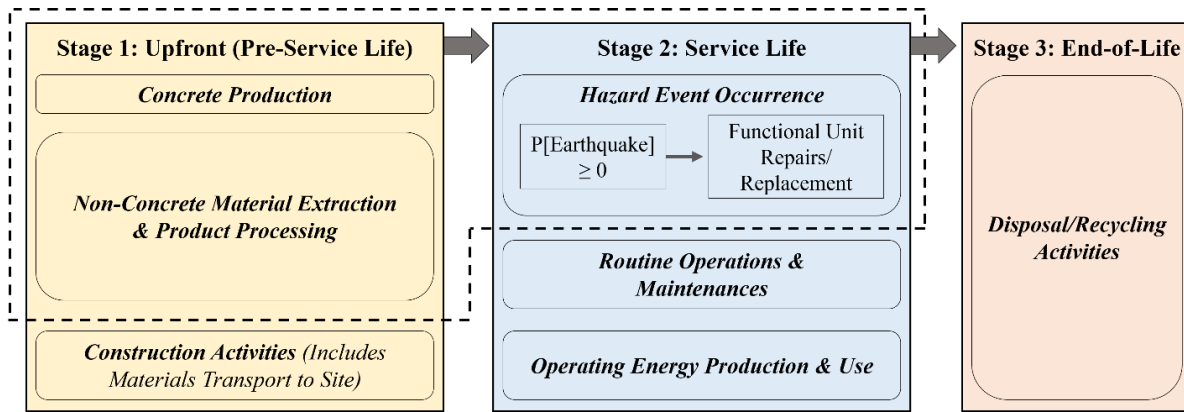


Figure 4.1. Life cycle system boundary showing stages inside the scope of current study.

4.2.4 INCORPORATING SEISMIC PERFORMANCE INTO INVENTORY AND IMPACT ANALYSES

To evaluate the environmental impacts and seismic performance of the chosen functional unit, we first quantify the embodied carbon produced from manufacturing the concrete and all other materials used in the initial construction of a building. Second, we estimate the mechanical properties of each selected concrete mix material variations (normal concrete, fly ash concrete, and RCA concrete). The mechanical properties are introduced into nonlinear dynamic simulation models of the building to quantify the influence of these concrete mixes on structural response under seismic loads. Seismic response (*e.g.* drifts, floor accelerations) is simulated as a function of ground motion intensity, characterizing structural response up to the point of collapse (Vamvatsikos & Cornell, 2002). Third, a probabilistic seismic loss analysis estimates the expected levels of earthquake-induced damage and required repair actions for structural and non-structural building components over the range of ground shaking intensities considered in dynamic analysis. Here, seismic losses are quantified in terms of both *economic costs* (dollar value necessary to conduct post-earthquake component repairs and/or replace the building) and *embodied carbon*.

Finally, life cycle seismic performance is quantified in terms of upfront and seismic losses, considering the likelihood of occurrences for ground shaking events of varying intensities.

4.3 CASE STUDY

The methodology presented herein is employed to assess life cycle building performance, in terms of possible economic and environmental costs, when a building is constructed with alternative concretes and considering seismic risks. We first discuss the structural design details—corresponding to the upfront life cycle stage—and the building’s earthquake (dynamic) response and structural/economic losses—corresponding to the hazard event/post-earthquake life cycle stage—before assessing the functional unit’s life cycle environmental impacts.

4.3.1 STRUCTURAL DESIGN CHARACTERISTICS OF CASE STUDY BUILDING

The RC building functional unit meets seismic code requirements for an assumed study site in southern Los Angeles for concrete “special” moment resisting frames (ACI, 2011; ASCE, 2010; ICC, 2009). The footprint of each building is 120 feet by 180 feet (36.6 m by 54.9 m); beams are 15 feet (4.6 m) long; columns are 15 feet (4.6 m) tall at the first story and 13 feet (4.0 m) at all others. Member sizes and reinforcement were determined from code force requirements and drift limitations, as well as capacity design provisions (*e.g.*, strong column-weak beam requirements). The building was designed by Haselton *et al.* (2011).

Investigation of the functional unit in this study considers variations in the properties of the structural concrete. The baseline (“normal”) concrete mix contains both Portland cement and virgin aggregate. The first alternative design set varies in terms of percent replacement of cement with Class F fly ash; concretes in which 20%, 40%, and 60% of cement is replaced with fly ash are considered. The second set varies in terms of percent replacement of virgin coarse aggregate with RCA; here, 30%, 60%, and 100% of coarse aggregate needs are replaced with RCA in different cases. These replacement percentages are taken from those commonly found in the literature of each concrete type (Hansen, & Narud, 1983; Ravindrarajah, & Tam, 1985; Langley *et al.*, 1989; Topcu, & Guncan, 1995; Naik, Singh, & Ramme, 1998).

Table 4.1 summarizes the varying quantities of a cementitious material (cement and/or fly ash), water, fine aggregate, and coarse aggregate (virgin stone and/or RCA) that compose each concrete mix. The mix design for the baseline concrete is proportioned based on ACI 211/318

guidelines to achieve a 28-day compressive strength of 5,200 psi (around 35.8 MPa) (ACI 211, 2009; ACI 318, 2011). This value is the “average-required strength”, defined as f'_{cr} , which would be specified in construction drawings and used in all structural design calculations. The material volumes of the six other concrete mixes are proportioned to reach the same 28-day f'_{cr} value. Two key changes are required for these mix designs. First, fly ash has a lower water demand than cement, meaning that to achieve the same strength level, the water/binder ratio decreases with increasing replacement percentage of fly ash (Lam, Wong, & Poon, 1998; Langley et al., 1989). Second, due to the higher porosity of RCA, water content must increase with greater amounts of RCA, subsequently increasing cement content to hold constant levels of workability, water/binder ratio, and strength for each mix (Hansen & Narud, 1983). Mix designs with admixtures such as superplasticizers are not considered here, due to the challenge of quantifying the environmental impacts of such materials. The mix designs provided in Table 4.1 are developed from a comprehensive review of previous research of mix designs and mechanical properties of these alternative concretes. The results of this literature survey consist several hundred data points that describe the percent increase or decrease in material volumes from those of a normal concrete mix having concrete strengths close to the target strength of this study.

Table 4.1. Mix designs with alternative concrete materials.

RC Building Variations	Water/Binder Ratio	Water (lb/ft³)³	Cement (lb/ft³)	Fly Ash (lb/ft³)	Fine Aggregate (lb/ft³)	Virgin Coarse Aggregate (lb/ft³)	Coarse RCA (lb/ft³)
Normal Concrete ¹	0.38	270	711	0	1,250	1,708	0
20% Fly Ash ²	0.36	256	568	142		1,708	0
40% Fly Ash	0.35	248	426	284		1,708	0
60% Fly Ash	0.30	182	284	426		1,708	0
30% RCA	0.38	278	732	0		1,195	512
60% RCA	0.38	286	753	0		683	1,025
100% RCA	0.38	294	775	0		0	1,708

¹ Normal (baseline) concrete mix has 0% fly ash and 0% coarse RCA.

² Percentages indicate % replacement of traditional concrete material by alternative material.

³ 1 lb/ft³ = approximately 16 kg/m³.

Each building contains the same inventory of non-structural building components, based on typical quantities of these components in office buildings (Haselton Baker Risk Group, 2016).

The non-structural components considered are: concrete roof tiles; staircases; exterior concrete cladding; exterior glazed curtain walls; suspended ceiling tiles; carpeted floor tiles; interior wall partitions; HVAC systems; and water service piping systems. This inventory of non-structural components, although not exhaustive, is representative of those components most likely to be damaged under the ground shaking intensities investigated here and thus, most likely to contribute to post-earthquake losses (Haselton Baker Risk Group, 2016; Ramirez et al., 2012).

4.3.2 MECHANICAL PROPERTIES OF ALTERNATIVE CONCRETES FOR CASE STUDY BUILDING

To determine the mechanical properties of the alternative concretes used in this study for use in constitutive material models in dynamic simulation models, we conducted a comprehensive literature review of over 100 journal articles that investigated changes in compressive strength, elastic modulus, bond strength, and stress-strain behavior from replacement of cement with fly ash, or replacement of virgin coarse aggregate with RCA.

Davis *et al.* (1937) published one of the earliest investigations on the influence of replacing cement with a supplementary cementitious material like fly ash on mechanical properties (ASTM C618-15, 2015). That study showed that the cementitious nature of fly ash causes concretes with this supplemental material initially to strengthen more slowly over time, but at later ages to achieve higher compressive strengths than normal cement concrete. This trend has been confirmed by many subsequent investigations on the mechanical behavior of fly ash concrete (Langley *et al.*, 1989; Naik *et al.*, 1998). In general, these studies demonstrate that compressive strength increases with greater replacement volumes of fly ash. There is some disagreement, however, as to whether concrete stiffness (i.e., elastic modulus) increases (Siddique, 2004), with the majority of studies suggesting no significant change (Malhotra, 1986). There is a lack of documented investigation on the stress-strain behavior of fly ash in concrete. Among those studies that have quantified this response, *e.g.* Lam *et al.* (1998) or Maher and Balaguru (1993), the findings suggest little to no change from the stress-strain behavior of normal concrete beyond the difference in strength.

For RCA concretes, Frondistou-Yannas (1977) and Ravindrarajah and Tam (1985) demonstrated that the replacement of virgin aggregate with RCA can significantly decrease both concrete's compressive strength and elastic modulus; Topçu and Guncan (1995) determined that these properties decrease further with increasing presence of RCA. Hansen and Narud (1983) also found that the strength, mechanical properties, and chemical composition of RCA concrete is

influenced by the quality of the original concrete and by the presence of old mortar attached to the RCA. Other studies have shown that as replacement percentage of RCA increases, concrete peak stress decreases and strain at peak stress increases (Bairagi, Ravande, & Pareek, 1993). In addition, numerous studies have quantified the influence of RCA on the ductility of concrete. There is some disagreement in the literature, however, as to whether RCA concrete is more brittle compared to normal concrete (Xiao & Falkner, 2007; Xiao, Li, & Zhang, 2005), more ductile (Topcu & Guncan, 1995), or exhibits no change in post-peak response (Ruhl & Atkinson, 1999).

Analysis of the data reviewed here identifies how use of alternative concretes changes material volumes, compressive strength, elastic modulus, bond strength, and material ductility of baseline normal concrete mixes. Given the differences between the studies reviewed (*e.g.* different chosen ages for data collection, different target strengths for each mix, etc.), we normalized the results for each alternative concrete mix (*e.g.* 20% fly ash) by those of their respective normal concrete case. In predicting the maximum compressive strength of each concrete we note that over time, concrete strength increases from that of the target average-required strength. In this study, we consider that the mechanical properties of the selected concrete designs after one year represent a common baseline. The material volumes (cement, fine aggregate, *etc.*) are selected based on the mix designs in the literature review that correspond—for each concrete type—to their desired one-year baseline mechanical properties.

After one year in service, we estimate that the concrete compressive strength of the normal concrete will increase to 6,040 psi, or 41.6 MPa, based on mix proportioning guidelines published by the Portland Cement Association in Kosmatka, Kerkhoff, & Panarese (2003). The compressive strength of RCA concretes increases over time, but does not reach the same long-term strength of a normal concrete, according to the data from the literature review. Based on the data assembled in the literature review, the findings in Table 4.2 demonstrate how the slow-hardening properties of fly ash—especially in the first 90 days—produce a one-year strength for the 20% fly ash concrete only 1% lower than the normal concrete control design, while the 40% and 60% mixes are predicted to be 5% and 10% stronger, respectively. Although only a small number of studies have been published on the stress-strain behavior of fly ash concrete, the papers reviewed suggest that it is appropriate to assume no change in the shape, other than increased maximum compressive strength/peak stress, of concrete stress-strain curves for fly ash concretes. By comparison, it is

assumed that RCA concretes are somewhat more ductile materials than normal concretes (around 30% more ductile in the case of the 100% RCA concrete). Effects on mechanical properties from long term material deterioration of the alternative concrete materials are not considered here.

4.3.3 STRUCTURAL SIMULATION MODELS OF CASE STUDY BUILDING

The calculated mechanical properties are incorporated into constitutive material models in a series of nonlinear simulation models representing the functional unit. Each building variation is modeled as a two-dimensional, three-bay frame in the *OpenSEES* nonlinear seismic analysis program (PEER, 2014). In this study, the structural elements of the computational model are first represented with distributed plasticity beam-column elements and elastic joint shear panel springs. Reinforcing steel is represented by a Giuffr -Menegotto-Pinto reinforcing steel model with isotropic strain hardening (Filippou, Popov, & Bertero, 1983) modified to capture rebar buckling (Dhakal and Maekawa 2002). Both confined and unconfined concrete sections are modeled with the Kent-Scott-Park material with zero tensile strength (Scott, Park, & Priestley, 1982), considering the material properties for each alternative concrete material described in Section 4.3.2. A geometric transformation is also applied to the structural elements to capture P- Δ effects.

Subsequently, a building model with lumped plasticity element representing the beams and columns is calibrated based on the pushover analysis of the distributed plasticity element models to use in the dynamic analysis. In the lumped plasticity approach, beam-columns are represented with elastic elements and concentrated hinge springs that have been assigned a material model capable of capturing concrete spalling, rebar buckling effects at large deformation, cyclic deteriorating, and bond slip (Ibarra, *et al.*, 2005). The plastic hinge rotations (pre-yield and post-capping) capacities of the lumped plasticity beams and columns were systematically calibrated (*e.g.* the same scale factor applied to all beams in a given model; a second scale factor applied to all columns) from the normal concrete model from Haselton *et al.* (2011) to match the force-deformation responses of the distributed plasticity models for the alternative concretes.

Pushover results show that despite the slight increases in later-age concrete strength for the fly ash concretes there are minimal differences in the base shear strength or ductility capacity for these design variations (Figure 4.2(a)). RCA content decreases slightly building stiffness and maximum base shear strength, and slightly increases structural ductility (Figure 4.2(c)). Analysis of the calibrated lumped plasticity models under a triangular pushover load distribution are shown

in Figure 4.2(b) and Figure 4.2(d) and also presented in Table 4.2. The model calibration changes the shape of the force-deformation response curve such that the initial stiffness for each lumped plasticity building model are essentially identical, thus giving each model the same fundamental period of $T_1 = 0.87$ sec. Based on these results, the influence of these concrete types on the dynamic response of each building is expected to be small.

Table 4.2. Properties of case study buildings with alternative concretes, showing concrete properties and building period and strength.

Functional Unit: RC Building Variations	Concrete Mechanical Properties		Pushover Results for Distributed Plasticity Building Models		Pushover Results for Lumped Plasticity Building Models	
	<i>Compressive Strength (psi)^{1*}</i>	<i>Elastic Modulus (ksi)</i>	<i>T₁(sec)²</i>	<i>Base Shear Strength (kips)^{**}</i>	<i>T₁(sec)³</i>	<i>Base Shear Strength (kips)</i>
Normal Concrete	6,040	4,430	0.81	4,550	0.87	4,600
20% Fly Ash	5,980	4,430	0.81	4,550		4,590
40% Fly Ash	6,340	4,430	0.80	4,580		4,610
60% Fly Ash	6,640	4,430	0.80	4,600		4,670
30% RCA	5,680	4,120	0.82	4,530		4,560
60% RCA	5,370	3,940	0.83	4,540		4,530
100% RCA	5,370	3,770	0.87	4,460		4,530

¹ Compressive strength after one-year. Average-required strength (f'_{cr}) targeted for 28 days is 5,200 psi (35.8 MPa) for all mixes

² Period from eigenvalues analysis, not considering cracked section properties.

³ Period from eigenvalues analysis, considering cracked section properties.

* 1 psi = 0.0069 MPa.

** Maximum base shear strength, for entire building (1 kip = 4,480 N).

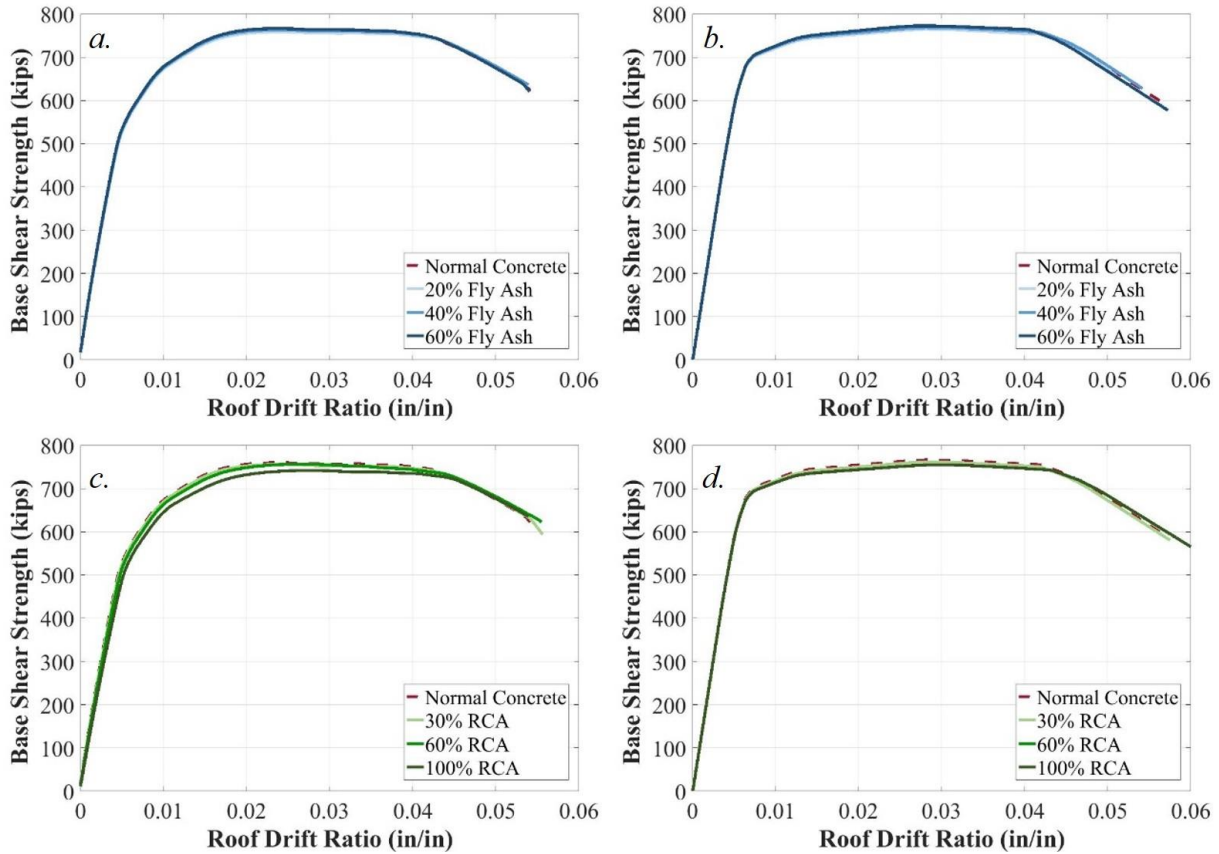


Figure 4.2. Static pushover results (per frame line) for a) distributed plasticity and b) lumped plasticity models of functional unit when designed with fly ash concrete; and c) distributed plasticity and d) lumped plasticity models of functional unit when designed with RCA concrete (1 kip = 4,480 N).

4.3.4 SEISMIC PERFORMANCE OF CASE STUDY BUILDING WITH ALTERNATIVE CONCRETES

4.3.4.1 SEISMIC HAZARD SCENARIOS

We characterize the seismic hazard analysis at the LA site based on twelve different ground shaking hazard levels, ranging from a return periods of 108 years, which corresponds to a shaking intensity of $S_a(T=0.87s)=0.34g$, to a return period of approximately 160,000 years, associated with $S_a(T=0.87s)=4.42g$ (Petersen *et al.*, 2008). These stripes are used to define structural response in the loss analysis (discussed below). Within the life cycle boundaries of the system assessed here, each hazard level may be considered as an individual scenario that potentially, but not necessarily, may be experienced by the building during its hazard event/post-hazard repair life cycle stage. To represent this seismic hazard, dynamic analysis is conducted with a set of thirty California earthquake records of strong ground motions at firm sites with site-to-source distances

ranging from 15-33 km and magnitudes between 6.5-6.9 (Vamvatsikos & Cornell, 2006). These records are generally representative of the crustal ground motions that may occur at the study site.

4.3.4.2 DYNAMIC ANALYSIS RESULTS

In IDA, the recorded ground motion acceleration time histories are first scaled to a small value of ground motion intensity, quantified in terms of spectral acceleration at the first-mode period of the structure, denoted as $Sa(T_1)$. Structural response is then analyzed at increasing levels of $Sa(T_1)$, until observation of collapse. Collapse is defined in this study as being triggered whenever story drifts greater than 12% are recorded at any story, following the work of Haselton *et al.* (2011) for code-conforming RC frame buildings. For the dynamic analysis, five percent Rayleigh damping is applied to the nonlinear simulation models' first and third modes.

The IDA results provided in Table 4.3 show that, as expected from the pushover analyses, using either normal or fly ash concrete produces almost identical collapse capacities for the functional unit. By comparison, the IDA results for the functional unit constructed with RCA concrete show that the somewhat greater ductility of that structural concrete may enhance collapse capacity (by up to 16%), despite some reductions in the concrete strength. However, constructing the buildings with RCA concrete incurs larger story drifts and floor accelerations at a given shaking intensity than when employing normal concrete.

Table 4.3. Seismic analysis results for study buildings designed with each alternative concrete type.

Functional Unit: RC Building Variations	Median Collapse Capacity, $Sa(T_1=0.87s)$ [g]	Post-Earthquake Economic Cost¹	Post-Earthquake Embodied Carbon²
Normal Concrete	3.38	\$437,200	532
20% Fly Ash			528
40% Fly Ash			523
60% Fly Ash			522
30% RCA	3.61	\$457,100	543
60% RCA	3.77	\$496,800	586
100% RCA	3.95	\$536,500	616

¹ Total economic seismic cost over 50 years, considering expected annualized costs, discounted at 3%.

² Total median embodied carbon seismic impact summed over 50 years, accounting for uncertainties regarding quality/reliability of emissions data sources and uncertainties in repair material quantities and transportation distances.

4.3.4.3 SEISMIC LOSS ANALOGY METHODOLOGY

The seismic loss analysis approach for quantifying post-earthquake economic costs follows the seismic performance and probabilistic loss-estimation procedures developed by FEMA P-58

(ATC, 2012a). The FEMA P-58 procedure is a component based loss estimation procedure where by earthquake induced repair are costs are quantified by determining the level of damage in each component in the building, as a function of dynamic analysis results, and quantifying the sum of the costs needed to repair all building components. This methodology has been implemented here using the SP3 software to organize loss calculations (Haselton Baker Risk Group, 2016). In this approach, fragility curves assembled by the FEMA P-58 project define the probability that a given structural or non-structural component is in or exceeds a specified damage state (DS) as a function of a building's seismic demand, expressed as either peak floor accelerations or story drifts (ATC, 2012a, 2012b). The seismic demands are obtained from the dynamic analysis results described above. The repair and replacement cost and actions for a component are defined as a function of the severity of damage based on FEMA P-58 recommendations. For instance, a story drift ratio of 2.75% is expected to cause special-moment frame concrete beams and joints to exhibit residual drifts of up to 0.06 inches (0.15 centimeters), which will require patching of the first top inch (approximately 2.5 centimeters) of concrete cover (ATC, 2012a, 2012b).

FEMA P-58 damage fragilities and repair outcomes were developed from experimental testing, post-earthquake reconnaissance and expert judgment of structural components made with normal concrete. Conversations with concrete industry professionals suggest that the unit cost of both fly ash and RCA concrete is similar to that of normal concrete (personal communication, 2016). Moreover, given the lack of data regarding the seismic performance of fly ash concretes, we assume, for simplifications purposes, that the damage states and associated repair costs are the same for the alternative concretes. For example, we assume that a median drift of 2.75% corresponds to the same “slight” damage (*i.e.* in the FEMA-defined Damage State 2) to concrete beam-column components regardless of the type of concrete used.

The loss analysis calculations incorporate Monte Carlo simulation results for 10,000 realizations of potential damage outcomes for the functional unit at each hazard level, for each alternative concrete type. In the case of a realization predicting building collapse, the economic costs are taken as equal to the building replacement cost. For the purposes of this study, the same construction cost is assumed for each building, regardless of concrete type, using construction costs of \$230/ft³, tabulated by the Haselton Baker Risk Group (2016) and Ramirez et al. (2012).

4.3.4.4 ECONOMIC SEISMIC LOSS ANALYSIS RESULTS

Figure 4.3(a) shows a vulnerability function relating ground shaking intensity at each hazard level, expressed as $Sa(T_1=0.87s)$, to median post-earthquake economic cost at each shaking intensity. These costs represent the expected economic costs from post-earthquake repairs, should shaking of a particular intensity occur at the building site. Using normal concrete or fly ash concrete for the functional unit results in nearly identical engineering demand parameters at each hazard level. Therefore, component damage states and economic repair cost outcomes for the functional unit constructed with using normal concrete are also representative of those associated with fly ash concrete and are thus not shown on the figure. By comparison, the slightly more flexible and more ductile RCA concrete types introduce larger peak floor accelerations than in the normal concrete or fly ash designs, resulting in costlier non-collapse repair actions when certain components enter higher damage states at lower ground motion intensities. Although the probability of collapse for RCA building variations decreases as percentage of RCA concrete increases, Figure 4.3(b) shows that the reduction in building replacement (post-collapse) cost is countered by the increased non-collapse repair costs. As such, post-earthquake economic costs for RCA concrete buildings do not significantly differ from those of the baseline normal concrete building.

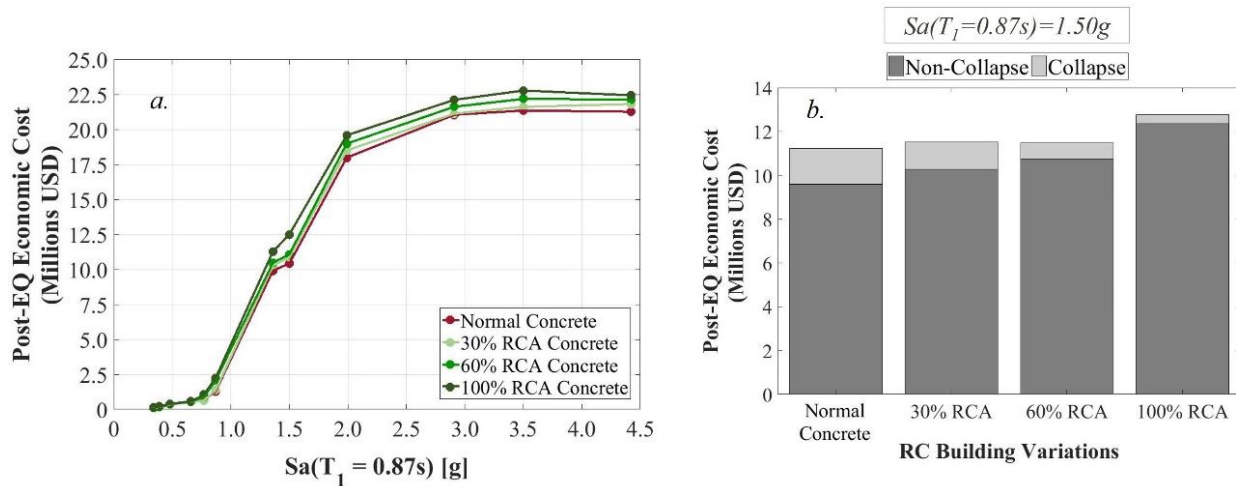


Figure 4.3. a) Vulnerability functions quantifying median post-earthquake economic costs for the normal concrete building and the RCA concrete buildings; b) post-earthquake economic costs deaggregated by median non-collapse and collapse at hazard level corresponding to $Sa(T_1=0.87s)=1.50g$ for normal concrete and RCA concrete functional unit variations.

We next quantify the expected annualized costs (EAC) for each RC building variation, as well as associated changes to the present value of the post-earthquake economic cost. EAC is

calculated by convolving the seismic hazard curve with the vulnerability function (Baker and Cornell 2003). Figure 4.4 shows that trends in annualized post-earthquake economic cost for the functional unit follow observations described above for the losses conditioned on each hazard level; fly ash concrete buildings have the *same* earthquake-induced economic costs as the normal concrete building, while the RCA concrete buildings have *similar* or somewhat *greater* annualized losses (roughly 23% more than the baseline normal concrete building, compared the 100% RCA case). Costs associated with the RCA concrete buildings increase with increasing aggregate replacement percentage. Table 4.3 lists the present value of these annualized post-earthquake economic costs, at a discount rate of 3%, and assessed over a service life of 50 years.

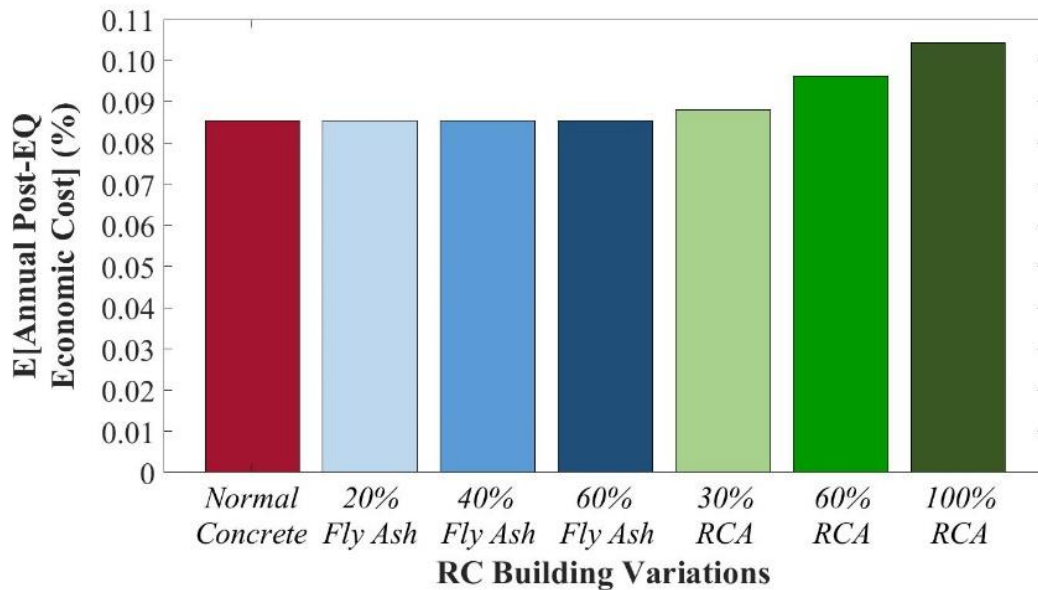


Figure 4.4. Expected annualized post-earthquake economic costs, expressed as annuities and normalized by total building replacement cost, for each RC building variation or functional unit.

4.3.5 LIFE CYCLE ENVIRONMENTAL IMPACTS OF CASE STUDY BUILDING WITH ALTERNATIVE CONCRETES

This section builds on the assessment of seismic economic costs to quantify how alternative concretes influence life cycle inventory emissions (*i.e.* embodied carbon of concrete production) of the functional unit, and then assesses the contribution of the varying unit concrete impacts to the building’s life cycle embodied carbon, at both upfront and post-hazard (*i.e.* service life) stages.

4.3.5.1 ENVIRONMENTAL IMPACT ANALYSIS PROCEDURE

The boundaries of this attributional LCA system consider emissions released during material production for structural and non-structural components. We use the *SimaPro* software to transform inventory emissions released during raw material manufacturing (from the Ecoinvent database) into resulting environmental impacts with the *Tool for the Reduction and Assessment of Chemical and other Environmental Impacts* (TRACI) (EPA, 2008; Goedkoop *et al.*, 2013). The Ecoinvent database is a European inventory, so we select materials and products representative of manufacturing practices and emissions standards for the United States. Emissions inventory data for all non-concrete materials are taken from existing allocation material processes in *SimaPro*.

4.3.5.2 LIFE CYCLE EMBODIED CARBON INVENTORY DATA FOR ALTERNATIVE CONCRETE PRODUCTION AND MANUFACTURING

A major contributing factor to differences between building life cycle embodied carbon impacts are variations in the CO₂ emissions released during the production of different concrete mix materials. The main sources of CO₂ emissions from cement production are the calcination of limestone, fuel combustion in the cement fuel kiln, and power generation for a cement plant (Huntzinger & Eatmon, 2009; Worrell *et al.*, 2001). When cement is replaced by fly ash, the embodied carbon impact of the fly ash is small, assuming that fly ash is generated by coal plant operation, regardless of demand for this material in concrete production (O'Brien *et al.*, 2009). Nevertheless, there are additional, albeit low, amounts of carbon emissions released from the capturing, milling, and refining of fly ash for commercial concrete applications (Flower & Sanjayan, 2007). RCA advocates argue that its use prevents more materials from entering landfills and supports a “closed-loop” recycling process (Weil, Jeske, & Schebek, 2006). While recycling existing concrete does reduce the burden placed on landfills and preserves stores of natural aggregate sources, the influence of RCA on embodied carbon depends on the energy used to crush and recycle the existing concrete. In addition, material transportation distances may differ between RCA and virgin aggregate (Marinkovic, Radonjanin, Malesev, & Ignjatovic, 2010; Meyer, 2009).

Figure 4.5 presents the *cradle-to-gate* system boundary for production of a unit (1 ft³ or 0.03 m³) of the “normal concrete” type. Figure 4.6 meanwhile show how the system boundaries change for production of a unit of concrete when using the two alternative materials, fly ash and RCA. Calculations for environmental impacts in terms of the embodied carbon from concrete materials consider: 1) material extraction and production of cement, fine aggregate (sand), and

virgin coarse aggregate; 2) collection and refinement of fly ash byproduct from coal production; 3) sorting and recycling of old concrete into coarse aggregate as RCA; 4) transportation of materials from extraction sources, to processing sites, to a concrete mix plant; and 5) energy production to power the concrete mix plant (following standard U.S. concrete mix practices). The system boundary for production of the alternative concrete mix materials (fly ash and RCA concretes) considers only the emissions and subsequent embodied carbon impact from production and commercial preparation of these materials for use in a concrete batch. In the case of fly ash, the production of the coal (the burning of which generates fly ash) is excluded. Similarly, in the case of the RCA materials, emissions and impacts from the life cycle of the concrete in its original form, including the dismantling of the structure and post-demolition waste-sorting, are excluded (Althaus *et al.*, 2005). Therefore, the only process impacts for RCA are those produced from the act of crushing the sorted waste into RCA and from the transportation emissions released while moving the RCA between the recycling plant and concrete mix plant.

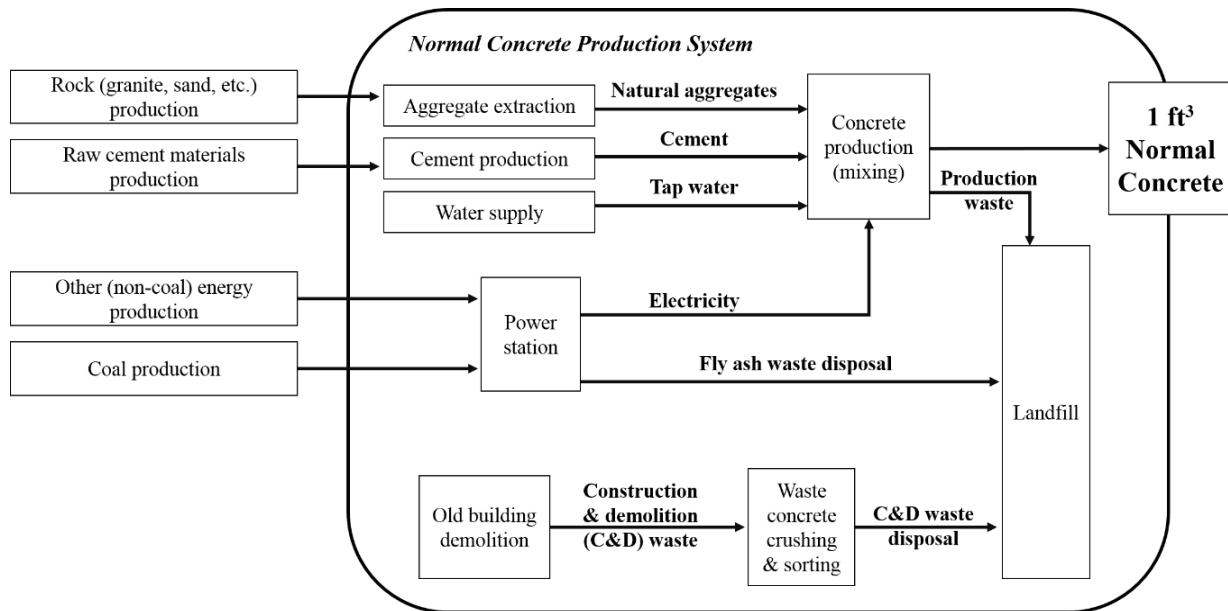


Figure 4.5. System boundary for production of one cubic foot (0.03 m³) of normal concrete, without any alternative materials.

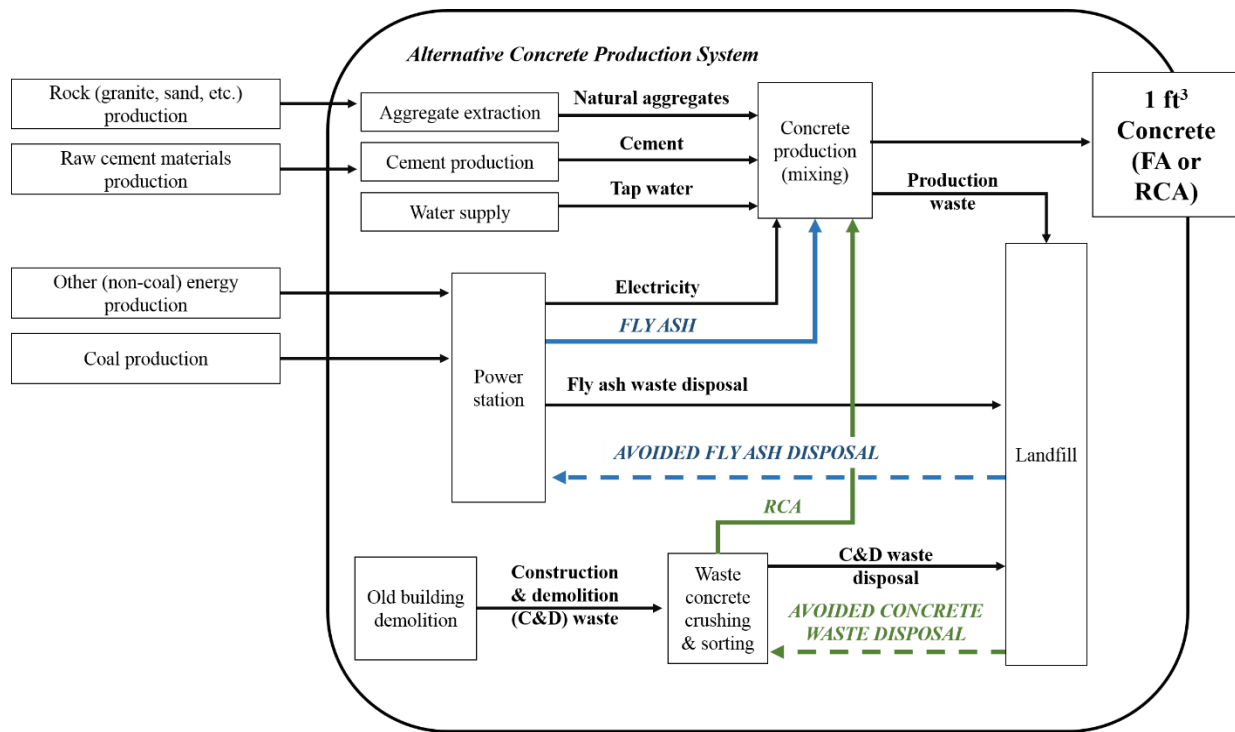


Figure 4.6. System boundaries for production of the functional unit when constructed with either fly ash or RCA concrete variations.

Here, we define a unique “assembly product stage” for each alternative concrete type to calculate life cycle inventory emissions from the production of raw materials, material transportation scenarios, and energy generated to produce a unit of concrete. The assembly product combines the emissions inventories of each concrete material and—using the TRACI methodology—allocates emissions to the total embodied carbon impact based on the specified material volumes, unit of energy, and ton-mileage.

Following U.S. concrete mix practices, we assume that the activity of concrete mixing to produce one cubic foot (0.03 m³) of material requires 14 MJ of energy (Nisbet, Marceau, & VanGeem, 2002). The emissions released by production of this energy are based on data for the energy sources commonly used in California. A 2006 survey of the California energy mix found that contribution of electricity to a site in Los Angeles is: 33% from coal; 21% from natural gas; 13% from wind power; 10% from nuclear power; 5% from biomass and natural waste; 6% from hydroelectric plants; and 12% from other, unspecified energy sources (Itron, 2006).

Figure 4.7 and Table 4.4 show the relative locations of material sources, processing plants, concrete mix plants, and study building site. There are no active coal plants in California, and most

coal power to the state is supplied from plants in Utah (EIA, 2016). Therefore, we assume that the fly ash used in these mixes comes from Utah. A uniform probability distribution of transportation distances are selected for each material (cementitious material, fly ash or cement; fine aggregate; or coarse aggregate, virgin or recycled) based on the location of existing quarries, cement plants, recycling plants, and concrete mix plants in California at the time of this study. This distribution of transportation distances represents a range of possible assumptions about the geographic location of concrete materials. Transport emissions vary depending on the class and emissions standards of the freight vehicles; in this study, transport impact includes emissions released by moving a specific ton-mileage between locations in the concrete production chain. Transport impact calculations assume that freight trucks achieve the Euro04 emissions standard, which is considered here as equivalent to the current U.S. standard (EPA, 2016a). The sensitivity of the results to varying transportation distances is discussed below.

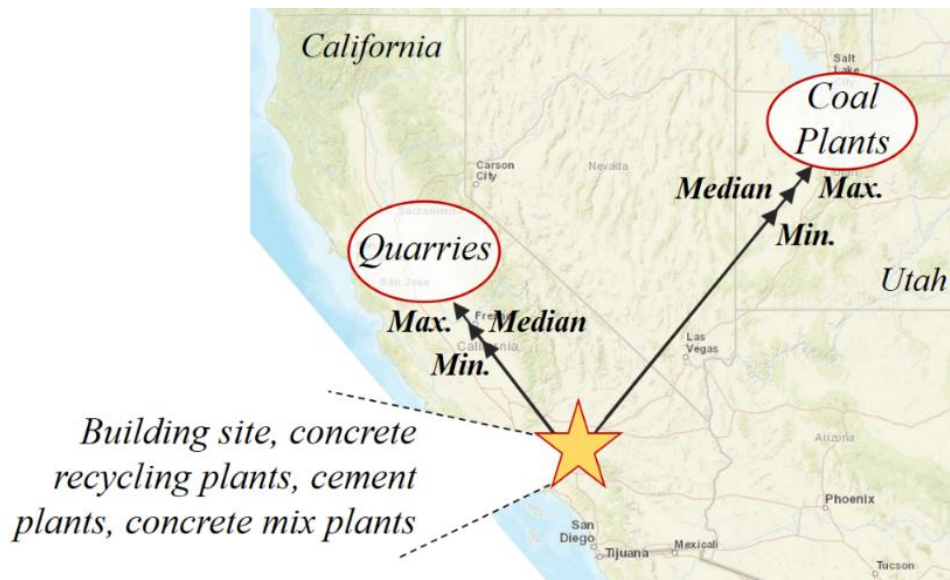


Figure 4.7. Map showing relative locations of material sources, processing plants, potential concrete mix plants, and building site assumed in this study.

Table 4.4. Distances between potential material extraction/processing sites to concrete mix plant site in southern Los Angeles.

Distance Type	Cement Distances (Miles) ¹	Fly Ash Transport Distances (Miles)	Virgin Aggregate Distances (Miles)	RCA Distances (Miles)
Minimum	3	570	47	14
Median	37	590	165	26
Maximum	94	606	344	82

¹ 1 mile = 1.6 kilometers.

4.3.5.3 EMBODIED CARBON ASSOCIATED WITH ALTERNATIVE CONCRETE PRODUCTION AND MANUFACTURING

Considering the life cycle inventory emissions for each material in a given concrete mix and the potential variations in material transportation distances, we allocate a unit embodied carbon impact to each concrete mix material. The sensitivity of the results to these assumptions for the unit embodied carbon of each material is discussed below.

The embodied carbon impact from producing 1 unit of fly ash (*e.g.* 1 lb or 0.45 kg) is approximately 92% lower than the unit cement production impact, considering uncertainties in emissions data quality and reliability. Therefore, replacing just 20% of cement with fly ash will reduce concrete unit embodied carbon, even when considering the further distance of a coal plant (fly ash source) from a concrete plant compared to the distance of the cement sources. The embodied carbon to process waste concrete into a unit of RCA is 30% lower than that generated by production of a unit of virgin coarse aggregate. However, replacing more virgin coarse aggregate with RCA also requires higher volumes of the most embodied carbon-intensive material (cement) in a mix design, (as shown in Table 4.1). As a result, when comparing the minimum RCA concrete material distances to the normal concrete mix with the furthest material distances, increasing the percentage of RCA can slightly decrease concrete unit embodied carbon. Despite this beneficial reduction in transportation impact, in general, the unit embodied carbon of concrete increases with addition of RCA due to the required additional cement content.

The range of assumptions made for this study (boundary of the production system for a unit of concrete, transportation distances, *etc.*) introduces multiple sources of uncertainty in the calculated embodied carbon impacts. Therefore, we conduct an uncertainty analysis, using Monte Carlo simulation, to quantify the distribution of potential embodied carbon impacts for a unit of concrete, given uncertainties in the actual value of each input parameter. The parameters analyzed here are: 1) unit embodied carbon impacts from manufacturing each concrete mix material, *i.e.* cement, fly ash, virgin aggregate, and RCA; 2) unit embodied carbon impact from energy generation (for mixing the concrete); 3) unit embodied carbon impact released by transportation emissions; 4) transportation shipping distances for each concrete mix material. For a given parameter (*e.g.* unit impact for cement production), the uncertainty analysis quantifies the distribution of unit concrete embodied carbon impacts considering the variability in this parameter's assumed value and median values for the impacts of all other parameters. In this

analysis, each parameter is varied individually over a uniform distribution of 10,000 possible outcomes. The distribution of transportation distances are bounded by the maximum and minimum values defined by the known locations of existing aggregate quarries, coal plants, *etc.*, listed in Table 4.4. The distribution of unit embodied carbon for material extraction/manufacturing, energy production, and transportation emission impacts, are bounded by limits 20% lower and 20% greater than the median impacts specified in the life cycle inventory data.

Table 4.5 presents the median unit embodied carbon impact for each individual concrete mix material input (cement, fly ash, *etc.*), as well as the combined median embodied carbon impact for a unit of concrete. The results of the uncertainty analysis demonstrate that the distribution of concrete unit embodied carbon impacts is most sensitive to variations in the transportation distances of virgin aggregate from extraction source/processing sites (quarries) to a concrete plant, as presented in Figure 4.8(d). This trend occurs because the distances between virgin aggregate quarries and concrete plants are further than those for other materials—such as between cement and concrete plants—combined with the heavier weight of the fine and coarse virgin aggregate compared to the weight of other materials—such as the lighter weight fly ash, which is transported over further distances. These calculations assume that virgin aggregate is processed at the quarry before transportation to a concrete plant. In addition to virgin aggregate transport distance, the distribution of concrete embodied carbon is also sensitive to the variability in embodied carbon impact from production of a unit of cement (Figure 4.8(a)), which is the most carbon-intensive material production process in the concrete manufacturing system boundary.

Reduce, Reuse, Resilience: Tradeoffs in Life Cycle Seismic Performance Associated with the Use of Fly Ash or Recycled Concrete Aggregate in Reinforced Concrete Buildings

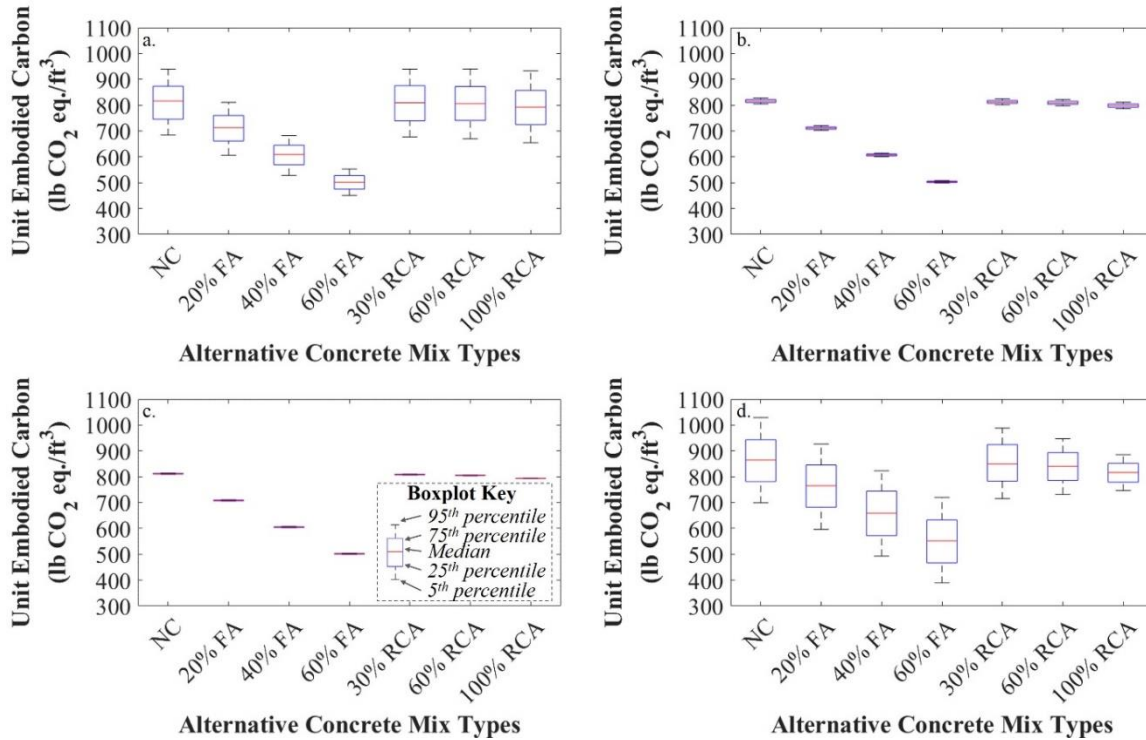


Figure 4.8. Results of uncertainty analysis, showing how distributions of concrete unit embodied carbon vary with respect to changes in a) cement unit material embodied carbon impact, b) transport distance between cement production facility and concrete plant, c) virgin aggregate unit embodied carbon impact, and d) transport distance between virgin aggregate source and the concrete plant. The legend on Figure 4.8(c) shows key boxplot features. (1 lb = 0.45 kg).

Table 4.5. Results of uncertainty analysis showing how unit embodied carbon impacts for concrete mix materials influence unit concrete and total upfront building embodied carbon impacts due to a) variations in cement unit embodied carbon impact, and b) variations in virgin aggregate transport distances.

Median Unit Material Impacts (lb/lb CO ₂ eq.)*				
		Cement Production		9.00x10 ⁻¹
		Fly Ash Production		8.00x10 ⁻³
		Virgin Aggregate Quarrying/Production		4.40x10 ⁻³
		Concrete Recycling		1.30x10 ⁻³
RC Building Variations	a) Median Upfront Embodied Carbon ¹		b) Median Upfront Embodied Carbon ²	
	Unit Concrete Impact (lbs/ft ³ CO ₂ eq.)*	Total Upfront Building Impact (tons CO ₂ eq.)*	Unit Concrete Impact (lbs/ft ³ CO ₂ eq.)	Total Upfront Building Impact (tons CO ₂ eq.)
Normal Concrete	805	1,820	867	1,880
20% Fly Ash	702	1,740	758	1,790
40% Fly Ash	604	1,660	651	1,700
60% Fly Ash	500	1,580	554	1,620
30% RCA	807	1,830	855	1,870
60% RCA	797	1,820	835	1,850
100% RCA	790	1,810	813	1,830

¹ Median impacts considering distribution of cement unit production embodied carbon impacts.

² Median impacts considering distribution of virgin aggregate transportation distances.

* 1.0 lb = 0.45 kg. 1 lb/ft³ = approximately 16 kg/m³. 1 ton = approximately 987 kg.

4.3.5.4 EMBODIED CARBON ASSOCIATED WITH FUNCTIONAL UNIT PRODUCTION AND MANUFACTURING

The unit embodied carbon for each concrete type is used to quantify the total life cycle embodied carbon for the functional unit, *i.e.* an entire 4-story RC building. Upfront embodied carbon for an entire building is computed here as the sum of the CO₂ equivalents associated with manufacturing all structural and non-structural building components. Figure 4.9 presents the system boundary associated with production of a functional unit, including non-concrete building products. Calculation of the volume of each material input to the functional unit is determined from normative building quantities defined in the FEMA P-58 loss analysis methodology (ATC, 2012a, 2012b; Haselton Baker Risk Group, 2016) and from estimations of total building material volumes made in previous work by the authors (Welsh-Huggins & Liel, 2016, 2017). The functional unit production system boundary impacts from the manufacturing and production activities for all building materials, but not for the emissions associated with transporting concrete and building components from manufacturing plants to the presumed building site.

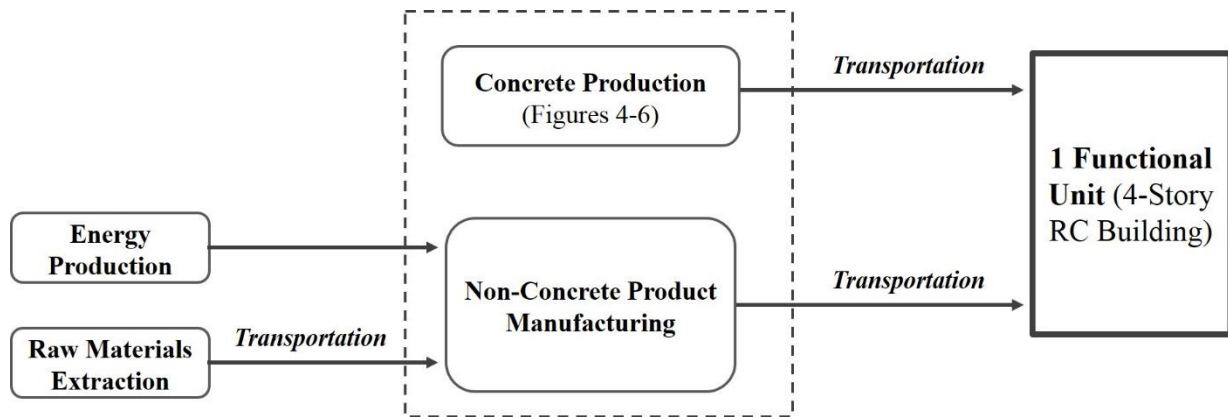


Figure 4.9. System boundary for production of a functional unit (code-conforming, 4-story, RC space frame building), which is constructed with alternative types of structural concrete.

Previous calculations by the authors of the upfront embodied carbon for typical RC buildings did not consider sources of uncertainty in the assumptions made regarding quantities and volumes of structural and non-structural materials used in building construction. Therefore, another round of uncertainty analysis, again using Monte Carlo simulation, is conducted to determine the sensitivity of upfront embodied carbon impacts to variations in assumptions about material quantities and concrete unit impacts. A total of 53 parameters are varied individually in

this case, to consider distributions in the quantity of every single material, structural or non-structural, that composes the functional unit, as well as inputs to the alternative concrete variations.

Assumptions about the quantities of certain components and materials, such as the non-structural steel in ceiling tile components, contain significant sources of uncertainty, due to lack of confidence in the reliability of available data (Edelen & Ingwersen, 2016). In these cases, the uniform distribution for the Monte Carlo simulation is bounded by minimum and maximum limits 20% lower and 20% greater than the previously employed median quantities. Where more detailed information is available—such as assumptions for the dimensions of beam-column structural members—the known maximum and minimum values bound the uniform distribution. Since the focus of this study is the influence of alternative concrete designs on the functional unit’s life cycle impacts, unit embodied carbon impacts of non-concrete materials are not varied.

Figure 4.10 presents the median upfront embodied carbon for a functional unit (results also shown in Table 4.5). The uncertainties in the assumptions for non-concrete material quantities are the same for the building, regardless of the alternative concrete type used, so results are only shown for construction of the functional unit with the baseline normal concrete. Consistent with other building life cycle analyses studies (*e.g.* Guggemos & Horvath, 2005; Junnila & Horvath, 2003), variations in the quantities of non-structural steel can significantly influence the total functional unit embodied carbon, but Figure 4.10 shows that, for these buildings, variations in the unit impact of concrete and in the size of concrete structural members will also lead to large variations in upfront embodied carbon outcomes for the functional unit.

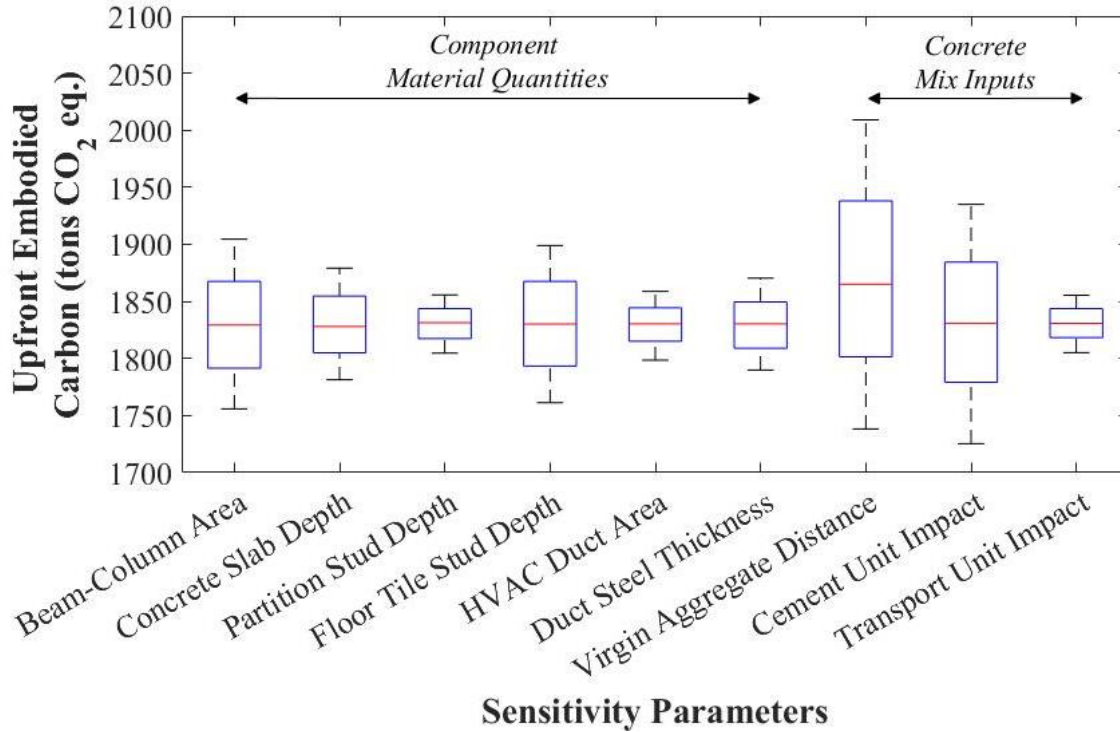


Figure 4.10. Sensitivity of upfront embodied carbon for a functional unit constructed with normal concrete. The parameters on the left are material quantities for structural and non-structural building components, while the parameters on the right are inputs to a unit of concrete. (1 ton = 987 kg).

4.3.5.5 EMBODIED CARBON ASSOCIATED WITH POST-EARTHQUAKE LOSSES

Quantifying the environmental impacts—here, embodied carbon—of seismic losses is a still-developing field. Moreover, only a few published studies have investigated this topic relative to changes in structural material properties, such as Rodriguez-Nikl *et al.* (2012) described above or in the study by Welsh-Huggins and Liel (2017, which applied scale factor multipliers to increase unit embodied carbon of higher strength concrete designs). Welsh-Huggins and Liel (2016) details our procedure to combine the results of loss analysis calculations, i.e. identification of damaged components and repair costs, with descriptions of repair actions, to quantify specific material volumes necessary for building component repairs. For each realization in the loss analysis, the material quantities for post-earthquake repairs and replacement are multiplied by their respective unit embodied carbon impacts. Unit embodied carbon impacts for the concrete materials are computed using the median impact values presented in Section 4.3.5.3.

Figure 4.11 presents vulnerability functions comparing median post-earthquake embodied carbon (median unit embodied carbon impacts for post-earthquake manufacturing of all building

repair/replacement materials) as a function of the ground shaking intensity, when the functional unit is constructed with each of the seven alternative concrete types. At low levels of shaking ($Sa(T_1=0.87s) < 1.37g$), nonstructural components dominate repair actions meaning that post-earthquake repairs produce similar levels of embodied carbon regardless of the functional unit. However, slight differences in the results are observed depending on the structural response from dynamic analysis, and levels of damage experienced by each building. Specifically, the buildings with a higher percentage of RCA experience greater peak floor acceleration and interstory drifts, due to their larger flexibility and ductility. These demands lead to somewhat larger embodied carbon seismic losses for these buildings.

At higher hazard levels, losses are dominated by structural repairs or post-collapse replacement. In this scenario, the higher unit embodied carbon impacts of the RCA concretes outweighs savings from the lower probabilities of collapse of these buildings, which means that embodied carbon losses for the RCA concrete buildings remain higher than when the functional unit uses fly ash or normal concretes. By comparison, the lower unit embodied carbon impacts of the fly ash concretes means that post-earthquake embodied carbon may be lower at hazard levels with greater shaking intensities than at those with slightly lower shaking intensities, where repairs to structural concrete elements are more likely than nonstructural repairs (see the dip in these results in Figure 4.11 at approximately 2.5g). At greater shaking intensities where more components require replacement instead of repairs, this decreased impact may also occur given that the embodied carbon associated with manufacturing repair materials may exceed that of manufacturing a component entirely anew.

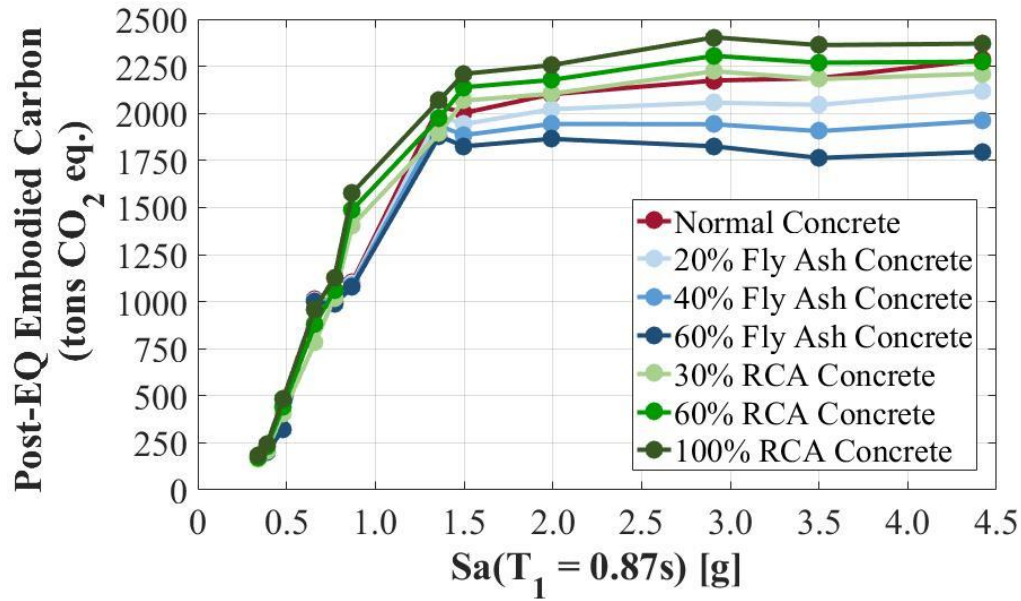


Figure 4.11 Vulnerability functions quantifying changes in median post-earthquake embodied carbon when the functional unit is constructed with each alternative concrete type, considering median unit impacts, transportation distances, and material quantities. (1 ton = 987 kg).

4.3.5.6 UNCERTAINTY OF EMBODIED CARBON IMPACTS IN POST-EARTHQUAKE LIFE CYCLE STAGE

The results shown in Figure 4.11 represent a deterministic calculation of the embodied carbon associated with each building’s post-earthquake life cycle stage. However, these calculations are based on a series of assumptions regarding the repair material quantities for each damage state of each building component, as well as the potential unit embodied carbon impacts of each alternative concrete type. Next, uncertainty analysis is used to quantify the sensitivity of the post-earthquake embodied carbon outcomes to variations in assumptions made for the seismic loss analysis.

We first identify the material and component types for which repair quantity assumptions are most likely to impact post-earthquake embodied carbon values. In Chapter 3, Welsh-Huggins and Liel (2017) found that beam-column components, repairs to ceiling tiles, interior wall partitions, and exterior concrete cladding components can contribute significantly to embodied carbon generated by post-earthquake repairs. The results of the uncertainty/sensitivity study presented in Figure 4.10, which examines assumptions affecting upfront embodied carbon, suggest that variations to the beam-column dimensions, the depth of the floor slabs, the size of the metal studs in wall partitions and floor tiles, and the area and thickness of HVAC ducts may also influence distributions of total post-earthquake repair embodied carbon.

Accordingly, we select a set of materials (required to repair both non-structural and structural components) for which the unit repair quantities in each damage state are expected to produce uncertainty in the functional unit’s post-earthquake embodied carbon outcomes. In addition, the sensitivity of the post-earthquake embodied carbon outcomes to variations in the unit embodied carbon impacts of the alternative concretes is also considered (the complete list of uncertainty analysis parameters is presented in Table 4.6). Thus, uncertainties in post-earthquake embodied carbon outcomes at each hazard level include those related to 1) levels of damage (*i.e.* probabilities of being in each damage state and number of units damaged) for each component, 2) unit quantities of repair materials at each damage state for various components, and 3) embodied carbon impacts from producing a unit of each alternative concrete, which includes variations in the unit environmental impacts from raw material production, freight transportation, and concrete plant energy generation, as well as distributions of material transportation distances from their processing/extraction source to a concrete mixing plant. As described above, the uncertainty analysis uses Monte Carlo simulation to vary each parameter in Table 4.6 individually to quantify its impact on the distributions of embodied carbon associated with hazard level seismic loss.

Table 4.6. Material repair quantities and concrete embodied carbon impact parameters varied in uncertainty analysis of post-earthquake embodied carbon outcomes.

Assumption Category	Parameter Quantity
<i>Beam-column repairs</i>	Structural concrete volume
<i>Exterior cladding repairs</i>	Non-structural concrete volume
<i>Floor slab repairs</i>	Concrete depth
<i>HVAC system repairs</i>	Non-structural steel depth
<i>Interior partition repairs</i>	Paint area
	Gypsum board volume
	Non-structural steel stud volume
	Wallpaper area
<i>Raised access floor tile repairs</i>	Non-structural steel tracking volume
<i>Suspended ceiling tile repairs</i>	Fiber glass panel area
	Non-structural steel tracking volume
<i>Alternative concrete embodied carbon impact variables</i>	Cement production unit impact
	Fly ash production unit impact
	Virgin aggregate (coarse & fine) production unit impact
	RCA production unit impact
	Electricity generation unit impact
	Freight transport emissions unit impact
	Cement transportation distance
	Fly ash transportation distance
	Virgin aggregate transportation distance
RCA transportation distance	

Figure 4.12 presents the uncertainty analysis results for the three parameters that contribute the most variability to post-earthquake embodied carbon outcomes: structural concrete repair quantities, non-structural steel repair quantities (dominated by ceiling tile steel repairs), and virgin aggregate transportation distances. The influence of repair material quantity assumptions on fly ash concrete building is the same as for the normal concrete building. As such, fly ash concrete building results are shown only to illustrate the influence of transportation distance assumptions on post-earthquake embodied carbon. In addition, trends (although not magnitudes) in the variability of post-earthquake embodied carbon outcomes are similar for the three RCA concrete buildings, and so are presented only for one alternative concrete design (60% RCA).

At moderate ground shaking intensities ($Sa(T_1=0.87s)=1.50g$), Figure 4.12(a) demonstrates that non-structural steel repair quantity assumptions produce more variability in post-earthquake embodied carbon for the more flexible and ductile RCA concrete building than for the normal concrete building, due to increased non-structural losses. At greater shaking intensities (e.g. Figure 4.12(b) for $Sa(T_1=0.87s)=2.91g$), uncertainty in assumptions for beam-column concrete repair quantities produce significant variability in post-earthquake embodied carbon for all RC building variations, due to increasing likelihood of structural repairs/total collapse. The results of the uncertainty analysis suggest, however, that variations in damaged material repair quantities, while significant, will not greatly change trends in post-earthquake embodied carbon.

Similar to the upfront embodied carbon uncertainty analysis (Figure 4.8), the results in Figure 4.12 show that, regardless of hazard level, post-earthquake embodied carbon outcomes are most sensitive to variations in virgin aggregate transportation distances. The findings suggest that constructing with RCA concrete will decrease sensitivity to virgin aggregate transportation distance, compared to using either normal concrete or fly ash concretes; this finding is unsurprising due to the lesser quantities of virgin aggregate in these RC building variations. Despite the variability in these transport distance assumptions, the 75th percentile of the fly ash concrete building's impacts is only marginally larger than that of the RCA concrete building, due to the higher seismic demand of the RCA concrete. In general, assumptions about the influence of material transport distance and access to cementitious materials on post-earthquake embodied carbon will have significant implications for future studies investigating post-hazard supply chain routes and material availability (a topic beyond the scope of the current research).

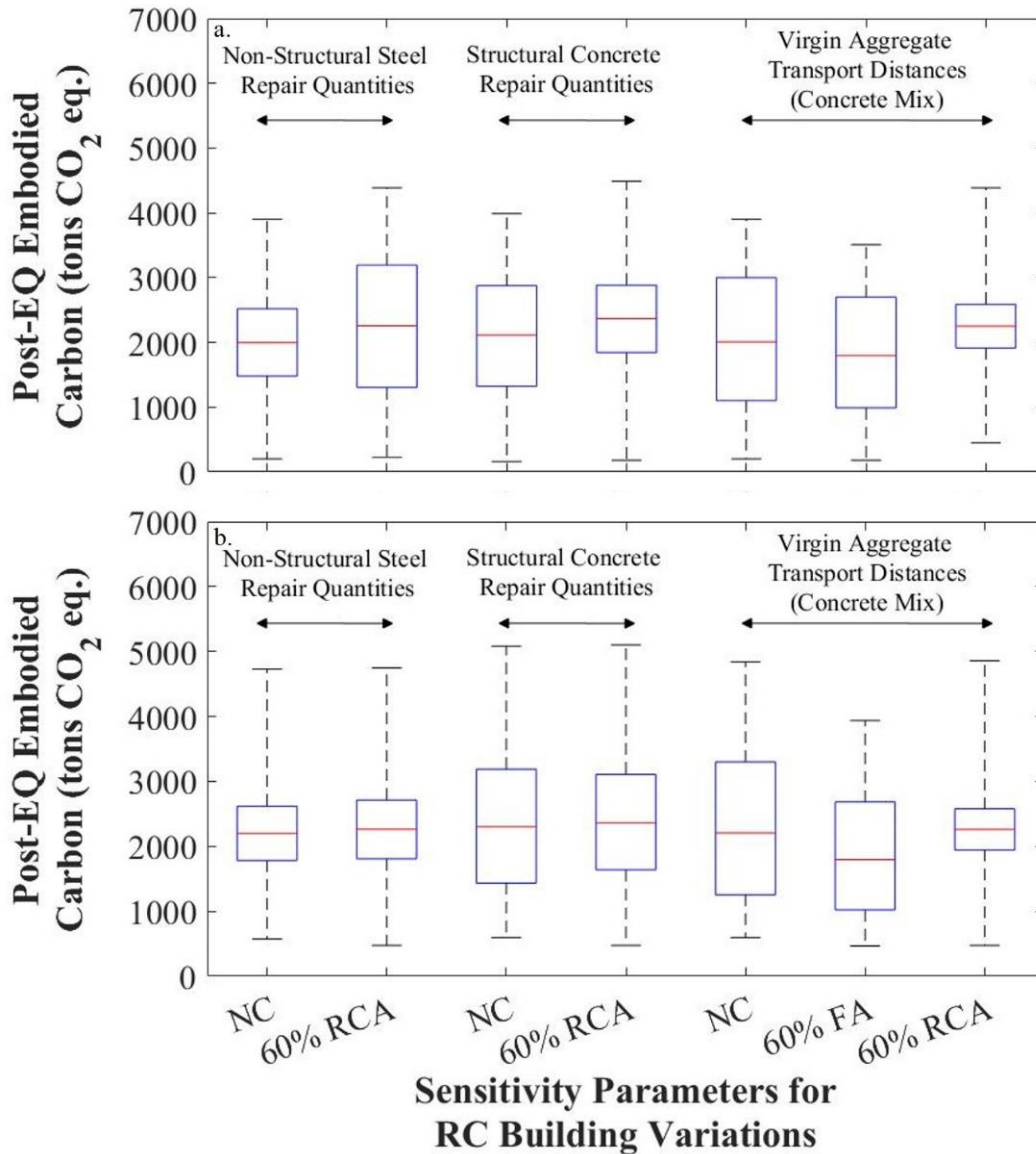


Figure 4.12. Distributions of post-earthquake embodied carbon, considering uncertainties in quantities of repair materials and alternative concrete impact assumptions at a) $S_a(T_1=0.87s)=1.50g$; and b) $S_a(T_1=0.87s)=2.91g$. Figure 4.8(c) shows legend of boxplot features. (1 ton = 987 kg).

4.3.5.7 INFLUENCE OF POST-EARTHQUAKE EMBODIED CARBON ON TOTAL LIFE CYCLE ENVIRONMENTAL IMPACTS

Each of the hazard levels analyzed in the post-earthquake life cycle stage represent potential ground shaking scenarios that may occur during the service life of the functional unit. Next, the calculations described in Section 4.3.4.3 (for computing annualized post-earthquake economic costs) are employed to quantify “total” service life post-earthquake embodied carbon impacts, accounting for the likelihood of different levels of ground shaking occurring. Based on the findings

presented in Chapter 3, the so-called total embodied carbon seismic loss considers no discount rate and, instead, simply sums the “annual” loss over 50 years (Welsh-Huggins & Liel, 2017). Figure 4.13 presents these total life cycle post-earthquake embodied carbon impacts, which represent median values taken from the distributions of all possible variations in embodied carbon outcomes.

Figure 4.13 demonstrates that trends in the magnitude of total post-earthquake embodied carbon (summed over the assumed 50 year service life of the functional unit) are similar to those of the post-earthquake embodied carbon vulnerability functions. Total post-earthquake embodied carbon *decreases* with increasing replacement of cement with fly ash in the building and *increases* with larger replacement of virgin coarse aggregate by RCA in the building. Compared to the total (median) post-earthquake embodied carbon of the functional unit with normal concrete, these results suggest that replacement of 60% of cement with fly ash could decrease total post-earthquake expected carbon by 7.5%. Conversely, replacement of 100% of coarse aggregate with RCA could increase median total post-earthquake expected carbon by 16%. These total post-earthquake embodied carbon values range from the carbon emissions equivalent of driving a typical passenger car roughly 1,140,000 miles, or around 1,830,000 kilometers (for the functional unit constructed with 60% fly ash concrete) to that of driving a car approximately 1,370,000 miles, or around 22,000,000 kilometers (when constructing with 100% RCA concrete) (EPA, 2016b).

These findings also suggest tradeoffs between the upfront and post-earthquake life cycle stage embodied carbon outcomes. Relative to the baseline functional unit, the as-modeled properties of fly ash concretes do not change building collapse capacity or post-earthquake, non-concrete repair impacts. However, fly ash concrete upfront/post-collapse impacts are lower than those of the normal concrete building. Comparatively, the as-modeled properties of RCA concretes increase the magnitude of post-earthquake embodied carbon impacts. Relative to the baseline functional unit, however, the RCA concrete as-modeled properties do reduce upfront *and* post-earthquake transportation-related embodied carbon impacts and also improve collapse capacity.

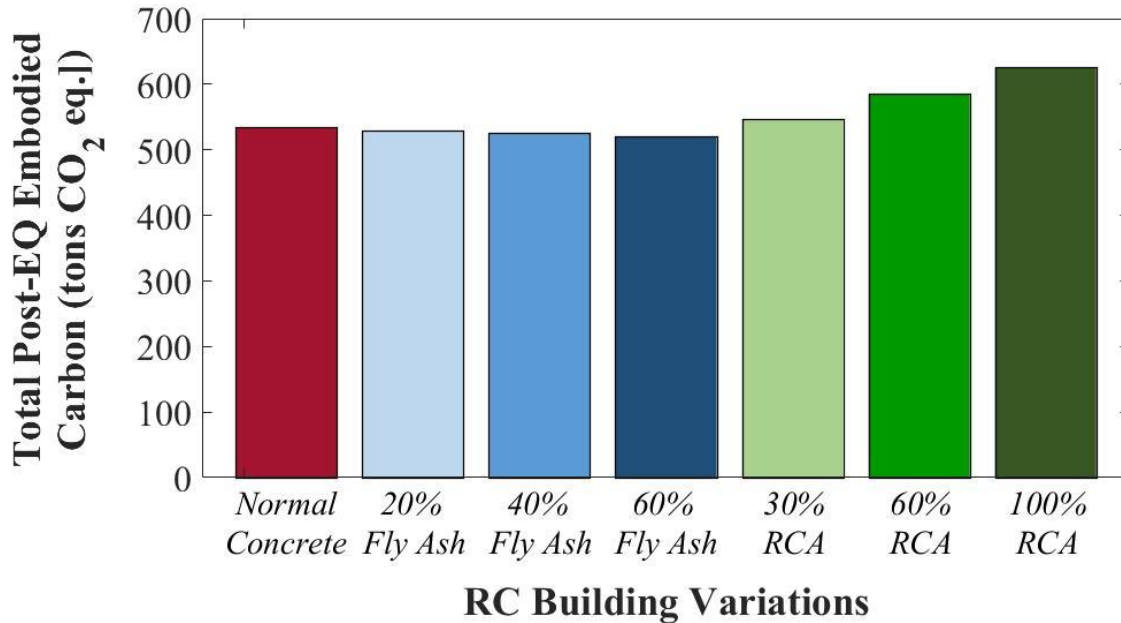


Figure 4.13. Total post-earthquake embodied carbon. Results represent median values, considering distributions of all possible embodied carbon outcomes, conditioned on hazard scenario frequencies of occurrence. (1 ton = 987 kg).

4.4 CONCLUSIONS

This chapter investigates the influence of “green” concrete mixes (here, those designed with fly ash replacing cement or with recycled concrete replacing coarse aggregate) on the life cycle seismic performance of reinforced concrete buildings. To do so, a life cycle analysis is conducted for a functional unit that represents a 4-story, seismically designed, modern, code-compliant, reinforced concrete building in southern Los Angeles. This study employs nonlinear dynamic simulation, probabilistic accounting of embodied carbon, and probabilistic seismic loss assessment in terms of both economic and environmental metrics to quantify impacts from two life cycle stages: upfront (pre-service life) and post-hazard (during service life).

The results suggest that the unit embodied carbon for manufacturing the concretes varied in this study correlates to their cement content and the transportation distances of virgin aggregates. As such, the embodied carbon generated from concrete production in each life cycle stage decreases with replacement of cement by fly ash in concrete and increases with replacement of virgin coarse aggregate by RCA (due to increased cement requirements) in concrete. Thus, fly ash concretes reduce upfront embodied carbon associated with material manufacturing, while RCA

concretes reduce upfront embodied carbon associated with transportation emissions. Although not quantified here, construction with fly ash or RCA concrete also helps to avoid waste impacts from industrial byproducts of coal burning and structural demolition.

Results in the post-hazard life cycle stage suggest that the functional unit's collapse capacity increases slightly with higher percentages of RCA in concrete, due to a somewhat more ductile material level response, while adding fly ash to concrete does not change seismic response. However, RCA concrete buildings also experience higher engineering demands, meaning that they incur greater magnitude and percent contributions of non-collapse damage at each hazard level than do normal concrete buildings. Therefore, post-earthquake economic costs and embodied carbon increase when the functional unit is constructed with a higher percentage of RCA structural concrete, compared to when using normal concrete. Conversely, post-earthquake embodied carbon impacts decrease with increasing higher percentages of fly ash in a building's structural concrete, but economic costs of this stage are unchanged from those of a building using normal concrete. Thus, fly ash concrete buildings reduce post-earthquake embodied carbon associated with concrete repairs, but do not improve seismic performance. RCA concrete buildings, meanwhile, slightly improve collapse capacity, but increase post-earthquake embodied carbon impacts.

The results of a series of uncertainty analyses at the two life cycle stages demonstrate potential variability in the results, due to sources of uncertainty in the life cycle system boundary and the assumptions about material quantities and embodied carbon impacts. The uncertainty analysis shows that while variations in the chosen assumptions for construction and repair material quantities may change the magnitude of (upfront or post-hazard) embodied carbon outcomes, overall trends remain similar. However, the results are most influenced by variations in assumptions regarding transport distances of virgin aggregates, either coarse or fine. Changes in virgin aggregate transportation distances produce greater variability in embodied carbon impacts when constructing the functional unit with normal concrete or fly ash concrete, compared to using RCA concretes. This trend occurs because construction with fly ash or normal concrete requires transportation of the same ton-mileage (or kilogram-kilometer) of virgin aggregate, regardless of transportation distance, while the RCA mixes contain decreasing volumes of virgin aggregate.

Overall, the findings demonstrate that replacing cement with fly ash reduces embodied carbon impacts at both the upfront (by up to 45%) and post-earthquake (by over 7%) life cycle

stages, compared to designing a building with normal concrete. Thus, construction with fly ash concretes may provide an effective design tool achieving a building with low embodied carbon impact over its entire life cycle, even in the context of possible occurrence of a hazard event during its service life. Comparatively, replacing virgin coarse aggregate with RCA in concrete reduces the variability in upfront embodied carbon impacts, but increases the magnitude of post-earthquake economic costs and embodied carbon impacts (up to 23% for economic cost and up to 16% for embodied carbon), relative to a normal concrete building. Therefore, replacing virgin coarse aggregate with RCA benefits “green” hazard-resilient life cycle performance when the objective is to either: 1) improve collapse capacity (increased by 16% from the normal concrete baseline), or 2) decrease coarse virgin aggregate transportation impacts.

Future investigation of this topic should quantify associated life cycle social impacts/costs, as well as other categories of environmental impacts, beyond just embodied carbon. These expansions in scope will support more holistic life cycle sustainability analyses and assessments of infrastructure designed and constructed built with alternative structural materials. With respect to the computational analysis used herein, future work should employ time-dependent models of concrete mechanical properties, to better quantify changes in seismic performance of buildings constructed with alternative concretes, like those assessed here, from material degradation (such as from chloride intrusion) or with later-age strength gains (due to the slow-hardening nature of fly ash concretes). Despite these limitations, the findings from this study support a new direction of research for other engineers, one that investigates how changes at both the material and whole-building levels will influence structural life cycle resilience and sustainability.

Chapter 5 CONCLUSIONS

5.1 SUMMARY

The 21st century building stock has a growing number of buildings designed with green features. The built environment also possesses an increasing vulnerability to extreme hazard events from larger populations and dense urban environments that could be impacted by earthquakes, hurricanes and other disasters. Recent studies have identified a connection between seismic design decisions and reduced post-hazard environmental impacts, but there has been limited quantification or testing of the hazard performance of common green building features. Similarly, some green building rating systems have introduced pilot credits that recognize hazard-resistance as a component of life cycle “greenness,” but such credits are not widely adopted and typically follow a prescriptive, not performance-based, approach; furthermore, the scientific basis for the value of these credits is not well-established. The goal of this dissertation is to quantify the influence of hazard resistant design principles on green building performance—namely, life cycle environmental impact—and to quantify the influence of green building design principles on hazard resilience, focusing here on seismic performance. In doing so, this work also develops a life cycle assessment framework for holistic evaluation of green and hazard resistance performance.

Each of the three chapters uses the same presumed site location in southern Los Angeles, and a set of modern reinforced concrete office buildings in Los Angeles. Chapter 2 presents a framework for the joint assessment of building environmental impact and hazard performance, in the context of green building design choices and earthquake risks to the built environment. The framework is illustrated through an examination of the seismic performance of office buildings with green roofs with different characteristics, evaluated through non-linear dynamic analysis and assembly-based loss analysis and environmental impact assessment. The results from these analyses provide an initial illustration in this dissertation of the challenging tradeoffs for building design decision-makers, as each building offers varying economic, environmental and hazard performance strengths and weaknesses. Chapter 3 investigates the idea that “green” buildings could be designed to withstand higher earthquake and other extreme loads as a tool to reduce environmental impacts associated with post-hazard repairs. To do so, seismic performance and life cycle embodied carbon are quantified for 30 reinforced concrete buildings varying by lateral

strength, ductility capacity, frame type, and height using nonlinear dynamic simulation and probabilistic environmental and economic loss assessment. Chapter 4 presents a holistic life cycle assessment of the influence of alternative concretes (designed with fly ash replacing cement or with recycled concrete replacing coarse aggregate) on building seismic performance. Upfront embodied carbon and seismic performance are computed for a functional unit defined as a 4-story, code-compliant, reinforced concrete building, where upfront construction and post-hazard repair environmental impacts are computed with respect to the series of alternative concrete mix designs.

5.2 FINDINGS

This dissertation makes several methodological contributions toward the development of more holistic life cycle analyses that include the occurrence of hazard events during a structure's lifespan. In addition, the previous chapters, when taken together, provide insight into the tradeoffs and synergies between seismic performance and life cycle environmental impact in support of broader goals for the intersection of hazard-resistant and green building design. Finally, the results of these studies point to remaining knowledge gaps in this field and avenues for future research.

5.2.1 METHODOLOGICAL CONTRIBUTIONS

This dissertation presents an innovative methodology to transform building component damage fragilities into specific material volumes for post-hazard component restoration and then to translate these material quantities into distributions of post-hazard environmental impacts. This framework is not limited in application to only earthquake hazards or buildings; the same approach could be taken to link damage fragilities and subsequent environmental impacts for a wide range of infrastructure types (such as bridges or pipelines) and hazard events (including other acute hazards, such as hurricanes, and including chronic hazards, such as time-dependent material degradation). Moreover, although the framework results were presented in this dissertation with respect to embodied carbon, the same calculations could be made for any environmental impact (*e.g.* acidification, eutrophication, etc.) of concern. Overall, the framework provides a tool to assess the environmental impacts and hazard resistance of buildings in tandem, rather than as isolated considerations.

In addition, this dissertation applies the concept of multi-objective analysis (MOA) to evaluate the multi-metric, systems-based nature of building life cycle analysis. A major challenge

for the integration of green building and hazard-resistant design philosophies is comparing the relative impact of design and analysis categories across multiple units of measurement. In some cases, other researchers have chosen to monetize environmental impact analysis results and present a total monetary score for integrated green-resilience. However, converting to a single unit of measurement removes the nuanced importance inherent to the specific units of measurement of each technical, social, economic, and environmental category. The results in Chapter 3 show that a MOA approach can provide a useful decision-making tool to quantify structural performance (*e.g.* material strength as lbs/ft², collapse capacity as spectral acceleration etc.) alongside life cycle cost (monetary units) and life cycle environmental impacts (*e.g.* greenhouse gas emissions, embodied energy, water consumption, etc.), because MOA results support a more holistic understanding of the costs and benefits of different design decisions. In addition, the results of Chapter 4 demonstrate how traditional life cycle analysis and assessment methodologies can be adapted to holistically quantify total economic and environmental costs/impacts produced over a structure's lifespan, considering alternative structural materials (such as more "green" concretes) alongside potential occurrence of acute hazards (including, but not limited to earthquake events).

5.2.2 INFLUENCE OF STRUCTURAL AND MATERIAL CHANGES ON BUILDING LIFE CYCLE ENVIRONMENTAL IMPACT AND SEISMIC PERFORMANCE

Chapter 2 first presents the life cycle assessment framework employed throughout this thesis to evaluate impacts of green and hazard-resistant design decisions. The framework is illustrated in this chapter with a case study of an office building in Los Angeles, designed with and without different vegetated or green roof systems, and at risk from varying seismic ground shaking hazard scenarios. This chapter shows that the buildings with larger roof loads (and hence higher member sizes) experience more seismic damage during intense shaking, but better withstand low-to-moderate shaking. Damaged buildings with higher roof loads are associated with greater post-hazard CO₂ emissions, due to greater volumes of material to repair/replace larger structural members. This study indirectly identifies the influence of member size and design strength on environmental and seismic performance, where members are "up-sized" to support green roof systems. The findings from this chapter suggest that structural changes to support added green roof mass can negatively impact seismic performance, in terms of decreased hazard resistance and subsequently increased post-earthquake embodied carbon. However, reductions in operational

energy consumption from the use of green roof systems may counterbalance life cycle environmental impacts, depending on the expected level of seismic hazard for a building lifespan.

Chapter 3 is motivated by qualitative suggestions by professional engineering organizations that designing a building to withstand higher seismic, or other hazardous, load cases could result in a “greener” building, from reduced post-hazard losses. The results of this study suggest that increasing lateral strength does reduce embodied carbon seismic losses. Trends in seismic losses for enhanced ductility designs are less clear, however, because embodied carbon losses relate to the percentage and magnitude of contribution of non-collapse versus collapse losses; that is, collapse losses tend to decrease with higher ductility capacity, but at the expense of larger non-collapse losses. In conclusion, the results show that increases in upfront embodied carbon required to achieve enhanced lateral strength can be offset by significant reduction in future post-earthquake losses, for a net savings in embodied carbon. These benefits from enhanced strength will be more significant in regions of high seismicity. Enhanced ductility capacity, however, can increase upfront embodied carbon (due to larger member sizes) *and* post-earthquake embodied carbon (from more non-structural losses). Chapter 3 also introduces the MOA method described above. Normalizing the results of each building to those of a baseline structure across multiple design and analysis categories quantifies the relative strengths and weaknesses of each design for decision-making prioritization. The MOA results suggest that enhanced lateral strength can produce more resilient (higher collapse capacities and lower economic seismic loss) and greener (lower seismic loss embodied carbon) outcomes than a code-compliant design. Moreover, upfront increases in embodied carbon can be offset by avoided post-earthquake impacts, compared to potential losses for the code-compliant baseline. The results of this analysis suggest that, in some cases, enhancing design goals for hazard resistance (*i.e.* increasing lateral strength) can support green building design objectives by reducing hazard-related embodied carbon.

Chapter 4 considers the influence on building seismic performance from using alternative concretes presumed to be “green.” The study shows that the unit embodied carbon of these concretes correlates to their cement content, such that embodied carbon *decreases* with replacement of cement by fly ash and *increases* with replacement of virgin coarse aggregate by recycled concrete (due to increased cement requirements). In addition, the collapse capacity of a building increases with higher percentages of RCA concrete due to a somewhat more ductile

material level response. However, RCA concrete buildings also experience higher engineering demands, meaning that they incur greater magnitude and percent contribution of non-collapse damage at each considered hazard level than do normal concrete buildings. Replacing cement with fly ash in concrete slightly enhances compressive strength, but these gains are insufficient to either improve collapse capacity or reduce seismic demand. In total, probabilistic seismic loss analysis shows that, for buildings with higher percentage of RCA in concrete, post-earthquake economic costs and embodied carbon *increase*, compared to a normal concrete building. Instead, for buildings with higher percentage of fly ash in concrete, post-earthquake embodied carbon *decrease*, while post-earthquake economic costs are *unchanged* from a normal concrete building. Expanded use of fly ash concrete in the future may be limited by continued divestment from coal plant power in the U.S., but at the present moment adoption of fly ash concretes in RC building design supports goals for both green building outcomes and hazard resistant objectives, in terms of reduced upfront and post-earthquake embodied carbon. In contrast, the many existing concrete structures in the U.S. offer consistent sources of old concrete to recycle into aggregate. However, buildings constructed with RCA concrete—despite protecting depleting sources of natural resources, like granite—worsen seismic performance in terms of economic and embodied carbon losses, despite enhancing collapse capacity, relative to a normal concrete building.

5.2.3 TRADEOFFS BETWEEN GREEN DESIGN AND HAZARD-RESISTANT DESIGN

Taken individually, Chapter 2-Chapter 4 identify and evaluate building design and analysis tradeoffs among green design and hazard-resistant objectives within their own study boundaries and specific building variations. The overall findings from this dissertation, however, have implications far beyond the medium height, reinforced concrete buildings in southern Los Angeles that were the focus of these studies. The following discussion can inform decision-making for integrating sustainable and resilient practices in a broad range of building design scenarios:

5.2.3.1 RELATIONSHIP BETWEEN BUILDING DAMAGE AND POST-EARTHQUAKE EMBODIED CARBON

The results of Chapter 3 and Chapter 4 show that high non-structural losses increase non-collapse contributions to embodied carbon, which can subsequently increase total hazard level environmental impacts (even compared to another building with a higher collapse risk). Indeed, at hazard levels dominated by non-collapse impacts, the material quantities needed to restore damaged non-structural components often require production of larger volumes of more CO₂-

intensive materials than are required to repair damaged structural components at the same shaking intensities. Chapter 4 also shows, that for two buildings having similar probabilities of collapse and similar levels of non-collapse damage, the building with a larger building replacement cost in terms of embodied carbon, may experience higher total seismic losses. This finding suggests that perhaps more of the upfront (total building) investment cost should be made in the quality and hazard-resistance of non-structural components, to reduce their potential damage in future hazard events. The importance of non-structural component repairs for post-earthquakes environmental impacts are expected to be similar regardless of the building type, structural material, environmental impacts of concern, or regional natural hazard chosen for assessment.

5.2.3.2 IMPACT OF BUILDING DUCTILITY CAPACITY ON ENVIRONMENTAL IMPACTS

Previous studies have documented how improved ductility capacity increases non-structural loss, because damage is more dispersed throughout a structure. In addition, the findings of Chapter 3 and Chapter 4 suggest that structural design for enhanced ductility/deformation capacity may require changes in structural member size or material properties that will increase building embodied carbon, at both upfront and post-collapse building life cycle stages. The results further demonstrate that when two buildings have similar collapse probabilities at a given shaking intensity, the more ductile building can produce higher total post-earthquake embodied carbon, due to the increased magnitude and percentage of non-structural losses.

These relationships between ductility capacity and life cycle embodied carbon are expected to be similar for buildings of other material types or structural systems, like steel. Impacts from upfront embodied carbon relate to volumes of materials based on member size, while post-hazard levels of embodied carbon are connected to how non-structural components experience seismic demands within a structure. The findings of these studies therefore contribute to a growing discussion in the structural engineering community, which debates the benefits of enhanced ductility capacity if it supports goals of collapse prevention, but not immediate occupancy. For example, if the goal of a building designer is to reduce collapse probability, enhanced ductility capacity may support this objective. However, if the design goal is to achieve rapid post-hazard restoration of full building functionality or to reduce overall environmental impact, it may be more beneficial to enhance lateral strength instead of ductility/deformation capacity, due to the greater volume of non-structural losses from a more ductile structure.

5.2.3.3 IMPACT OF LATERAL STRENGTH ON ENVIRONMENTAL IMPACTS

The results of the studies presented here show a more direct relationship between increasing lateral strength and reducing post-hazard environmental impact than with enhancing ductility capacity. However, “up-sizing” structural member dimensions to achieve gains in lateral strength, as described in Chapter 2-Chapter 3, introduces tradeoffs between higher upfront embodied carbon impact, from the larger material volumes of bigger member sizes and enhanced collapse capacity and/or reduced non-structural and structural losses. Enhanced lateral strength is expected to be generally beneficial in regions of high seismic risk, where even structures with code-compliant strengths are vulnerable to exceedance by rare ground motions and the benefits in terms of reduced post-earthquake damage outweigh the upfront carbon costs, regardless of structure type (building, bridge, etc.) or material choice (steel, concrete, etc.).

5.2.3.4 IMPACT OF GREEN TECHNOLOGIES ON HAZARD RESISTANCE

Chapters 2 and 4 demonstrate that designing “green,” with respect to either non-structural components like green, vegetated roofs, or structural material design choices like fly ash concrete, is not necessarily harmful to hazard resistance, but can, in certain cases, introduce conflicts between different design objectives. For example, the green roof systems in Chapter 2 reduce operational energy costs, but may change building response under seismic loads and require up-sizing of structural members. Similarly, using recycled concrete as aggregate in new concrete may make a building more ductile, thus somewhat increasing collapse capacity. However, this recycled aggregate concrete requires greater cement content, which can substantially increase unit environmental impacts. The findings of these chapters encourage engineers to assess other green building features, like solar panels or energy-efficient window glazing, or other alternative building materials, like modular timber construction or concrete that replaces cement with blast slag, in the context of hazard performance objectives and to not assume that designing for sustainability goals need be a compromise on a structure’s hazard resistance.

5.3 FUTURE WORK

There are several possible avenues for future research that could either improve understanding of the relationship between seismic performance and life cycle environmental impact of modern buildings (including, but not limited to, RC frame structures) or extend the results presented in the preceding chapters. These future research directions can be broadly organized into several

categories: experimental testing and model development for green materials/green building features, treatment of sources of analysis, and decision-making analysis tools.

5.3.1 EXPERIMENTAL TESTING AND MODEL DEVELOPMENT FOR GREEN MATERIALS AND BUILDING FEATURES

One of the limitations of the seismic analysis results discussed in this dissertation is the lack of damage fragility functions developed specifically for green building features, such as the vegetated, green roofs presented in 1.1, or components made of innovative structural materials, such as the alternative concrete designs evaluated in Chapter 4. Experimental testing of these types of components and/or materials would help to develop representative equations of the relationships between hazard intensity, expected levels and type of damage, and economic repair costs to better predict the seismic performance of green building features, which are increasingly common in real-world structural applications. Efforts should also be made to document seismic damage to these components in reconnaissance activities after future earthquakes.

Expanding the analysis presented in Chapter 4 to consider other types of building materials, such as timber or steel, or other alternative concrete types, such as replacement of cement with additional supplementary cementitious materials like slag or silica fume, would further elucidate how structural material choice influence tradeoffs between green building and hazard-resistant design principles. In addition to analyzing other building materials, future model development should consider the time-dependent materials properties to better represent potential longer-term changes in concrete strength or material degradation caused by chemical attacks like chloride intrusion. Future work should analyze the structural response of buildings with structural material models that include mechanical properties degradation over time and subsequently how seismic performance is affected by the occurrence of hazard events at different points in time.

5.3.2 TREATMENT OF UNCERTAINTIES

Chapter 4 presents the results of several uncertainty analyses that investigate the sensitivity of upfront and post-earthquake embodied carbon outcomes to assumptions about material quantities and unit embodied carbon impacts. Lack of confidence in the reliability of available literature sources that define building construction and repair material quantities can produce significant uncertainty and variability in the magnitude of embodied carbon impacts for a structure, but are

unlikely to change overall trends between different building designs. However, this study provides only an introductory exploration of how variability in structural design, post-hazard repair, and embodied carbon assumptions may affect life cycle environmental impacts. Future studies should revisit this topic in more detail.

Another opportunity to account for hazard damage variability would be to quantify post-earthquake embodied carbon (or other environmental impacts) for either the occurrence of multiple earthquake events over a building's lifespan or for damage incurred in mainshock-aftershock earthquake sequences. After each hazard event, assuming collapse does not occur, building component repairs and replacement are required to restore functionality and continue the structure's service life. The proposed analysis would provide an important understanding of how present value environmental impacts of smaller, repeated post-hazard repair activities over a building lifespan compares to the impact of building restoration after only one large hazard event.

5.3.3 DECISION-MAKING ANALYSIS TOOLS

A final area for future work is development of analysis tools and methodologies with practical utility to evaluate the relative value of different seismic design decisions, in the context of both green building design and hazard-resistant design. Three suggestions are offered to meet this goal:

- Development of a software tool, or add-in to an existing loss analysis program like the Seismic Prediction Performance Program, which would translate damage fragilities and repair actions into repair material volumes and associated embodied carbon impacts. Such a software tool should also compare upfront carbon impacts, as is already being integrated in some building information modeling (BIM) programs.
- Seismic design codes regulate structural response by placing limits on permissible levels of floor accelerations and story drifts at design level hazard intensities. Future development of the building code, or green building rating systems, could take a similar approach by specifying maximum allowable upfront and/or post-hazard environmental impacts. Then, designers could demonstrate that both initial material production of selected structural and non-structural systems, as well as potential post-hazard repairs for incurred damage at design level hazard events, will not exceed this environmental impact limit.
- Similarly, the decision to enhance lateral strength above code-mandatory levels will depend on the desired life cycle objectives of a designer, but offers a possible avenue for

incorporating principles of hazard-resistance into green building rating systems. For example, structures with regional seismic, or other extreme load, hazard risk could be credited for demonstrating increases in lateral strength above code-minimum specifications. Moreover, these credits could potentially be awarded as proportional to a design's proposed level of increased strength.

5.4 CONCLUDING REMARKS

With increasing urban hazard vulnerability, potential life cycle environmental impacts and hazard performance of buildings must be considered in tandem, not in isolation. The longevity of infrastructure in the 21st century will depend on harmonious, not harmful, interactions with the natural environment, and a structure's ability to not just withstand hazard events, but to adapt from them. This dissertation provides a new framework within which these holistic performance levels can be assessed and presents multi-objective analysis as a tool to evaluate the multi-metric nature of joint hazard-resistant and green building design. In addition, these studies identify and quantify several tradeoffs between upfront and post-hazard impacts for building designers to consider when selecting structural design systems, structural materials, or green building non-structural components. This research shows that hazard-resistant design principles can assist green building objectives for life cycle environmental impacts and, at the same time, green design philosophies can support performance-based engineering goals for life cycle hazard resilience. The analysis approach suggested here and its subsequent findings encourage inclusion of green building factors in hazard-resilient design practices and vice versa, and more broadly, encourage consideration of both economic and environmental impacts when calculating the life cycle cost of seismic losses.

REFERENCES

- ACI 211. (2009). *211.1-91: Standard Practice for Selecting Proportions for Normal, Heavyweight, and Mass Concrete*. ACI Committee 211. Farmington Hills, MI: American Concrete Institute.
- ACI 318. (2011). *Building code requirements for structural concrete (ACI 318-11) and commentary (ACI 318R-11)*. Farmington Hills, MI: American Concrete Institute.
- Almufti, I., & Willford, M. (2013). The resilience-based earthquake design initiative (REDi™) rating system. *Arup Publications*, (October).
- Althaus, H.-J., Kellenberger, D., Doka, G., & Künniger, T. (2005). Manufacturing and disposal of building materials and inventorying infrastructure inecoinvent. *The International Journal of Life Cycle Assessment*, 10(1), 35–42.
- Anagnos, T., Comerio, M. C., & Stewart, J. P. (2016). Earthquake loss estimates and policy implications for nonductile concrete buildings in Los Angeles. *Earthquake Spectra*, 32(4), 1951–1973.
- Arroyo, D., Ordaz, M., & Teran-Gilmore, A. (2015). Seismic loss estimation and environmental issues. *Earthquake Spectra*, 31(3), 1285–1308.
- ASCE. (2010). *Minimum design loads for buildings and other structures: ASCE/SEI 7-10*. Reston, VA: American Society of Civil Engineers.
- ASHRAE. (2014). *Advanced energy design guide for small to medium office buildings*. Atlanta, GA: ASHRAE.
- ASTM C618-15. (2015). *Standard specification for coal fly ash and raw or calcined natural pozzolan for use in concrete*. West Conshohocken, PA: ASTM International. Retrieved from www.astm.org
- ATC. (2012a). *Seismic performance assessment of buildings. Volume 1 - Methodology* (Vol. 1). Redwood City, CA: Applied Technology Council.
- ATC. (2012b). *Seismic performance assessment of buildings. Volume 2 - implementation guide* (Vol. 2). Redwood City, CA: Applied Technology Council.
- Bairagi, N. K., Ravande, K., & Pareek, V. K. (1993). Behaviour of concrete with different proportions of natural and recycled aggregates. *Resources, Conservation and Recycling*, 9(1–2), 109–126.
- Baker, J. (2011). Conditional mean spectrum: tool for ground-motion selection. *Journal of Structural Engineering*, 137(3), 322–331.
- Baker, J. (2015). Efficient analytical fragility function fitting using dynamic structural analysis. *Earthquake Spectra*, 31, 579–599.
- Baker, J. W., & Cornell, C. A. (2003). Uncertainty specification and propagation for loss estimation using FOSM methods. *PEER Report*, (2003/07).
- Berke, P. R. (1995). Natural-hazard reduction and sustainable development: a global assessment. *Journal of Planning Literature*, 9(4), 370–382.
- Bilec, M. M., Ries, R. J., & Matthews, H. S. (2010). Life-cycle assessment modeling of construction processes for buildings. *Journal of Infrastructure Systems*, 16(3), 199–205.
- Bilec, M., Ries, R., Matthews, H. S., & Sharrard, A. L. (2006). Example of a hybrid life-cycle assessment of construction processes. *Journal of Infrastructure Systems*, 12(December), 207–215.
- Bocchini, P., Frangopol, D. M., Ummenhofer, T., & Zinke, T. (2014). Resilience and sustainability of civil infrastructure: toward a unified approach. *Journal of Infrastructure Systems*, 4014004, 1–16.
- Bokalders, V., & Block, M. (2010). *The Whole Building Handbook*. London: earthscan.
- BREEAM. (2015). What is BREEAM? Retrieved from www.breeam.org

References

- Bruneau, M., Chang, S. E., Eguchi, R. T., Lee, G. C., O'Rourke, D., Reinhorn, A. M., ... von Winterfeldt, D. (2004). A framework to quantitatively assess and enhance the seismic resilience of communities. In *13th World Conference on Earthquake Engineering*. Vancouver, Canada.
- Carbon Leadership Forum. North American product category rules for ISO 14025 type III environmental product declarations and/or GHG protocol conformant product "carbon footprint" of concrete (2012).
- Carmody, M. O., Jasarevic, M., Omenzetter, P., Clifton, G. C., & Fassman, E. A. (2009). Seismic response of green roofs. In *2009 NZSEE Conference* (pp. 1–9).
- CEC. (2008). Green building in North America. In *Secretariat Report to Council under Article 13 of the North American Agreement on Environmental Cooperation*. Commission for Environmental Cooperation. Retrieved from www.cec.org/Storage/61/5386_GB_Report_EN.pdf
- Changqing, W., & Jianzhuang, X. (2013). Study of the seismic response of a recycled aggregate concrete frame structure. *Earthq. Eng. & Eng. Vib.*, *12*(4), 669–680.
- Ching, E. (2014). *Building construction illustrated*. Hoboken, New Jersey: Wiley.
- Chiu, C. K., Chen, M. R., & Chiu, C. H. (2013). Financial and environmental payback periods of seismic retrofit investments for reinforced concrete buildings estimated using a novel method. *J. Archit. Eng.*, *19*(2), 112–118.
- Ciroth, A., & Srocka, M. (2008). How to obtain a precise and representative estimate for parameters in LCA. A case study for the functional unit. *International Journal of Life Cycle Assessment*, *13*(3), 265–277.
- Cole, R. J., & Kernan, P. C. (1996). Life-cycle energy use in office buildings. *Building and Environment*, *31*(4), 307–317.
- Comber, M. V., & Poland, C. D. (2013). Disaster resilience and sustainable design: quantifying the benefits of a holistic design approach. *Structures Congress 2013*, 2717–2728.
- Comber, M. V., Poland, C., & Sinclair, M. (2012). Environmental impact seismic assessment: application of performance-based earthquake engineering methodologies to optimize environmental performance. *Structures Congress 2012*, 910–921.
- Cook, S. M. (2014). Sustainable wastewater management: modeling and decision strategies for unused medications and wastewater solids. *University of Michigan, Ph.D. Thes.*
- Court, A. B., Morris, P., Simonen, K., Trusty, W. B., Webster, M., & Heintz, J. A. (2012). *Seismic performance assessment of buildings: volume 4 methodology for assessing environmental impacts*. FEMA P-58-4.
- Court, A., Simonen, K., Webster, M., Trusty, W., & Morris, P. (2012). Linking next-generation performance-based seismic design criteria to environmental performance (ATC-86 and ATC-58). In *Structures Congress 2012* (pp. 922–928).
- Cowing, M. M., Pate, M. E., & Glynn, P. W. (2004). Dynamic modeling of the tradeoff between productivity and safety in critical engineering systems. *Reliability Engineering and System Safety*, *86*, 269–284.
- Davis, M., & Porter, K. (2016). The public's role in seismic design provisions. *Earthquake Spectra*, *In Press*.
- Davis, R. E., Carlson, R. W., Kelly, J. W., & Davis, H. E. (1937). Properties of cements and concretes containing fly ash. *ACI Journal*, *33*(5), 577–612.
- Dhokal, R. P., & Maekawa, K. (2002). Modeling for postyield buckling of reinforcement. *Journal of Structural Engineering*, *128*(9), 1139–1147.
- DOE. (2012). *2011 Buildings energy data book*. Silver Spring, MD: Department of Energy.
- Edelen, A., & Ingwersen, W. (2016). *Guidance on data quality assessment for life cycle inventory data*. Cincinnati, OH.
- EIA. (2016). California profile data, reserves and supply. *U.S. Energy Information Administration*.

References

- Ekvall, T., & Weidema, B. P. (2004). LCA methodology system boundaries and input data in Consequential life cycle inventory analysis. *International Journal of Life Cycle Assessment*, 9(3), 161–171.
- EPA. (2008). *Life cycle assessment: principles and practice*. U.S. Environmental Protection Agency. Cincinnati, OH.
- EPA. (2016a). Emission standards reference guide for on-road and nonroad vehicles and engines. U.S. Environmental Protection Agency. Retrieved from <https://www.epa.gov/emission-standards-reference-guide>
- EPA. (2016b). Greenhouse gas equivalencies calculator. Retrieved from <http://www.epa.gov/energy/greenhouse-gas-equivalencies-calculator>
- Etzeberria, M., Marí, A. R., & Vazquez, E. (2007). Recycled aggregate concrete as structural material. *Materials and Structures*, 40, 529–541.
- Evangelista, L., & de Brito, J. (2010). Durability performance of concrete made with fine recycled concrete aggregates. *Cement and Concrete Composites*, 32(1), 9–14.
- Feese, C., Li, Y., & Bulleit, W. M. (2014). Assessment of seismic damage of buildings and related environmental impacts. *J. Perform. Constr. Facil.*, 29(4), 1–10.
- Filippou, F., Popov, E., & Bertero, V. (1983). Effect of bond deterioration on hysteretic behavior of concrete joints. Report EERC 83-19. *Earthquake Engineering Research Center, University of California, Berkeley*.
- Flint, M. M., Baker, J. W., & Billington, S. L. (2014). A modular framework for performance-based durability engineering: From exposure to impacts. *Structural Safety*, 50, 78–93.
- Flower, D. J. M., & Sanjayan, J. G. (2007). Green house gas emissions due to concrete manufacture. *International Journal of Life Cycle Assessment*, 12(5), 282–288.
- Frondistou-Yannas, S. (1977). Waste concrete as aggregate for new concrete. *ACI Journal*, 74(8), 373–376.
- Gartner, E. (2004). Industrially interesting approaches to “low-CO₂” cements. *Cement and Concrete Research*, 34(9), 1489–1498.
- General Services Administration. (2011). *The benefits and challenges of green roofs on public and commercial buildings: a report of the United States General Services Administration*.
- Goedkoop, M., Oele, M., Leijting, J., Ponsioen, T., & Meijer, E. (2013). *Introduction to LCA with SimaPro*. Amersfoort, The Netherlands: PréSustainability.
- Goulet, C. A., Haselton, C. B., Mitrani-reiser, J., Beck, J. L., Deierlein, G. G., Porter, K. A., & Stewart, J. P. (2007). Evaluation of the seismic performance of a code-conforming reinforced-concrete frame building — from seismic hazard to collapse safety and economic losses. *Earthquake Engng Struct. Dyn.*, 36, 1973–1997.
- Gromala, D. S., Kapur, O., Kochkin, V., Line, P., Passman, S., Reeder, A., & Trusty, W. (2010). *Natural hazards and sustainability for residential buildings*. FEMA P-798.
- Guggemos, A. A., & Horvath, A. (2005). Comparison of environmental effects of steel- and concrete-framed Buildings. *Journal of Infrastructure Systems*, 11(2), 93–101.
- Hammond, G. P., & Jones, C. I. (2006). *Inventory of carbon and energy (ICE), version 1.5a Beta*. Bath, UK.
- Hammond, G. P., & Jones, C. I. (2008). Embodied energy and carbon in construction materials. *Energy*, 161(2), 87–98.
- Hansen, T. C., & Narud, H. (1983). Strength of recycled concrete made from crushed concrete coarse aggregate. *Concrete International*, 5(1), 79–83.
- Haselton, C. B., & Deierlein, G. G. (2007). *Assessing Seismic Collapse Safety of Modern Reinforced Concrete Moment Frame Buildings*. Palo Alto, CA.
- Haselton, C. B., Goulet, C. A., Mitrani-reiser, J., Beck, J. L., Deierlein, G. G., Porter, K. A., & Stewart, J. P. (2008).

References

- An Assessment to Benchmark the Seismic Performance of a Code-Conforming Reinforced Concrete Moment-Frame Building*. Berkeley, CA.
- Haselton, C. B., Liel, A. B., Deierlein, G. G., Dean, B. S., & Chou, J. H. (2011). Seismic collapse safety of reinforced concrete buildings. I: assessment of ductile moment frames. *Journal of Structural Engineering*, 137(4), 481–491.
- Haselton, C. B., Liel, A. B., Taylor-Lange, S. C., & Deierlein, G. G. (2016). Calibration of model to simulate response of reinforced concrete beam-columns to collapse. *ACI Structural Journal*, 113(6), 1141–1152.
- Haselton Baker Risk Group. (2016). Seismic Performance Prediction Program. Retrieved from <http://www.hbrisk.com/>
- Hendrickson, C., Horvath, a, Joshi, S., & Lave, L. (1998). Economic input-output models for environmental life-cycle assessment. *Environmental Science & Technology*, 32, 184a–191a.
- Horvath, A., & Hendrickson, C. (1998). Steel versus steel-reinforced concrete bridges: environmental assessment. *Journal of Infrastructure Systems*, 4(3), 111–117.
- Hossain, K. A., & Gencturk, B. (2014). Life-cycle environmental impact assessment of reinforced concrete buildings subjected to natural hazards. *J. Archit. Eng.*, A4014001(In Press).
- Huntzinger, D. N., & Eatmon, T. D. (2009). A life-cycle assessment of Portland cement manufacturing: comparing the traditional process with alternative technologies. *Journal of Cleaner Production*, 17(7), 668–675.
- Ibarra, L. F., Medina, R. a., & Krawinkler, H. (2005). Hysteretic models that incorporate strength and stiffness deterioration. *Earthquake Engineering & Structural Dynamics*, 34(12), 1489–1511.
- ICC. (2009). *2009 international building code*. Country Club Hills, IL.: International Code Council.
- ISO IEC. (2006). *ISO 14044: Environmental management — life cycle assessment — requirements and guidelines*. International Organization for Standardization. Geneva, Switzerland. Retrieved from http://www.iso.org/iso/iso_catalogue/catalogue_tc/catalogue_detail.htm?csnumber=38498
- Itron. (2006). California commercial end-use survey (CEUS). *California Energy Commission, CEC-400-20*.
- Jacquet, J., Hagel, K., Hauert, C., Marotzke, J., Röhl, T., & Milinski, M. (2013). Intra- and intergenerational discounting in the climate game. *Nature Climate Change*, 3(12), 1025–1028.
- Jalayer, F., & Cornell, C. A. (2009). Alternative non-linear demand estimation methods for probability-based seismic assessments. *Earthquake Engineering & Structural Dynamics*, 38, 951–972.
- Johnson, T. W. (1996). Comparison of environmental impacts of steel and concrete as building materials using the life cycle assessment Method (M.S. Thesis). *U.S. Military Academy*.
- Juenger, M. C. G., Winnefeld, F., Provis, J. L., & Ideker, J. H. (2011). Advances in alternative cementitious binders. *Cement and Concrete Research*, 41(12), 1232–1243.
- Junnla, S., & Horvath, A. (2003). Life-Cycle environmental effects of an office building. *Journal of Infrastructure Systems*, 9(December), 157–166.
- Kajikawa, Y. (2008). Research core and framework of sustainability science. *Sustainability Science*, 3(2), 215–239.
- Kosmatka, S. H., Kerkhoff, B., & Panarese, W. C. (2003). *Design and control design and control of concrete mixtures*. Portland Cement Association (14th ed., Vol. EB001). Shokie, Illinois: Portland Cement Association.
- Lam, L., Wong, Y. L., & Poon, C. S. (1998). Effect of fly ash and silica fume on compressive and fracture behaviors of concrete. *Cement and Concrete Research*, 28(2), 271–283.
- Langley, W. S., Crette, G. G., & Malhotra, V. M. (1989). Structural concrete incorporating high volumes of ASTM Class F fly ash. *ACI Materials Journal*, 86(5), 507–514.

References

- Lawson, A. M., Bersani, K. S., Fahim-Nader, M., & Guo, J. (2002). Benchmark input-output accounts of the United States, 1997. *Survey of Current Business*, (December), 19–109.
- Liel, A. B., & Deierlein, G. G. (2013). Cost-Benefit Evaluation of Seismic Risk Mitigation Alternatives for Older Concrete Frame Buildings. *Earthquake Spectra*, 29(4), 1391–1411.
- Lin, T., Harmsen, S. C., Baker, J. W., & Luco, N. (2013). Conditional spectrum computation incorporating multiple causal earthquakes and ground-motion prediction models. *Bulletin of the Seismological Society of America*, 103(2A), 1103–1116.
- Maher, B. M. H., & Balaguru, P. N. (1993). Properties of flowable high-volume fly ash-cement composite. *J. Mater. Civ. Eng.*, 5(2), 212–225.
- Malhotra, V. M. (1986). Superplasticized fly ash concrete for structural applications. *Concrete International*, 8(12), 28–31.
- Malhotra, V. M. (1990). Durability of concrete incorporating high-volume of low-calcium (ASTM Class F) fly ash. *Cement and Concrete Composites*, 12(4), 271–277.
- Marinkovic, S., Radonjanin, V., Malesev, M., & Ignjatovic, I. (2010). Comparative environmental assessment of natural and recycled aggregate concrete. *Waste Management*, 30(11), 2255–2264.
- Mehta, P. K., & Gjordv, O. E. (1982). Properties of portland cement concrete containing fly ash and condensed silica-fume. *Cement and Concrete Research*, 12(5), 587–595.
- Menna, C., Asprone, D., Jalayer, F., Prota, A., & Manfredi, G. (2013). Assessment of ecological sustainability of a building subjected to potential seismic events during its lifetime. *International Journal of Life Cycle Assessment*, 18(2), 504–515.
- Meyer, C. (2009). The greening of the concrete industry. *Cement and Concrete Composites*, 31(8), 601–605.
- Mileti, D. S., & Peek-Gottschlich, L. (2001). Hazards and sustainable development in the United States. *Risk Management*, 3(1), 61–70.
- Mitrani-Reiser, J., Haselton, C., Goulet, C., Porter, K., Beck, J., & Deierlein, G. (2007). Evaluation of the seismic performance of a code-conforming reinforced-concrete frame building - Part II: loss estimation. *Earthquake Engng Struct. Dyn.*, 36(13), 1973–1997.
- Moehle, J. P., & Deierlein, G. G. (2004). A framework methodology for performance-based earthquake engineering. In *Proceedings of 13th World Conference on Earthquake Engineering*. Vancouver, Canada.
- Moehle, J. P., Hooper, J. D., & Lubke, C. D. (2008). *Seismic design of reinforced concrete special moment frames: a guide for practicing engineers. NEHRP Seismic Design Technical Brief No. 1*. Gaithersburg, MD. Retrieved from <http://nvlpubs.nist.gov/nistpubs/gcr/2008/gcr08-917-1.pdf>
- Naik, T. R., Singh, S., & Ramme, B. (1998). Mechanical properties and durability of concrete made with blended fly ash. *ACI Materials Journal*, 95(4), 454–462.
- Nisbet, M. A., Marceau, M. L., & VanGeem, M. G. (2002). Life cycle inventory of Portland cement concrete. *Portland Cement Association*.
- NRCA. (2007). *The NRCA green roof systems manual*. Rosemont, IL: National Roofing Contractors Association.
- O'Brien, K. R., Ménaché, J., & O'Moore, L. M. (2009). Impact of fly ash content and fly ash transportation distance on embodied greenhouse gas emissions and water consumption in concrete. *International Journal of Life Cycle Assessment*, 14(7), 621–629.
- Padgett, J. E., & Tapia, C. (2013). Sustainability of natural hazard risk mitigation: life cycle analysis of environmental indicators for bridge infrastructure. *Journal of Infrastructure Systems*, 19(December), 395–408.
- Padgett, J., & Li, Y. (2016). Risk-based assessment of sustainability and hazard resistance of structural design. *J. Perform. Constr. Facil.*, 30(2).

References

- Pate-Cornell, M. E. (1984). Discounting in risk analysis: capital vs. human safety. In M. Grigoriu (Ed.), *Risk, structural engineering and human error*. Waterloo, Canada: University of Waterloo.
- Peck, S., & Kuhn, M. (2003). *Design guidelines for green roofs*. Toronto, Canada. Retrieved from http://www.epa.gov/region8/greenroof/pdf/design_guidelines_for_green_roofs.pdf
- PEER. (2014). The open system for earthquake engineering simulation. Retrieved from www.opensees.berkeley.org
- Petersen, M. ., Frankel, A. D., Harmsen, S. C., Mueller, C. S., Haller, K. M., Wheeler, R. L., ... Rukstales, K. S. (2008). *Documentation for the 2008 update of the United States national seismic hazard maps*.
- Porter, K. (2003). An overview of PEER's performance-based earthquake engineering methodology. In *Ninth International Conference on Applications of Statistics and Probability in Civil Engineering (ICASP9)*. San Francisco, CA: Civil Engineering Risk and Reliability Association (CERRA).
- Porter, K. A. (2016). Safe Enough ? A Building Code to Protect Our Cities and Our Lives. *Eathquake Spectra*, 32(2), 677–695.
- Porter, K. A., Beck, J. L., Shaikhutdinov, R. V., Au, S. K., Mizukoshi, K., Miyamura, M., ... Masuda, M. (2004). Effect of seismic risk on lifetime property value. *Earthquake Spectra*, 20(4), 1211–1237.
- Porter, K. A., Kiremidjian, A. S., & LeGrue, J. S. (2001). Assembly-based vulnerability of buildings and its use in performance evaluation. *Earthquake Spectra*, 17, 291–312.
- Porter, K., Kennedy, R., & Bachman, R. (2007). Creating fragility functions for performance-based earthquake engineering. *Earthquake Spectra*, 23(2), 471–489.
- Portland Concrete Association. (2012). Functional resilience: prerequisite for green buildings. Retrieved from www.sustainableconcrete.org
- Ramirez, C. M., Liel, A. B., Haselton, C. B., Mitrani-Reiser, J., Haselton, C. B., Spear, A. D., ... Miranda, E. (2012). Expected earthquake damage and repair costs in reinforced concrete frame buildings. *Earthquake Engineering & Structural Dynamics*, 41(11), 1455–1475.
- Ravindrarajah, R. S., & Tam, C. T. (1985). Properties of concrete made with crushed concrete as coarse aggregate. *Magazine of Concrete Research*, 37(130), 29–38.
- RILEM. (1991). *Fly ash in concrete: properties and performance*. (E. Wesche, Ed.). London.
- Rodriguez-Nikl, T. (2015). Linking disaster resilience and sustainability. *Civil Engineering and Environmental Systems*, 32(1–2), 157–169.
- Rodriguez-Nikl, T., Christiansen, J. W., & Walters, K. (2012). Reliability-based life cycle assessment of green concrete structures. *American Concrete Institute: Special Publication*, 289, 1–13.
- Ruhl, M., & Atkinson, G. (1999). The influence of recycled aggregate on the stress-strain relation of concrete. In *Darmstadt Concrete* (Vol. 14). Darmstadt, Germany.
- Ryan, K., Sayani, P., Baez, Y., & Mitrani-Reiser, J. (2009). Comparative life cycle performance assessment of conventional and seismic isolated buildings. In *International Symposium on Seismic Response Controlled Buildings for Sustainable Society, Tokyo, Japn.*
- Sagoe-Crentsil, K. K., Brown, T., & Taylor, A. H. (2001). Performance of concrete made with commercially produced coarse recycled concrete aggregate. *Cement and Concrete Research*, 31(5), 707–712.
- Saiz, S., Kennedy, C., Bass, B., & Pressnail, K. (2006). Comparative life cycle assessment of standard and green roofs. *Environmental Science & Technology*, 40(13), 4312–6. Retrieved from <http://www.ncbi.nlm.nih.gov/pubmed/16856752>
- Sarkisian, M., Brunn, G., Nasr, M., Hachem, M., & Hu, L. (2011). Predicting the environmental impact of structures in regions of high seismic risk. In *AEI 2011* (pp. 263–271).

References

- Schelling, T. C. (1995). Intergenerational discounting. *Energy Policy*, 23(4–5), 395–401.
- Schwab, A. K., & Brower, D. J. (1999). *Sustainable development and natural hazards mitigation*. Raleigh, North Carolina: North Carolina Division of Emergency Management.
- Scott, B. D., Park, R., & Priestley, M. J. N. (1982). Stress–strain behavior of concrete confined by overlapping hoops at low and high strain rates. *ACI Journal*, 79(1), 13–27.
- Serres, N., Braymand, S., & Feugeas, F. (2016). Environmental evaluation of concrete made from recycled concrete aggregate implementing life cycle assessment. *Journal of Building Engineering*, 5, 24–33.
- Sharrard, A. L., Matthews, H. S., & Ries, R. J. (2008). Using an input-output-based hybrid life-cycle assessment model. *Journal of Infrastructure System*, 14(December), 327–336.
- Siddique, R. (2004). Performance characteristics of high-volume Class F fly ash concrete. *Cement and Concrete Research*, 34(3), 487–493.
- Simion, I. M., Ghinea, C., Maxineasa, S. G., Taranu, N., Bonoli, A., & Gavrilesco, M. (2013). Ecological footprint applied in the assessment of construction and demolition waste integrated management. *Environmental Engineering and Management Journal*, 12(4), 779–788.
- Simonen, K., Merrifield, S., Almufti, I., Strobel, K., & Tipler, J. (2015). Integrating environmental impacts as another measure of earthquake performance for tall buildings in high seismic zones. In *Structures Congress 2015* (pp. 933–944).
- Srubar III, W. (2014). Beyond LCAs and EPDs: importance of service-life prediction for green materials and structures. In *Proceedings of the Sustainable Structures Symposium; Portland, Oregon*.
- Tapia, C., & Padgett, J. E. (2012). Examining the integration of sustainability and natural hazard risk mitigation into life cycle analyses of structures. *Structures Congress 2012*, 1929–1940.
- Thormark, C. (2007). Energy and resources , material choice and recycling potential in low energy buildings. In *International CIB Conference SB07 Sustainable Construction, Materials & Practices* (pp. 1–6). Lisbon, Portugal.
- Tol, R. S. J. (2011). The social cost of carbon. *Annual Review of Resource Economics*, 3, 419–443.
- Topcu, I. B., & Guncan, N. F. (1995). Using waste concrete as aggregate. *Cement and Concrete Research*, 25(7), 1385–1390.
- USGBC. (2009). *Green building and LEED core concepts*. Washington D.C.
- USGBC. (2015). *LEED credit library. LEED BC+CD: v4 - LEEDv4*. Washington D.C.
- USRC. (2015). About the USCRC. Retrieved from <http://www.usrc.org/about-us>
- Vamvatsikos, D., & Cornell, C. A. (2002). Incremental dynamic analysis. *Earthquake Engineering & Structural Dynamics*, 31(3), 491–514
- Vamvatsikos, D., & Cornell, C. A. (2006). Direct estimation of the seismic demand and capacity of oscillators with multi-linear static pushovers through IDA. *Earthquake Engineering and Structural Dynamics*, 35(9), 1097–1117.
- Vieira, P. S., & Horvath, A. (2008). Assessing the end-of-life impacts of buildings. *Environmental Science and Technology*, 42(13), 4663–4669.
- Wei, H., Shohet, I. M., Skibniewski, J., & Shapira, S. (2016). Assessing the lifecycle sustainability costs and benefits of seismic mitigation designs for buildings. *J. Archit. Eng.*, 22(1), 1–13.
- Wei, H., Skibniewski, J., Shohet, I. M., & Yao, X. (2016). Lifecycle environmental performance of natural-hazard mitigation for buildings. *J. Perform. Constr. Facil.*, 30(3), 1–13.

References

- Weidema, B. P., Bauer, C., Hischer, R., Mutel, C., Nemecek, T., Reinhard, J., ... Wernet, G. (2013). Overview and methodology: Data quality guideline for the ecoinvent database version 3. *Ecoinvent Report*, 1(3).
- Weil, M., Jeske, U., & Schebek, L. (2006). Closed-loop recycling of construction and demolition waste in Germany in view of stricter environmental threshold values. *Waste Management & Research: The Journal of the International Solid Wastes and Public Cleansing Association, ISWA*, 24(3), 197–206.
- Weiler, S. K., & Scholz-Barth, K. (2009). *Green roof systems*. Hoboken, New Jersey: John Wiley & Sons, Inc.
- Welsh-Huggins, S. J., & Liel, A. B. (2016). A life-cycle framework for integrating green building and hazard-resistant design: examining the seismic impacts of buildings with green roofs. *Structure and Infrastructure Engineering*, 13(1), 19–33.
- Welsh-Huggins, S. J., & Liel, A. B. (2017). Is hazard resilience sustainable? Evaluating multi-objective outcomes from enhanced seismic design decisions for buildings. *Journal of Structural Engineering, Under Revi.*
- Werner, W., & Burns, J. (2012). Quantification and optimization of structural embodied energy and carbon. In *Structures Congress 2012* (pp. 929–940).
- Worrell, E., Price, L., Martin, N., Hendriks, C., & Meida, L. O. (2001). Carbon dioxide emissions from the global cement industry. *Annual Review of Energy Environment*, 26, 303–329. Retrieved from <http://www.annualreviews.org/doi/abs/10.1146/annurev.energy.26.1.303>
- Xiao, J., & Falkner, H. (2007). Bond behaviour between recycled aggregate concrete and steel rebars. *Construction and Building Materials*, 21(2), 395–401.
- Xiao, J., Li, J., & Zhang, C. (2005). Mechanical properties of recycled aggregate concrete under uniaxial loading. *Cement and Concrete Research*, 35(6), 1187–1194.
- Xiao, J., Li, W., & Poon, C. (2012). Recent studies on mechanical properties of recycled aggregate concrete in China—A review. *Science China Technological Sciences*, 55(6), 1463–1480.